QUARTZ CRYSTAL RESONATOR STUDIES IN HEII

by

Patrick William Retz, B.Sc.
Department of Physics
Bedford College
University of London

A thesis submitted for the degree of Doctor of Philosophy

at the University of London

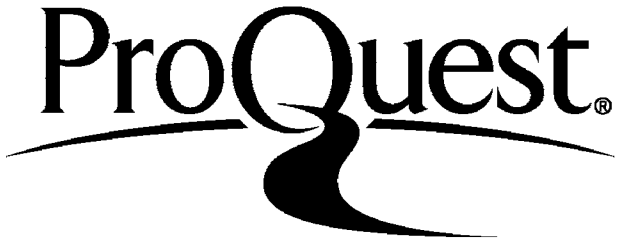

ABSTRACT

The interaction of HeII with a solid oscillating (20,34 and 48 MHz) boundary has been studied between 0.03K and T_λ by an experimental technique based on the measurements of the change in resonant frequency and Q factor of a shear-mode quartz crystal immersed in the liquid. The results show three separate aspects of this interaction. (i) Below 0.6K the measurements indicate a non-viscous mechanism which is attributed to the formation of a solid layer of ^4He atoms on the crystal surface. Estimates of the total adsorbed areal density reveal it to be a monolayer, characterised by a thermal mobilisation energy of 0.15K. (ii) Measurements in the middle temperature region ($0.6 < T < T_\lambda$) are used to determine the (complex) transverse acoustic impedance and hence the effective viscosity of HeII. The data is at sufficiently high frequencies to observe the breakdown in hydrodynamics which occurs when the viscous wave penetration depth δ becomes comparable to the phonon and roton mean free paths. (iii) Very precise measurements of the change in Q factor near T_λ show that the viscous wave samples an enhanced normal fluid density next to the crystal surface when δ becomes smaller than ξ, the superfluid healing length. A simple model is developed for the viscous losses in this region which enables an estimate to be made of the amplitude and temperature dependence of ξ. The results are found to be well described by a power law $\xi = \xi_o(1 - T/T_\lambda)^{-2/3}$ where $\xi_o = 0.08$ nm.

The transverse acoustic impedance of a weakly interacting Fermi-liquid is derived from an exact solution of the Landau kinetic equation. Explicit computations for a Fermi-gas are presented.

The work presented in this thesis is my own, or was done in collaboration with my Supervisor, Dr. M.J. Lea. My contribution was substantial and significant in all aspects of the work including experimental design, data collection, computations, theoretical calculations and interpretation.

M. J. Lea

25/8/83

P Reh

CONTENTS:

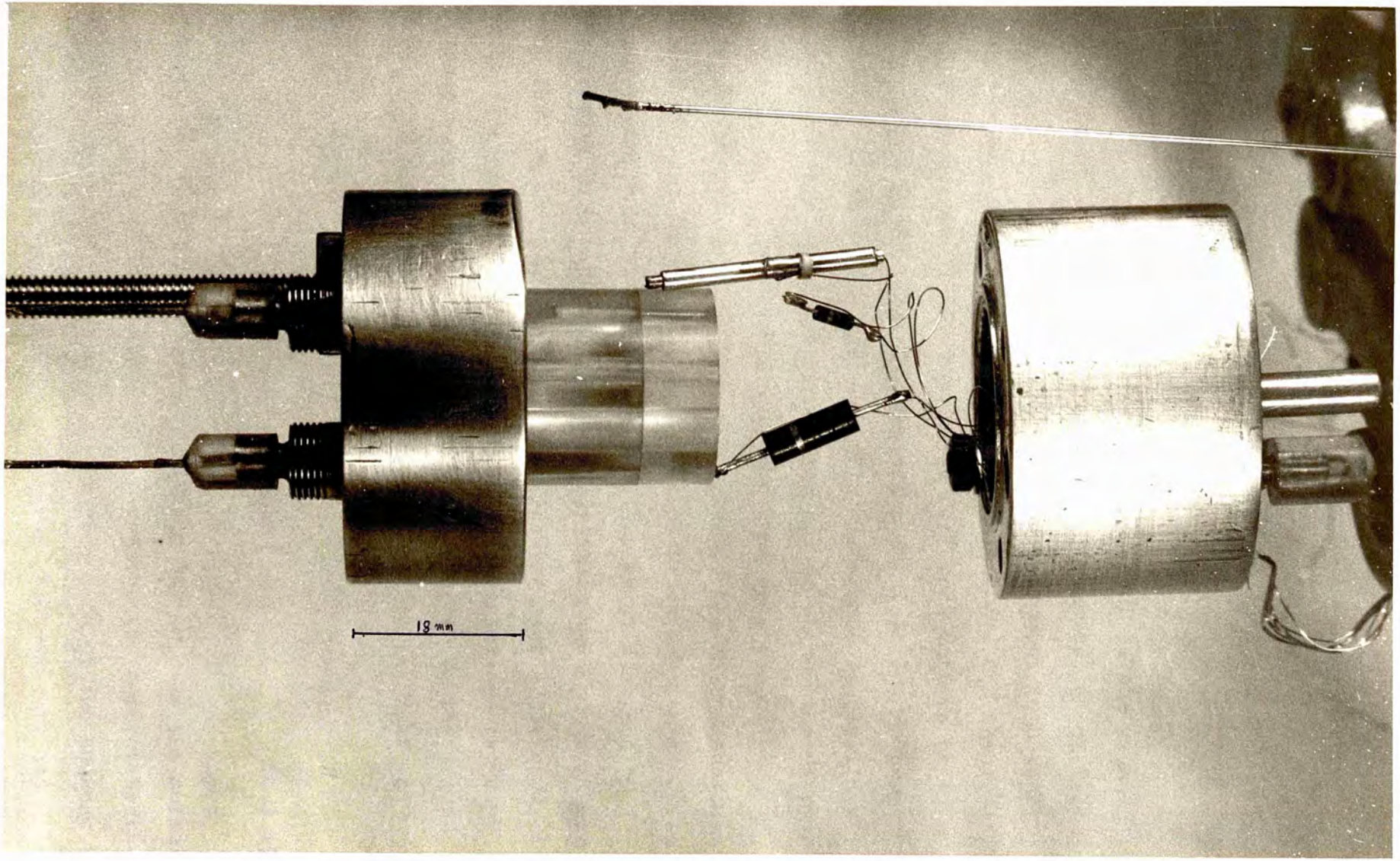
18 mm

CHAPTER ONE

1.0 QUARTZ CRYSTAL RESONATOR STUDIES IN HEII

1.1 Introduction

There has always been considerable interest in the unusual temperature dependence of the normal viscosity η of HeII and especially on its dependence on measurement technique. While there is satisfactory agreement between the temperature dependence of η from these different methods between T_λ and $\sim 1.6K$, large discrepancies occur at lower temperatures. Although the cause of this difference in capillary and slit flow experiments as being due to phonon boundary scattering has been known for some time only recently (Nadirashvili and Tsakadze (1978, 1979)) has an explanation been offered for this effect in oscillation experiments. In measurements of this kind the oscillating element e.g. vibrating wire, torsional crystal etc generates a viscous wave in the liquid which is rapidly attenuated over a distance δ, the viscous penetration depth. This characterises the distance away from the vibrating surface over which the liquid tends to participate in the oscillations and for HeII is given by

$$\delta = \sqrt{\eta/\pi\rho_n f} \qquad (1.1.1)$$

where f is the oscillation frequency and ρ_n is the normal density. A necessary condition to observe the correct hydrodynamic viscosity is that the mean free path of the phonons ℓ_p must be much less than δ. However, Nadirashvili and

Tsakadze have shown that at even moderate frequencies ($\sim$ kHz) and temperatures this condition is not satisfied. When this occurs the viscous damping is reduced which results in a lower viscosity value being measured.

In order to investigate this further we have developed a new high-freqency viscometer which uses the properties of an AT-cut quartz crystal. These crystals oscillate in thickness or shear mode, extremely pure since they have a large surface area to thickness ratio, and have a resonant frequency f_s of typically 5-20 MHz (fundamental) and Q factors in excess of 10^5. When immersed in a liquid of specific transverse acoustic impedance $Z = R + iX$ the viscous loading will cause a reduction in f_s and Q given by

$$\Delta f_s = \frac{2f_s X}{n\pi R_q} \qquad (1.1.2)$$

$$\Delta\left(\frac{1}{Q}\right) = \frac{4R}{n\pi R_q} \qquad (1.1.3)$$

for $X, R \ll R_q$. R_q is the specific acoustic impedance of the quartz and n is the harmonic number. From two-fluid hydrodynamics (Putterman (1974)) we can write

$$Z = R + iX = (1 - i)\sqrt{\eta\rho_n \pi f} \qquad (1.1.4)$$

from which the viscosity may be determined since the normal density is well known.

We have used this method to measure Z and hence η, from both X and R, between T_λ and 0.6K at SVP. In this

temperature range our results show deviations from equation (1.1.4) which support the earlier work of Nadirashvili and Tsakadze. Furthermore, the frequencies are sufficiently high to also observe the non-hydrodynamic region which occurs when both ℓ_p and ℓ_r, the roton mean free path, become comparable to δ.

Measurements of R near T_λ have also revealed deviations from equation (1.1.4) and have been interpreted in terms of the superfluid healing length $\xi_h(T)$. A number of experiments on helium-4 contained in restricted geometries or in the form of thin films have shown departures from bulk liquid behaviour. The depression of the lambda transistion temperature (Ihas and Pobell (1974), Brewer (1978)) and the reduction in the superfluid density (Henkel et al (1969), Scholtz et al (1974)) in such systems are well documented. The results from many of these experiments have been analysed in terms of the Ginzburg-Piteavskii [GP] (1958) phenomenological theory of HeII, the essential characteristics of which is the existence of a (complex) order parameter ψ and an associated temperature dependent superfluid healing length $\xi_h(T)$. The latter characterises the distance over which the order parameter builds up from zero at a non-superfluid boundary to its full value in bulk liquid. In the Mamaladze (1967) modification of the GP theory

$$\xi_h(T) = \xi_o \varepsilon^{-2/3} \qquad (1.1.5)$$

where $\varepsilon \equiv 1 - T/T_\lambda$ and $\xi_o = 0.16$ nm. Qualitatively, the

theory predicts that in systems of reduced dimensionality departures from bulk behaviour are expected to occur when ξ_h becomes of the order of the characteristic length of the experiment.

In oscillation experiments the viscous penetration depth δ plays the role of the characteristic length of the experiment. For temperatures within a few millikelvin of T_λ and at high frequencies δ is much less than $\xi_h(T)$ and hence an AT-cut quartz-crystal provides a very powerful technique for studying the superfluid healing length. Its main advantage over other experimental determination of this parameter e.g. in pores or fine channels is that it uses the simplest possible geometry i.e. a plane surface.

1.2 The Fundamental Equations

Since a quartz crystal is an electromechanical transducer, its properties are normally analysed by means of an equivalent circuit. This can be found by a combination of solving the wave equation inside the resonator, the appropriate piezoelectric equations and mechanical boundary conditions at the resonators' surface. Berlincourt et al (1964) and Berlincourt (1971) have used this method to derive the equivalent circuits for a number of piezoelectric resonators oscillating in a variety of modes. Various characteristic frequencies can be defined from the equivalent circuits electrical impedance. In the case of a planar piezoelectric resonator of thickness d oscillating in shear the motional

or mechanical resonant frequency f_s is

$$f_s = \frac{nv}{2d} \quad . \tag{1.2.1}$$

v is the velocity of the shear wave inside the resonator and n, an odd integer, is the harmonic number. For frequencies very near f_s the equivalent circuit takes the particularly simple form of a tuned series LCr circuit with $f_s = 1/2\pi\sqrt{LC}$. However for a complete description it is also necessary to include the crystals static capacitance C_o in parallel with the LCr branch. The circuit parameters can be completely defined in terms of the resonators' physical dimensions and the piezoelectric and dielectric constants of the resonator material.

The Q factor will depend on the intrinsic power loss arising from internal friction within the crystal, the crystal mounting and the geometry of the electrodes. On immersion in liquid there will be an additional power loss ΔP_ℓ due to the viscous wave excited in the liquid which can be estimated as follows. The elastic wave inside the crystal undergoes many reflections at the two crystal/liquid interfaces. If the transverse acoustic impedance of the resonator material and liquid are R_q and $Z = R + iX$ respectively then,

$$\text{Energy lost per reflection} = \Re e\left[1 - \left(\frac{R_q - Z}{R_q + Z}\right)^2\right]$$

$$\simeq \frac{4R}{R_q} \quad , \tag{1.2.2}$$

for $X,R \ll R_q$. Since there are v/d reflections per second the power radiated into the liquid is

$$\Delta P_\ell = \frac{4R}{R_q}\frac{v}{d} \quad . \tag{1.2.3}$$

From simple harmonic oscillation theory the Q factor is related to the power loss ΔP via

$$Q = \frac{2\pi f_s}{\Delta P} \tag{1.2.4}$$

If $Q_o, \Delta P_o$ and $Q, \Delta P$ are the Q factors and power losses in the crystal when in vacuum and when immersed in a liquid then since $\Delta P = \Delta P_o + \Delta P_\ell$,

$$\Delta\left(\frac{1}{Q}\right) \equiv \frac{1}{Q} - \frac{1}{Q_o} = \frac{4R}{n\pi R_q} \quad . \tag{1.2.5}$$

The viscous loading will also cause f_s to be lowered by an amount Δf_s through the phase shift which occurs at each reflection.

$$\text{Phase shift per reflection} = \tan^{-1}\left[\frac{\mathrm{Im}\left(\frac{R_q - Z}{R_q + Z}\right)}{\mathrm{Re}\left(\frac{R_q - Z}{R_q + Z}\right)}\right]$$

$$\simeq \frac{2X}{R_q} \quad , \tag{1.2.6}$$

for $X,R \ll R_q$. Therefore the phase shift per second is

$\frac{2X}{R_q} \cdot \frac{v}{d}$ and hence

$$\Delta f_s = \frac{2Xv}{R_q d} \cdot \frac{1}{2\pi}$$

or

$$\Delta f_s = \frac{2f_s X}{n\pi R_q} \qquad (1.2.7)$$

using equation (1.2.1). Hence providing that the liquid density is known equations (1.2.5), (1.2.7) and (1.1.4) can be used to give two independent determinations of the high-frequency viscosity. Although the above derivations are only approximate a more rigorous treatment involving the piezoelectric equations and the wave equation with boundary conditions yields an identical result. Equations (1.2.5) and (1.2.7) have also been quoted by Borovikov (1976).

1.3 Viscosity, Phonon and Roton Mean Free Paths

The concept of elementary excitations as developed by Landau and Khalatnikov (Landau (1941), Khalatnikov (1965, 1976)) is particularly useful in describing the properties of HeII for temperatures not in the immediate proximity of the lambda-point. In their model the weakly excited states of the assembly of helium atoms are regarded as a set of distinct elementary excitations. Each one has a definite energy ε and momentum p and behave like quasi-particles capable of motion throughout the system. At temperatures below 1.8K there are two predominant elementary excitations, each is associated with a different part of the dispersion

curve or energy spectrum. For small momenta $\varepsilon = cp$, where c is the velocity of sound, the excitations are called phonons. Roton excitations are associated with the minimum of the spectrum and are characterised by a parabolic dispersion relation of the form

$$\varepsilon = \Delta + \frac{(p - p_o)^2}{2\mu} \quad . \qquad (1.3.1)$$

Δ and p_o are the energy and momentum coordinates of the minimum and μ is the effective roton mass. The Landau parameters have been estimated at various temperatures from the neutron scattering experiments of Yarnell et al (1959) and Cowley and Woods (1971). Typical values for 1.1K, at SVP, are

$$\Delta/K_B = 8.65 \pm 0.04$$

$$p_o/\hbar = (19.1 \pm 0.1)\text{nm}^{-1}$$

$$\mu = 0.16\ m_4$$

where all the symbols have their usual meaning.

The concept of elementary excitations can be used providing few of these are present so that their interaction energy is small compared to their own energy. In this case the assembly of excitations can be considered as being comprised of an ideal gas of phonons and rotons. Furthermore, since both phonons and rotons can be excited individually it clearly follows that they possess integer spin and therefore obey Bose statistics. For rotons, however, the large value

of Δ justifies replacing the Bose distribution with that of the Boltzmann distribution for suitably low temperatures. From knowledge of the energy spectrum and the number distribution of the excitations it is possible by straightforward standard statistical mechanical methods to calculate the entire set of equilibrium properties of the liquid. These have been tabulated in a publication by Brooks and Donnelly (1977).

1.3.1 The normal viscosity η

The coefficients of viscosity and thermal conductivity are derived from the kinetic theory of the excitations which takes account of the various interactions between the phonons and rotons. Below 1.5K the five processes or interactions most likely to occur are the 4-phonon, 5-phonon, 4-roton, phonon-roton scattering and phonon-roton conversion. In a somewhat lengthy calculation Landau and Khalatnikov estimate the cross-sections for each of these interactions and hence deduce expressions for the various collision integrals. These, together with the phonon and roton equations of motion derived from the Boltzmann equation for the distribution of quasi-particles, enabled them to evaluate the normal viscosity. Expressing $\eta = \eta_p + \eta_r$, where η_p and η_r are the phonon and roton contributions, they found

$$\eta_r = \frac{p_o^2 \tau_r N_r}{15\mu} \quad . \tag{1.3.2}$$

N_r is the roton density and τ_r is the time characterising roton-roton scattering. They are given by the following

relations:

$$N_r = \frac{2p_o^2(\mu K_B T)^{1/2}}{(2\pi)^{3/2}\,\hbar^3}\, e^{-\Delta/K_B T} \qquad (1.3.3)$$

and

$$\frac{1}{\tau_r} = \frac{4p_o\mu|V_o'|^2}{\hbar^4}\, N_r \qquad (1.3.4)$$

where $|V_o'|$ is a constant and represents the matrix element for the roton-roton scattering transition. Substituting these last two equations into equation (1.3.2) gives

$$\eta_r = \frac{\hbar^4 p_o}{60\mu^2|V_o'|^2} \quad , \qquad (1.3.5)$$

a quantitiy independent of temperature. Khalatnikov also evaluates an expression for η_p (not quoted here) which contains the complete temperature dependence of η. The value of η_p is completely specified from the theory but the absolute magnitude of η_r is not since $|V_o'|$ is unknown. Khalatnikov notes, however, that between 1.5-1.9K η does not change very much with temperature (e.g. see figures 4.18) and the calculated value of η_p is very small. He therefore identifies the whole viscosity in this region with η_r. Using a value of $\eta_r = 12\mu P$, the total viscosity $\eta_p + \eta_r$ agrees very well with η from experiment (see Wilks (1967), section 7.9).

1.3.2 The phonon mean free path

Another parameter of the Landau-Khalatnikov treatment is the mean free path of the phonons ℓ_p between those collisions which scatter the flux of momentum. Khalatnikov calculates for $T > 0.9K$,

$$\ell_p = \frac{1}{16\tau' c}\left[\frac{1 + 8\tau'/\tau_p}{1 + \tau'/4\tau_p}\right] \qquad (1.3.6)$$

$$\frac{1}{\tau'} = \frac{6!N_r}{4\pi c}\left[\frac{p_o(K_B T/c)^2}{\hbar^2 \rho}\right]^2\left(\frac{2}{15} + \frac{33}{35^2}\left(\frac{p_o}{\mu c}\right)^2 + \frac{14}{75}\left(\frac{p_o}{\mu c}\right) A + A^2\right) \qquad (1.3.7)$$

and

$$\frac{1}{\tau_p} = \frac{(2\pi\hbar^3)K_B T^{12} 10^{43}}{4\pi(K_B T/c)^3} \quad . \qquad (1.3.8)$$

τ_p and τ' are the times characterising the 5-phonon process and phonon-roton scattering respectively. The value of A is estimated from

$$A = \frac{\rho^2}{p_o c}\left(\frac{\partial^2 \Delta}{\partial \rho^2} + \frac{1}{\mu}\left(\frac{\partial p_o}{\partial \rho}\right)^2\right) . \qquad (1.3.9)$$

The density derivatives of Δ and p_o are computed from the pressure data of Dietrich et al (1972) and Donnelly (1972). Khalatnikov (1976) quotes the following:

$$\frac{\rho^2}{\Delta}\frac{\partial^2\Delta}{\partial\rho^2} = -5.2$$

$$\frac{\rho}{p_o}\frac{\partial p_o}{\partial\rho} = +0.4$$

Substituting numerical values into equation (1.3.9) we find

$$\frac{1}{\ell_p} = 1.112 \times 10^8 T^{9/2} e^{-8.65/T}\left[\frac{1 + 8\tau'/\tau_p}{1 + \tau'/4\tau_p}\right] \qquad (1.3.10)$$

with

$$\frac{\tau'}{\tau_p} = 3.84 \times 10^{-4}\ T^{9/2}\ e^{8.65/T} \qquad (1.3.11)$$

where ℓ_p is in metres.

1.3.3 The roton mean free path

It is also possible to define a roton mean free path ℓ_r such that $\ell_r = \overline{|v_r|}/\tau_r$, where $\overline{|v_r|}$ is the mean magnitude of the roton velocity. From equation (1.3.1)

$$v_r = \frac{\partial\varepsilon}{\partial p} = \frac{p - p_o}{\mu}\ , \qquad (1.3.12)$$

and hence

$$\overline{|v_r|} = \frac{\int_0^\infty \frac{|p - p_o|}{\mu} e^{-\left(\Delta + \frac{(p - p_o)^2}{2\mu}\right)/K_B T} \frac{p^2}{2\pi\hbar^3} dp}{\int_0^\infty e^{-\left(\Delta + \frac{(p - p_o)^2}{2\mu}\right)/K_B T} \frac{p^2}{2\pi\hbar^3} dp} . \qquad (1.3.13)$$

Since the only significant contribution to the integral comes from values of p close to p_o we can take the limits of integration as $\pm \infty$. Introducing a variable $x = p - p_o$ then

$$\overline{|v_r|} = \frac{\int_{-\infty}^{\infty} \frac{|x|}{\mu} e^{-x^2/2\mu K_B T} (x^2 + 2p_o x + p_o^2) dx}{\int_{-\infty}^{\infty} e^{-x^2/2\mu K_B T} (x^2 + 2p_o x + p_o^2) dx} . \qquad (1.3.14)$$

These are standard integrals (see for example Dwight (1961)) and, after some algebraic simplification,

$$\overline{|v_r|} = \sqrt{\frac{2K_B T}{\pi\mu}} \left(\frac{1 + 2\mu K_B T/p_o^2}{1 + \mu K_B T/p_o^2}\right) , \qquad (1.3.15)$$

a result previously quoted by Khalatnikov (1956). The factor $2\mu K_B T/p_o^2$ is negligible below 1K and hence using equation (1.3.4)

$$\ell_r = \sqrt{\frac{2K_BT}{\pi\mu}}\,\frac{4p_o|V_o'|^2N_r}{\hbar^4} \quad . \qquad (1.3.16)$$

Eliminating the unknown constant $|V_o'|^2$ in favour of η_r, gives finally

$$\ell_r = \sqrt{\frac{2K_BT}{\pi\mu}}\,\frac{p_o^2N_r}{15\eta_r} \quad . \qquad (1.3.17)$$

Associating the viscosity minimum of 12.3 μP, taken from the data of Brewer and Edwards (1963), with the roton viscosity

$$\ell_r = 1.092 \times 10^{-12}e^{8.65/T} \qquad (1.3.18)$$

where ℓ_r is in metres. The temperature dependence of ℓ_p and ℓ_r and the viscous penetration depth at 20 MHz are shown in figure 5.1.

There have been modifications to the Landau-Khalatnikov theory and in particularly one by Roberts and Donnelly (1974) which gives the roton viscosity with no adjustable parameters. They calculate that

$$\frac{1}{\tau_r} = \sqrt{\frac{2K_BT}{\mu}}\,\pi\Gamma(\tfrac{1}{3})\left(\frac{p_o^2}{8\pi\rho K_BT}\right)^{2/3} \qquad (1.3.19)$$

where $\Gamma(\frac{1}{3}) = 2.679$ and ρ is the total density. Substituting τ_r into equation (1.3.2) and taking the pressure density of p_o into account

$$\eta_r = 5.77 \times 10^{-5}\rho^{8/9}T^{1/6}\mu^{-1/2}\ \mu P \quad . \qquad (1.3.20)$$

At SVP $\eta_r = 11.4\ \mu p^p$ which compares reasonably well with the viscosity minimum of Brewer and Edwards (1963). However, at higher pressures the agreement is not as good. Roberts and Donnelly point out that although it is reasonable to identify η_r with the minimum in η at SVP where the phonon contribution is small, this assumption is not necessarily well founded at elevated pressures. Lea and Fozooni (1982) have recently measured η_r as a function of pressure from SVP to 24 bar. Their results are in good agreement with those of Brewer and Edwards but they were unable to distinguish experimentally between a weak $\eta_r \alpha T^{1/6}$ dependence and a temperature independent roton viscosity.

1.4 The Superfluid Healing Length

For temperatures in the neighbourhood of the lambda-point the elementary excitation model cannot be applied because the excitations are so numerous that their interactions become important. There is, however, another approach used in this region which is an extension of the Landau theory (Landau and Lifshitz (1958)) of second order phase transitions to systems with surfaces. In this theory the thermodynamic potential (or the Gibbs free energy) of the system is expanded in a series of powers of some order parameter ψ which in equilibrium vanishes on one side of the transition point. The equilibrium value of this parameter on the other side of the phase transition is found by minimising the thermodynamic potential with respect to this paramter. A natural choice for the order parameter in helium-4 is the

superfluid density ρ_s since it vanishes at the lambda-point. However, it turns out that a more convenient quantity is

$$|\psi(\underline{r})|^2 = \frac{\rho_s(\underline{r})}{m_4} \quad . \tag{1.4.1}$$

By applying this variational approach Ginzburg and Pitaevskii (1958) obtained the following differential equation

$$\nabla^2\psi_o(\underline{r}') + \psi_o(\underline{r}') - \psi_o^3(\underline{r}') = 0 \tag{1.4.2}$$

where $\psi_o(\underline{r}')$ is the order parameter normalised to its bulk value:

$$|\psi_o(\underline{r}')|^2 = \frac{|\psi(\underline{r}')|^2}{\psi} = \frac{\rho_s(\underline{r}')}{\rho_s} \quad , \tag{1.4.3}$$

and

$$\underline{r}' = \underline{r}/\xi_h \tag{1.4.4}$$

$$\xi_h = \hbar/\sqrt{2m_4\alpha} \tag{1.4.5}$$

$$\nabla^2 = \frac{\partial^2}{\partial r'^2} \tag{1.4.6}$$

(N.B. Unless the spatial dependence is explicitly written it shall be assumed that ρ_s and ψ refer to the superfluid density and the order parameter in bulk i.e. for $r' \to \infty$). $\bar{r}'$ is the position vector in units of the healing length and α is the coefficient of $|\psi(\underline{r})|^2$ in the expansion of the thermodynamic potential. In the Mamaladze (1967) modification of their theory, if

$$\frac{\rho_s}{\rho} = k\varepsilon^{2/3} \qquad (1.4.7)$$

then

$$\alpha = \frac{\Delta C m_4 T_\lambda}{k}\ \varepsilon^{4/3} \qquad (1.4.8)$$

where $\rho(=\rho_n + \rho_s)$ is the total helium density and ΔC is the difference in the specific heats in the superfluid and normal states. Taking a value of $k = 2.41$ from the data of Tyson and Douglass (1966) and $\Delta C = 5.20 \times 10^6 JK^{-1}kg^{-1}$

$$\xi_h = \frac{\hbar}{m_4\sqrt{2\Delta C T_\lambda}}\varepsilon^{-2/3} \qquad (1.4.9)$$

$$= 0.16\ \varepsilon^{-2/3}nm\ .$$

This has a functional form consistent with the phenomenological theory of scaling (Fisher (1974)), Hohenberg et al (1976)) of critical behaviour. On the basis of scaling there should be only one intrinsic length ξ_c, the phase correlation length, describing the properties of the phase transition. Any other length such as the length describing the surface properties (ξ_h), or the onset length in finite geometries, should only differ from this length by a factor of the order unity but are expected to have the same temperature exponent. Hohenberg et al (1976) calculate that ξ_c is given by

$$\frac{\xi_c \rho_s}{T} = \frac{m_4^2 k_B}{4\pi\hbar^2} \qquad (1.4.10)$$

and hence $\xi_c \propto \varepsilon^{-2/3}$. However, there are some reservations about the validity of the Mamaladze modification which have been discussed in detail by Binder and Hohenberg (1972).

Equation (1.4.2) can be solved to obtain the form of the superfluid density profile in some simple geometries. In the case of helium-4 next to a solid wall, taken to be in the xy plane, the equation for the order parameter becomes

$$\xi_h^2 \frac{d^2\psi_o(z)}{dz^2} + \psi_o(z) - \psi_o^3(z) = 0 \quad . \qquad (1.4.11)$$

This has a first integral

$$\xi_h^2 \left(\frac{d\psi_o}{dz}\right)^2 + \psi_o^2 - \frac{\psi_o^4}{2} = A' \qquad (1.4.12)$$

where A' is a constant. A further integration gives

$$\int \frac{d\psi_o}{\sqrt{\psi_o^4 - 2\psi_o^2 + 2A}} = \frac{z}{\xi\sqrt{2}} + B' \quad . \qquad (1.4.13)$$

Clearly, the constants A' and B' are determined by the boundary conditions on ψ_o which in the bulk liquid or thick film limit, where the film thickness $d_f \gg \xi_h$, are

$$\frac{z}{\xi_h} = 0 \qquad \psi_o = 0 \qquad (1.4.14)$$

$$\frac{z}{\xi_h} \to \infty \qquad \begin{matrix} \psi_o \to 1 \\ \xi_h \dfrac{d\psi_o}{dz} \to 0 \end{matrix} \qquad (1.4.15)$$

and therefore $A' = \frac{1}{2}$. For this value of A' the L.H.S. of equation (1.4.13) can be integrated in closed form giving

$$\psi_o = \tanh(z/\xi_h\sqrt{2}) \qquad (1.4.16)$$

and hence the superfluid density profile is

$$\frac{\rho_s(z)}{\rho_s} = \tanh^2(z/\xi_h\sqrt{2}) \ . \qquad (1.4.17)$$

Sobyanin (1972) has extended the theory to include the effect of the attractive Van der Waals potential between the wall and helium atoms, however, his computations show that $\rho_s(z)$ is only slightly sensitive to the form of the external potential used.

Although the mean field approximation of Ginzburg-Pitaevskii-Mamaladze is a theory of the bulk liquid its major use has been in explaining phenomena observed in helium-4 contained in thin films and restricted geometries. In the case of thick films however there is an additional complication in that the boundary condition at the free liquid surface - whether ψ_o or its gradient is zero - is not clear. Experimental measurements tend to favour the former but neither choice will result in a value of $A' = \frac{1}{2}$ and therefore the integral in equation (1.4.13) cannot be carried out in closed form. ψ_o and hence the average superfluid density $\langle\rho_s\rangle$, found by integrating $|\psi_o|^2$ over the film thickness d_f, become elliptic functions of z/ξ_h. An analysis of this equation shows (Atkins and Rudnick (1970)) that for sufficiently small d_f, $\langle\rho_s\rangle$ is less than the superfluid density in bulk. Moreover when $\xi_h \sim d_f$ this depletion of ρ_s is

FIG. 1.1 ESTIMATES OF THE SUPERFLUID HEALING LENGTH

REFERENCE	SYSTEM	METHOD	ξ(nm)	ε RANGE
Ginzburg and Pitaevskii (1958) Mamaladze (1967)	Boundary	Theory: Superfluid healing length ξ_n	$0.163\ \varepsilon^{-2/3}$	$\varepsilon \leqslant 4.6 \times 10^{-3}$
Hohenberg, Aharony, Halperin and Saggia (1976)	Bulk	Theory: Phase correlation length ξ_c	$0.027\ \varepsilon^{-2/3}$	$\varepsilon > 0$
Williams and Rudnick (1970)	Bulk	Attenuation of first sound (16.8 kHz - 3.17 MHz). ξ equal to wavelength at temperature for maximum attenuation	$0.08\ \varepsilon^{-2/3}$	$4.6 \times 10^{-7} \leqslant \varepsilon \leqslant 5 \times 10^{-5}$
Ihas and Pobell (1974	Channels	ΔT_λ from measurements of the vanishing of second sound in narrow (μm) channels	$0.12 \pm 0.01\ \varepsilon^{-0.65 \pm 0.02}$	$2 \times 10^{-5} \leqslant \varepsilon \leqslant 2 \times 10^{-4}$
Henkel, Smith and Reppy (1969)	Pores	Determination of $\langle \rho_s \rangle$ from gravitational superflow through a slit.	$0.28 \pm 0.04\ \varepsilon^{-0.67 \pm 0.04}$	$2 \times 10^{-4} \leqslant \varepsilon \leqslant 0.2$

complete and $\langle \rho_s \rangle = 0$. Quantitatively this theory predicts that the onset temperature in thin films will be depressed by an amount ΔT_λ below the bulk transisiton temperature according to:

$$\frac{\Delta T_\lambda}{T_\lambda} = \left(\frac{\xi_o}{d_f}\right)^{3/2} \qquad (1.4.18)$$

The above equation and direct measurements of $\langle \rho_s \rangle$ have formed the basis for the determinations of ξ_o, a few of which are tabulated in figure 1.1. Also included in this table is one bulk estimate of ξ_o from the first sound attenuation experiments of Williams and Rudnick (1970). As can be seen all conform to the expected 2/3 temperature exponent but there are considerable variations in their amplitudes.

CHAPTER TWO

2.0 EXPERIMENTAL TECHNIQUES

2.1 Introduction

The most convenient method of determining the characteristic frequencies and Q factor of a piezoelectric crystal is by means of a transmission circuit (Anon (1957)) in which the crystal controls the magnitude of the transmitted signal. Such an arrangement was used in the experimental work described here and is shown in block diagram form in figure 2.3. The circuit was based on a Hewlett-Packard (HP) 8640B signal generator. Resonance was identified with the maximum transmitted signal. This position was locked-on to using the quadrature phase transmitted signal, which is zero at resonance, to control the driving frequency (via the d.c. frequency modulation facility) of the HP8640B. At low temperatures the stability and precision of the resonant frequency measurements was $\sim$ 0.1 Hz. The Q factor was estimated from the magnitude of the maximum transmitted signal. The AT-cut quartz crystal was operated at the 3rd (20.47 MHz), the 5th (34.09 MHz) and 7th (47.70 MHz) harmonics. Measurements were made at SVP between T_λ and $\sim$ 30 mK using a helium-3/helium-4 dilution refrigerator constructed by the Oxford Instrument Company Limited.

2.2 The Sonic Cell

The basic components of the sonic cell are shown schematically

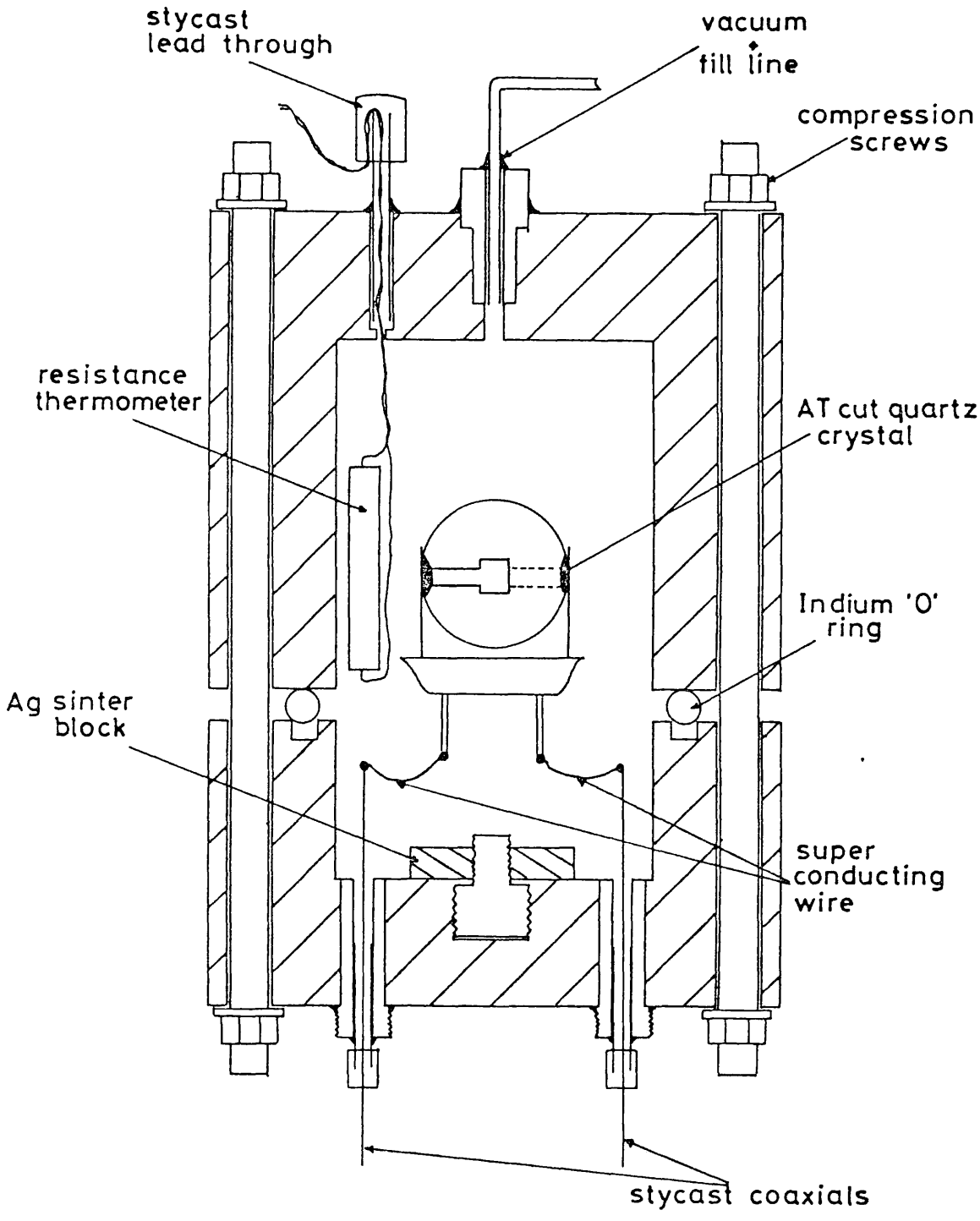

FIG.2.1 DIAGRAM OF THE SONIC CELL

in figure 2.1. The cell body consisted of two sections made from OFHC (Oxygen-Free High-Conductivity) copper which were sealed together by means of an indium O-ring compressed by four screws evenly spaced around the cells circumference. The cell was evacuated and helium gas introduced in the sample space via the capillary fill line situated on the upper section. Although this was thermally anchored to the mixing chamber, all five heat exchangers on the dilution unit and the 1.2 pot, it was undoubtably the major source of heat leak and prevented temperatures of less than 30 mK from being easily reached. From observations of the pressure change in the fill line during helium-4 condensation, the cell volume was estimated to be 2.9 cm^3. (Much of the dead space inside the cell had been reduced by a perspex cylinder which held both the crystal clamping assembly and the resistance thermometers in place - see photograph). On the lower section were situated the coaxial lead-throughs: Commercially available glass-to-metal seals were initially used but these were later replaced by laboratory made Stycast 1266 lead-throughs since these proved to be more resilient to thermal cycling. A later experiment carried out by Drs Lea and Fozooni confirmed that the cell was pressure tight to at least 21 atm. at 4.2K. A diagram of the gas-handling system is shown in figure 2.2.

Several different crystal clamping arrangements were designed and tested. Mechanically, the clamping assembly had to be flexible enough to allow for the thermal contraction of the quartz otherwise the crystal would fracture and also to

reduce the risk of producing impurity modes. A further consideration was to make the clamping assembly an integral part of the electrical circuit by clamping onto the crystal electrodes. With these points in mind the original laboratory built clamps consisted of small Cu/Be springs, gold plated for improved electrical contact, that pressed against the crystal electrodes. Although some degree of success was achieved, pressure contacts of this kind caused irreparable damage to the crystal surface and electrodes. Other arrangements including the excitation of electrodeless crystals by capacitative coupling, as reported by Smagin (1975), were also attempted but in the majority of cases the Q factors were undesirably low. By far the best clamping assembly in terms of performance and reliability was a commercially made one, the outline of which is shown in figure 2.1. They are used extensively by GEC (General Electric Company) in the manufacture of their high-frequency crystal units. The crystal is loósely clamped on the rim and held fast by a thin layer of 'Aquadag' (originally the crystals were held with a blob of silver araldyte but this was removed) painted over both the clamping post and gold electrode. This arrangement even survived after rapid and repeated immersion in liquid nitrogen. Short lengths of superconducting Niomax CN wire were used between the clamping terminals and the coaxial lead-throughs. This completed the electrical circuit and further ensured that below the superconducting transition temperature ($\sim$ 10K) of the wire the crystal was well isolated from the heat leak down the RF lines.

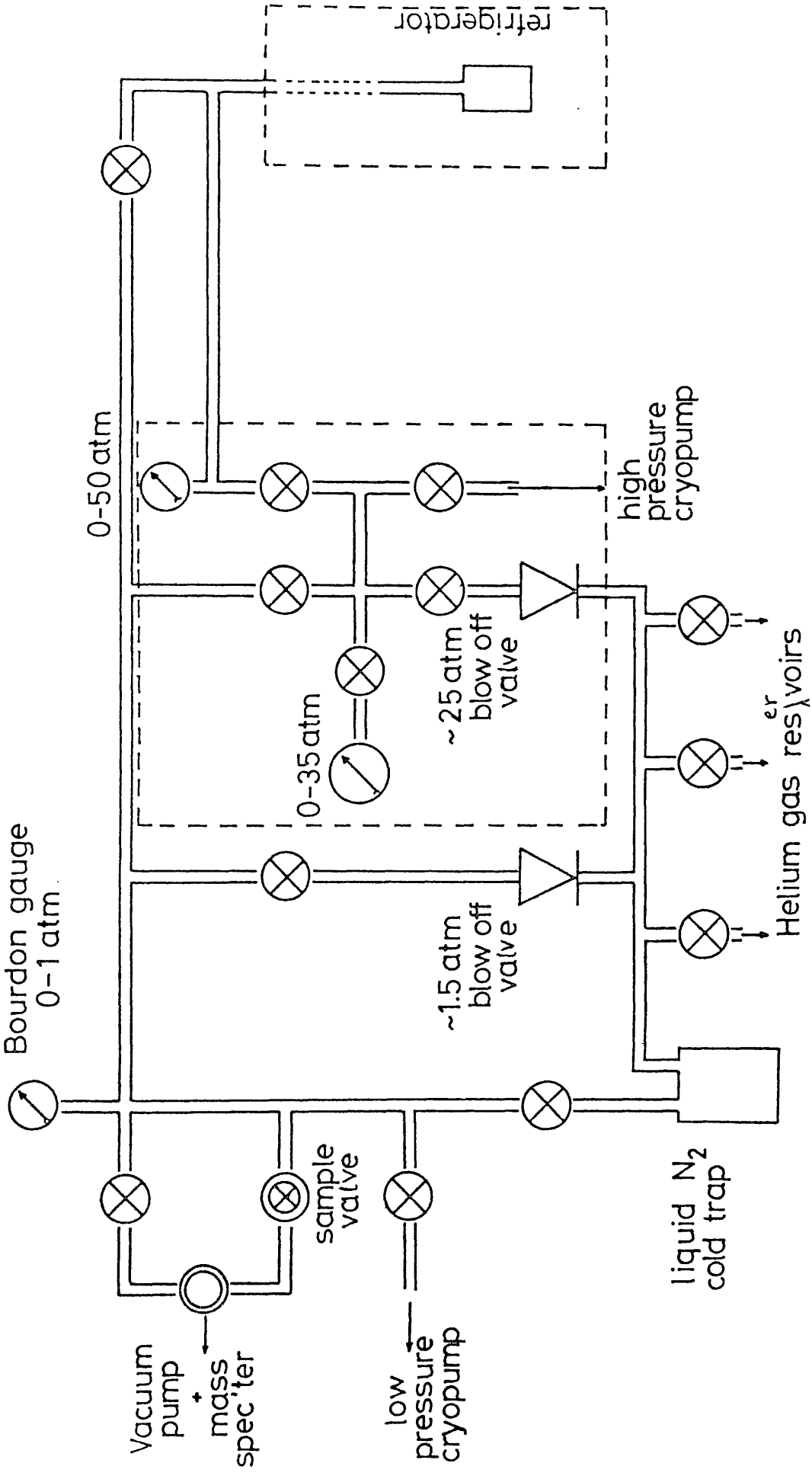

FIG.2.2 HIGH/LOW PRESSURE GAS-HANDLING SYSTEM

An important cell parameter is the time τ required for the helium sample to reach thermal equilibrium with the cell wall. If R_T is the thermal boundary resistance and C_t is the thermal capacity of the system then $\tau = C_t R_T$. Now the dominant contribution to R_T in this case (for a review of thermal boundary problem see Harrison (1979)) is the Kapitza boundary resistance and $R_T = R_k/A_i T^3$ where R_k is the Kapitza coefficient and A_i is the interface area between the cell wall and liquid helium. At millikelvin temperatures R_T (and hence τ) can become undesirably high, however, this can be circumvented by the introduction of sintered metal inside the cell. This has an extremely porous structure which results in a high surface area to volume ratio thereby increasing A_i and hence reducing R_T. The silver sinter block, kindly supplied by Dr N Kerley of the Oxford Instrument Company Limited, was made from Johnson-Mattheys' 'Cypher 88' silver powder and had a surface area to volume ratio of $\sim 10^6$ m^{-1}. It was cut into a block $8 \times 8 \times 1.5$ mm^3 which was tightly threaded into a copper post and screwed down until it pressed hard against the cell base. This volume of sinter was estimated to improve the cell thermalising time by a factor of 40!

The thermal boundary resistance and the heat leak from external sources e.g. fill line, RF lines etc were estimated from steady state measurements of RF heating of the helium sample. If the total rate of heat dissipation in the helium sample is $\dot{Q}$ and ΔT is the temperature difference that this maintains between the helium sample and cell then it was found that

$$\dot{Q} = 0.346\ T^3 \Delta T\ W \qquad (2.2.1)$$

$$= \Delta T / R_T$$

where

$$\dot{Q} = (21.6 + \text{RF power diss}^{n}\text{ in crystal})\ \text{nW} \qquad (2.2.2)$$

Taking $A_i = 9.6 \times 10^{-8} m^2$, the Kapitza boundary coefficient for the silver sinter/helium interface is $\sim 0.033\ K^4 m^2 W^{-1}$. This is higher than the value quoted by Lounasmaa (1974) and Harrison (1979) but bearing in mind that R_k depends critically on the condition of the surfaces and on the degree of thermal contact between the sinter and copper, it is not unreasonable. Equation (2.2.1) can also be used to calculate the corrections to the R10/R11 thermometry calibrations - see later - which at 50 mK is only 0.5 mK.

In a further RF heating experiment, τ was measured directly at several temperatures by observing the time taken for the helium sample to rise (or fall) by 1/e of of its initial temperature. At 18,25 and 58 mK τ was estimated to be 9, 6.7 and 1s respectively. Compared to the rate of cooling below 100 mK, these times were sufficiently small to ensure that thermal equilibrium always existed between the helium sample and the cell.

2.3 Quartz Crystals

The crystals used in these experiments were thickness-shear (TS) mode AT-cut quartz crystals. They are characterised

by a cut angle $\theta = 30^{o}\ 10'$ (see 'Standards on Piezoelectric Crystals' Anon (1949)) which results in a $df_s/dT \sim 0$ around room temperature and are therefore widely used in industrial instruments. A number of these crystals were kindly supplied by Dr E Read of the GEC-Hirst Research Centre, Wembley, Middlesex. They had a fundamental frequency of 6.83 MHz and had been specially selected for their high Q factors which at 20.47 MHz, the third harmonic, was $> 10^5$. The crystals were in the shape of flat discs, approximately 9 mm in diameter and only 0.25 mm thick. This gave an effective diameter to thickness ratio of 36 which was sufficient to ensure a pure thickness mode of oscillation. The electrodes were thin gold films, vacuum deposited onto the quartz surface. They were square shaped and had a surface area of approximately $\sqrt{2} \times \sqrt{2}$ mm^2.

Each crystal unit on arrival was first tested by plotting out its frequency response at resonance and measuring its Q factor with the transmission circuit of figure 2.3. Unfortunately the crystals were held fast to the clamping arrangement with large blobs of araldyte which may be ideal at room temperature but would have almostly certainly caused the quartz to fracture if cooled to cryogenic temperatures. Therefore the silver araldyte was dissolved with dimethyl formamide and replaced by a thin layer of Aquadag. Although the crystals were handled with great care small amounts of atmospheric dirt was found to drastically reduce their Q factors. However, cleaning the crystals ultrasonically in methanol for a few seconds and drying them in a stream of helium gas invariably improved the Q factor.

2.4 Electronics

The electronic components of the transmission circuit are shown in block diagram form in figure 2.3. The crystal was placed in a series resonant configuration and driven in c.w. (continuous wave) mode by a Hewlett-Packard (HP)8640B signal generator. The signal generator power levels used were - 43 dBm and - 53 dBm, where 0 dBm ≡ 1 mW, and represents the power dissipated in a 50 Ω load connected across the output terminals of the oscillator. At the lowest setting this produced an estimated power dissipation of 2 nW in the helium sample, i.e. less than 10% of the heat leak due to other sources. The transmitted signal was amplified by an Avantek high-gain (+ 40 dB), low-noise amplifier and finally detected by a Marconi-Saunders diode detector placed immediately after the amplifier. The frequency was recorded with a Philips PM6615 Universal Counter, triggered externally by an oven stabilised crystal oscillator with a stability factor, as quoted by the manufacturers, of 10^{-3} ppm. As a visual check, the pre-detected signal was monitored continuously on an oscilloscope.

A feedback circuit was used to keep the driving frequency locked-on to the crystal resonance. Its operation was based on the rapid phase change that occurs across the crystal on sweeping through the resonant frequency. The central component was a HP10514A mixer which in this mode acted as a phase detector: Its d.c. output was zero when the RF signals at its two inputs were $\pi/2$ out of phase. The mixer output was averaged and amplified by 20 dB using a Brookdeal 415

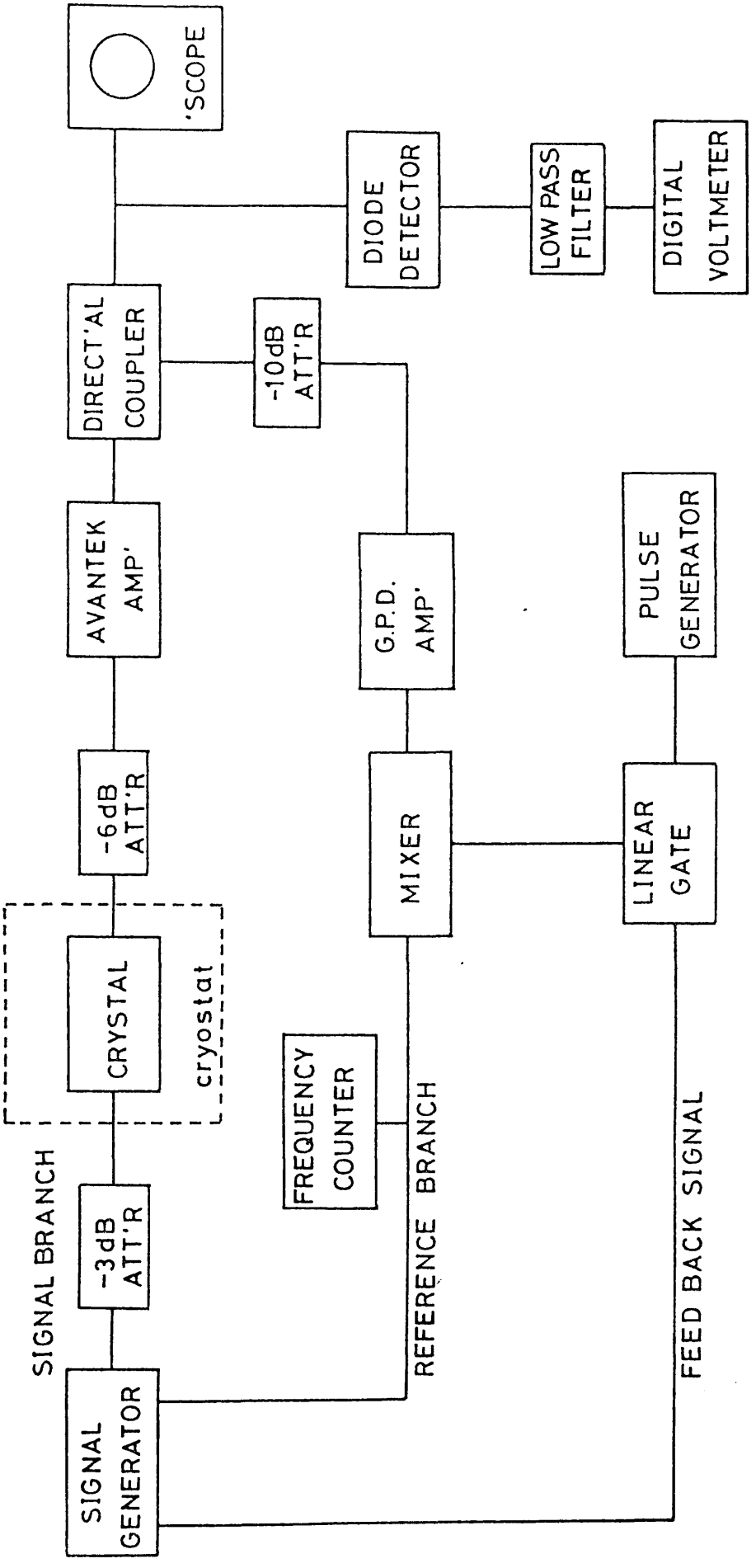

FIG.2.3 SCHEMATIC DIAGRAM OF THE ELECTRONICS

linear gate and returned to the signal generator via its d.c. frequency modulation facility. The FM setting was found by trial and error. Exessive frequency modulation caused the circuit to oscillate and an inadequate amount resulted in the circuit not locking-on. This latter position occurred at the frequency for which the feedback signal (mixer output level) was zero. This frequency was made to coincide with the frequency for the maximum transmitted signal by adjusting the length and hence the phase of the reference arm. The smallest coaxial length used produced a phase change, at 20 MHz, of $\sim$ 0.008 rads which gives an indication of the sensitivity of the feedback balancing procedure. The feedback loop was always adjusted at temperatures below 600 mK where the crystal resistance was practically constant.

The RF signal inside the cryostat was carried by purpose build coaxial lines. They were made from cupro-nickel tubing: the outer conductor was 5 mm in diameter and the inner one 2 mm in diameter. This ratio of conductor radii gave an impedance of about 50 Ω thereby roughly matching the impedance of the other electrical components. The outer conductor was thermally anchored to the 1.2 pot and all five heat exchangers. The inner and outer conductors were electrically isolated but thermally shorted by means of glass-to-metal seals positioned along the inner conductor. Figure 2.4 shows the power loss (in dB) in the RF coaxial lines from 1 to 500 MHz. Superimposed on this graph is the predicted $\sqrt{f}$ power loss law which is closely

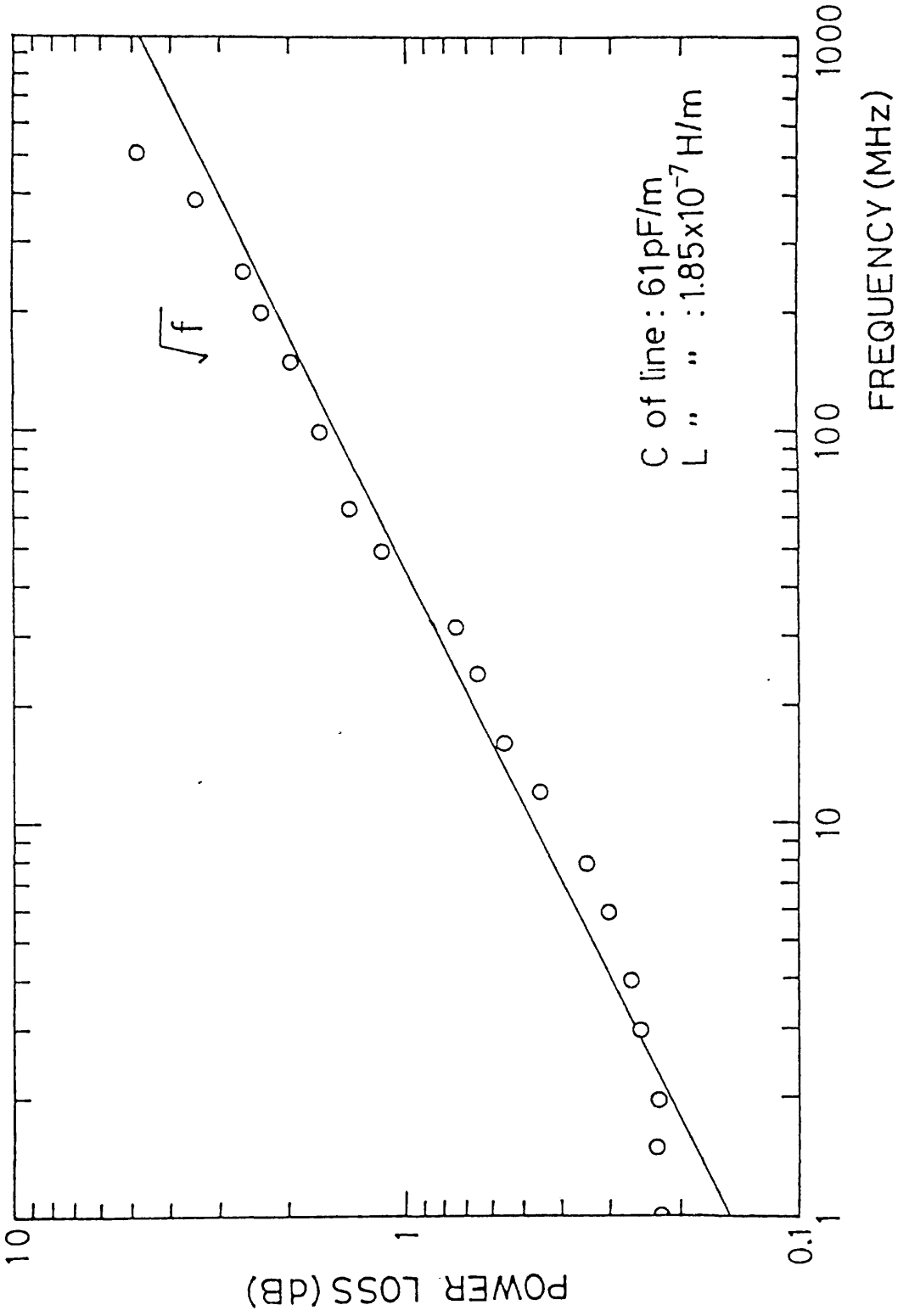

FIG.2.4 POWER LOSS IN THE CUPRO-NICKEL COAXIAL RF LINES

obeyed down to $\sim$ 2 MHz. Conventional 50 Ω coaxial cables were used outside the cryostat. Attenuators placed on either side of the cell served to suppress any standing waves and further ensured that the electrical load on both sides of the crystal was fifty ohms.

The linearity of the power response of the circuit was checked with the crystal leads shorted. The results are shown in figure 2.5 at 20, 34 and 48 MHz. The vertical axis is the d.c. output, s_o, from the diode detector (manufactured by Marconi-Saunders: type 6060) measured in millivolts. The RF signal power from the signal generator, in units of dBm, is plotted on the ~~ordinate~~ horizontal axis. If the latter is denoted by P then for $P < -55$ dBm, $P \alpha s_o^n$ where n is 1.00, 1.06 and 1.07 at 20, 34 and 48 MHz respectively.

2.5 RF Heating of Crystal and Helium Sample

From an analysis of the transmission circuit, if the RF power in the circuit is P_{rf} then the power dissipated in the crystal P_c when the crystals series resistance is r is

$$P_c = \frac{200r}{(100 + r)^2} \cdot P_{rf} \cdot \qquad (2.5.1)$$

P_{rf} is equal to the HP8640B setting, which represents the power dissipated in a 50 Ω load connected across its output terminals, reduced by - 3 dB by the variable attenuator. For $T < 600$ mK, $r \sim 100$ Ω at 20.47 MHz giving a

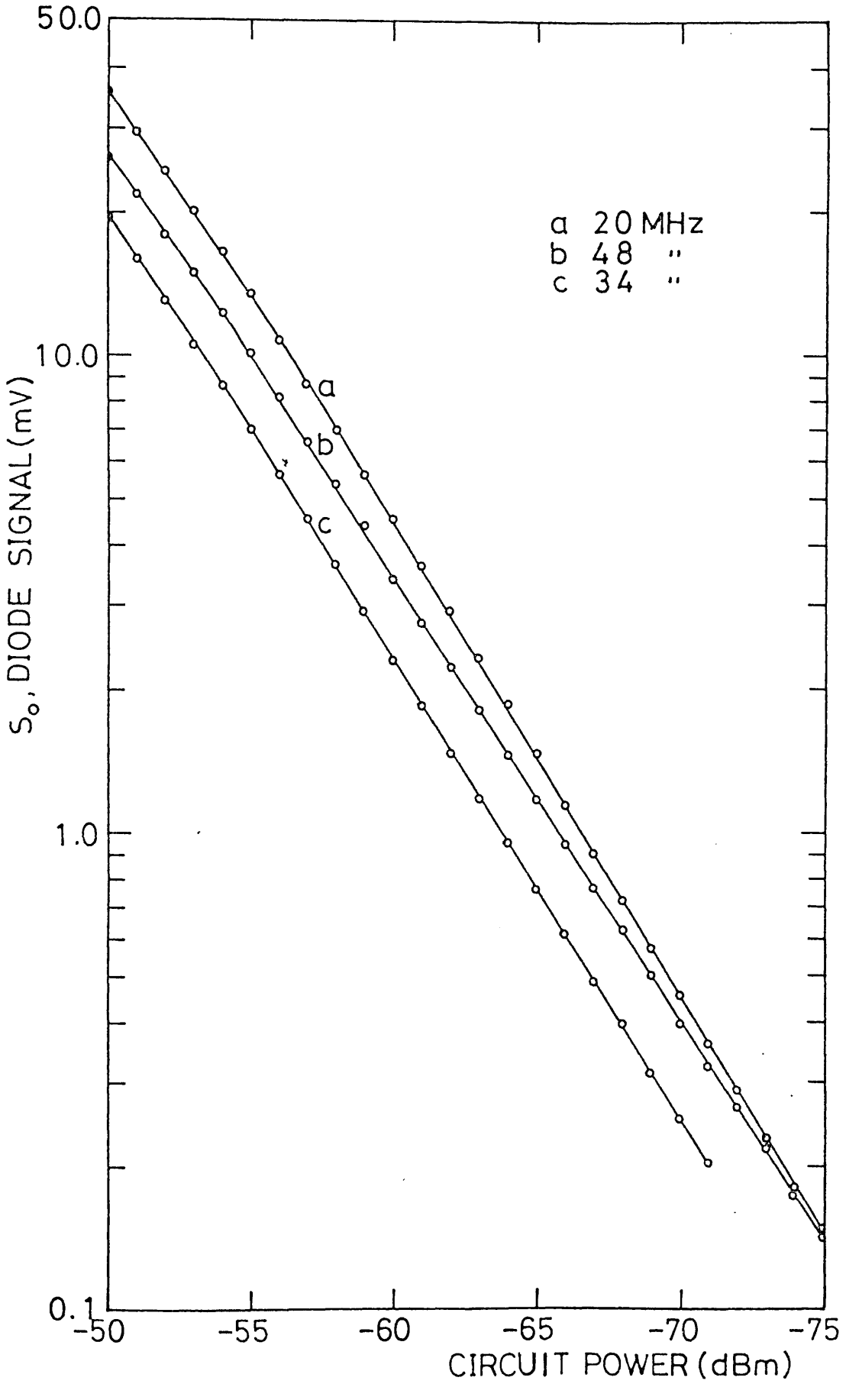

FIG. 2.5 DIODE DETECTOR CALIBRATION

$P_c \sim 2$ nW for $P_{rf} = (-53 - 3)$ dBm. Through the Kapitza effect this will maintain a temperature difference ΔT between the crystal and surrounding helium of $\Delta T = (R_k/A_i)P_c$. Taking $A_i \sim 10^{-5}$ m^2 i.e. the total electrode surface area and a typical value of $R_k T^3 \sim 0.01$ K^{4}m^{2}W^{-1} below 0.2K from Lounasmaa (1974), then $\Delta T \sim 2$ mK at 0.1K. At higher temperatures ($T > 0.2$K) $R_K T^3 \sim 0.001$ K^{4}m^{2}W^{-1} making $\Delta T < 0.2$ μK at 1K. Therefore the crystal and helium sample were in good thermal equilibrium for $T < 100$ mK.

Any power dependent behaviour was checked for by performing runs at higher power levels (the signal generator level was increased by an order of magnitude) but none was seen.

2.6 Thermometry

The thermometry associated with the dilution refrigerator has been developed over a considerable period of time and incorporates the more widely used thermometric devices described, for example, in Betts' (1976) book on 'Refrigeration and Thermometry Below 1 Kelvin'. On a run to run basis the most useful secondary thermometers were two carbon 'Speer' resistors, designated R4(½W, 100 Ω) and R8(½W, 470 Ω) which were used below and above 1.0K respectively. R4 had been calibrated against a CMN magnetic susceptibility thermometer, a Superconducting Reference Material (SRM) 767 unit and, at temperatures < 50 mK, against a Nuclear Orientation (NO) thermometer. The saturated vapour pressure of helium-4 had been used to calibrate R8 between 0.85 and 4.2K. Details of the above thermometers as used by the

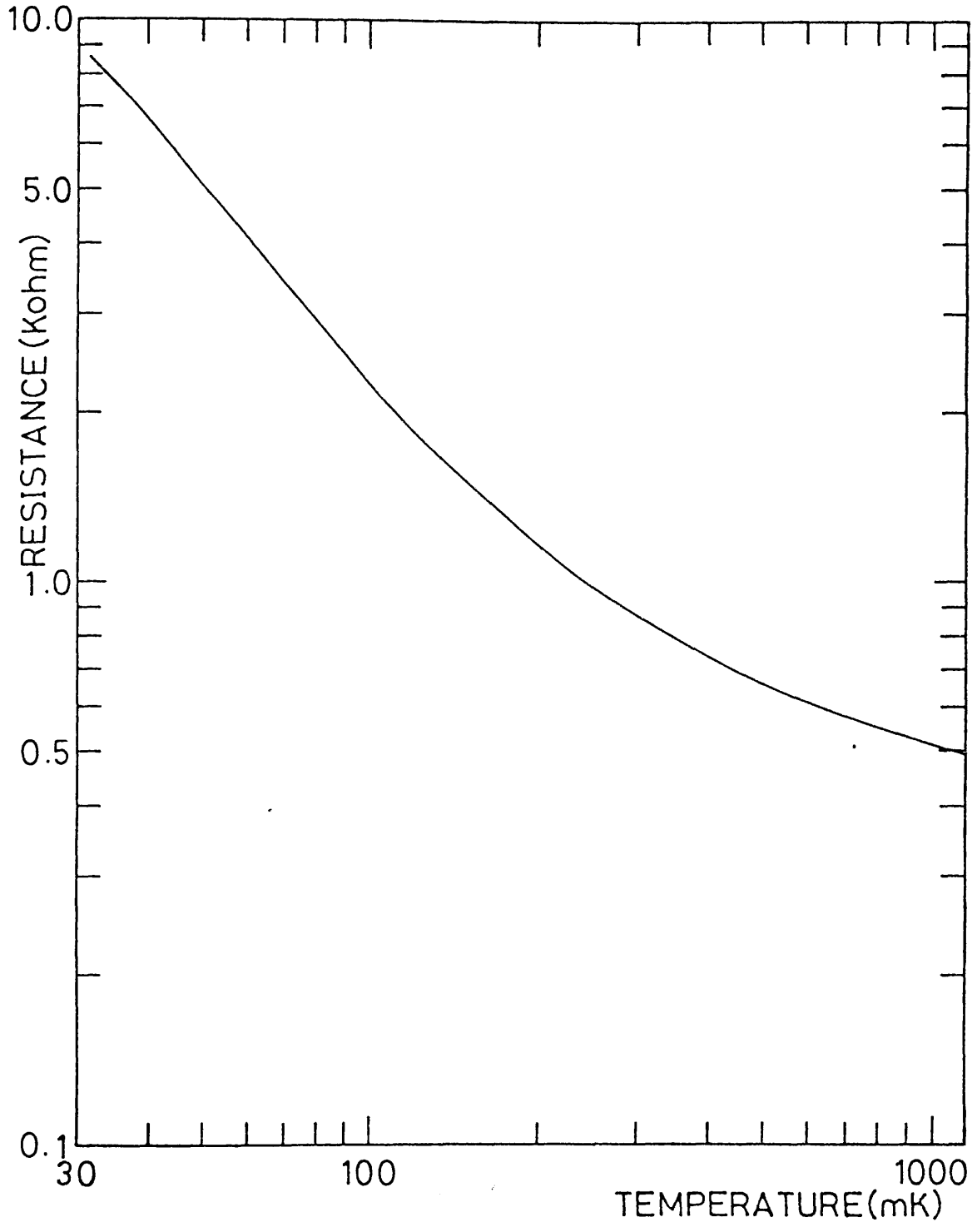

FIG.2.6 RESITOR CALIBRATION: R10

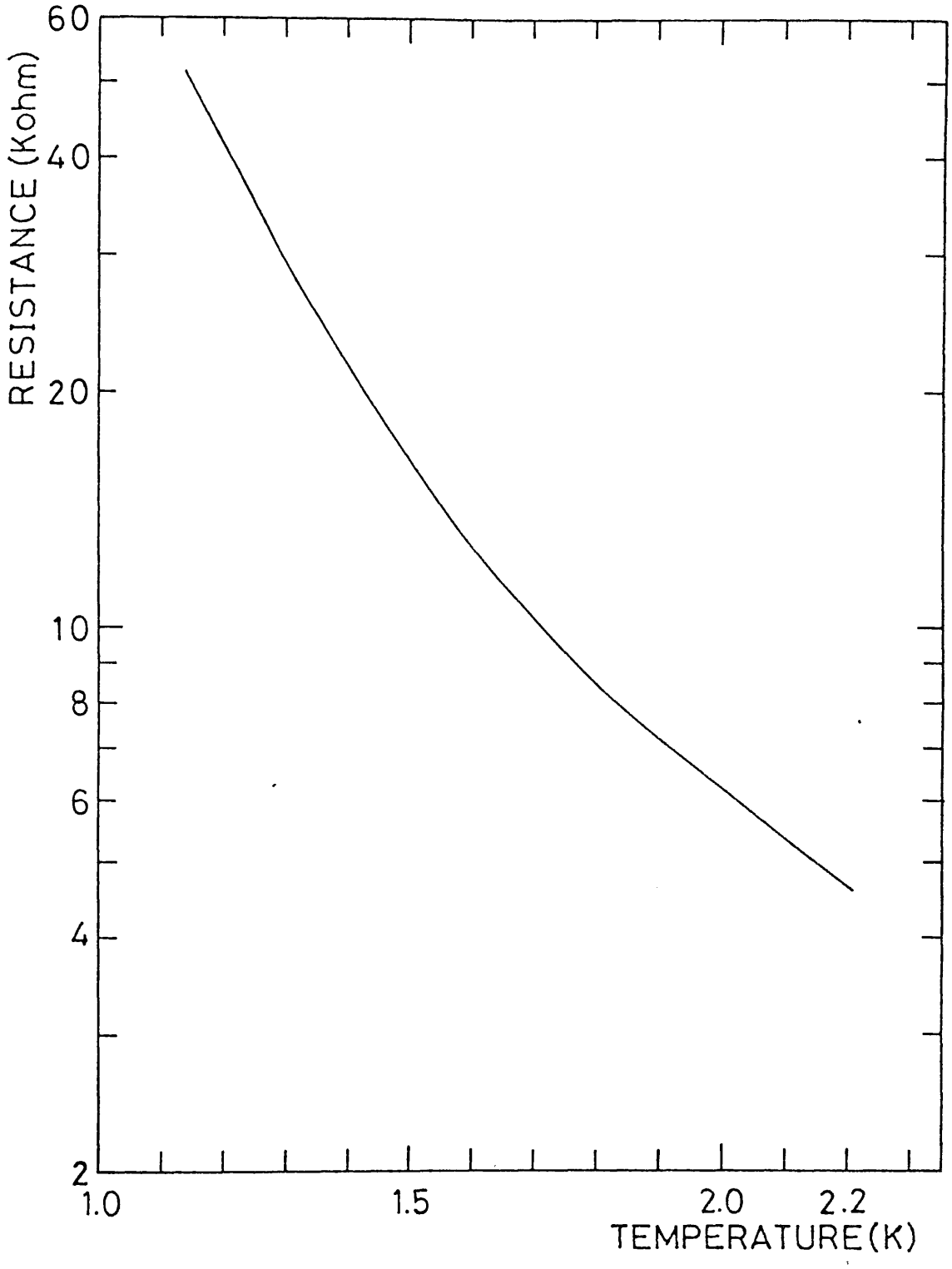

FIG.2.7 RESISTOR CALIBRATION: R11

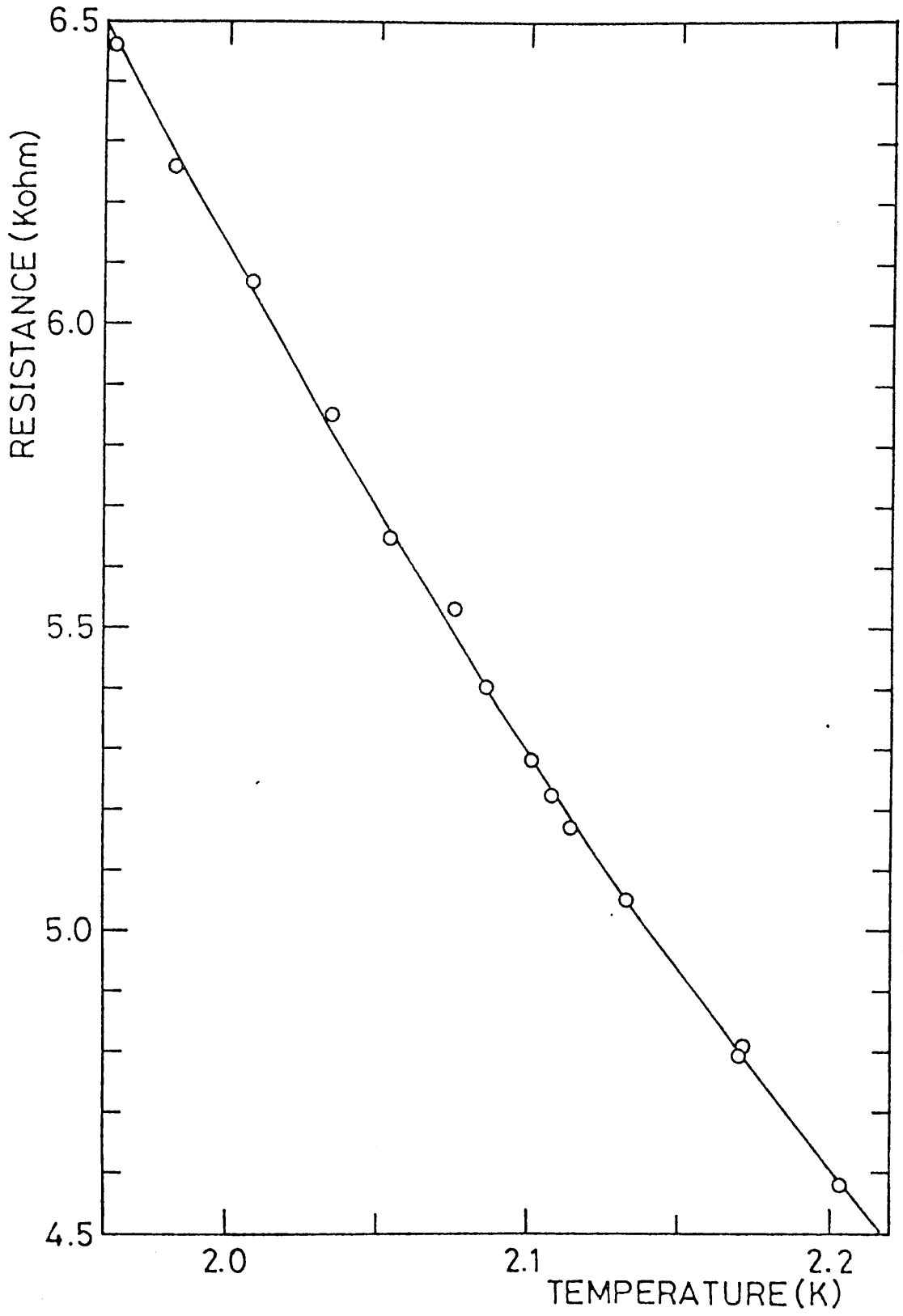

FIG.2.8 RESISTOR CALIBRATION OF R11 ABOVE 2K

Bedford College Low Temperature Group, together with their calibration procedures, has already been discussed by Butcher (1978). A further two resistance thermometers, designated R10(½W,100Ω Speer) and R11(⅛W,100Ω Allen-Bradley) were located inside the cell in order to provide a more accurate determination of the helium temperature. These were calibrated by a direct comparison with R4 and R8.

All temperatures in this work are in accordance with 'The 1976 Provisional 0.5 to 30K Temperature Scale' researched by the Bureau International des Poids et Mesurers (Anon (1979)).

2.6.1 R10 and R11: Measurement and error estimates

Resistance measurements were made with a 'Cryobridge S72' manufactured by the Czechoslovak Academy of Science. This instrument is based on an a.c. Wheatsone bridge with an operating frequency of 225 Hz. By using the built in comparison resistors, resistances in the range of 1 to 112,211 Ω could be measured to an accuracy of 0.1%. The bridge voltage was variable and had a range from 2 mV (r.m.s.) to 20 μV. In order to reduce the Joule heating effect, bridge settings of 200, 60 and 20 μV were used for R10 < 500 Ω < 2 kΩ and < 30 kΩ. Similar settings were used for R11.

The percentage error in T, determined from the scatter in the calibration points, for R10 was estimated to be ± 1.5% from 1.0-0.05K, ± 2% from 50-40 mK and ± 3% from 40-30 mK. In the case of R11 the percentage error in T was taken as ± 1% over its entire working range.

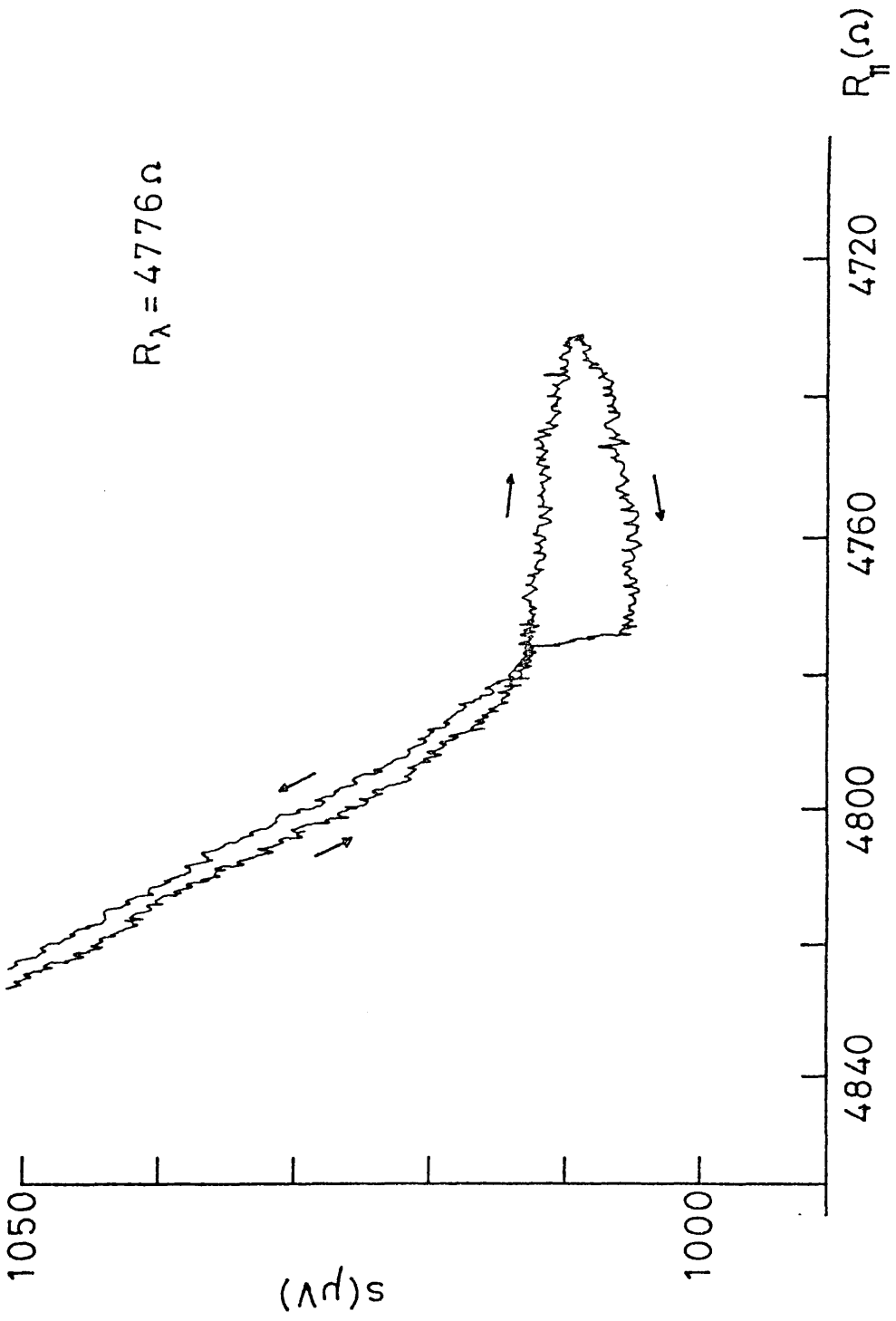

FIG.2.9 DIODE DETECTOR SIGNAL s NEAR THE LAMBDA-POINT

A further calibration point, $R11(T_\lambda)$, was obtained from the XY trace of the transmitted signal near T_λ and is shown in figure 2.9. The vertical axis was driven by the d.c. output from the diode detector whilst the out-of-balance signal from the Cryobridge was used to drive the horizontal axis. The sudden change in the transmitted signal s on cooling down, and the rapid change in curvature on warming up, corresponds to the lambda-point.

CHAPTER THREE

3.0 DATA REDUCTION AND ANALYSIS

3.1 The Raw Data

The experimental data in its basic form consisted of the lock-on frequency, f_3, and the d.c. signal from the diode detector at this frequency, s_3, as a function of temperature T. A typical set of data obtained during a helium-4 run at 20.47 MHz is shown in figures 3.1 and 3.2. Below T_λ, both f_3 and s_3 increase rapidly and then begin to level off at roughly 0.6K. For $T < 0.6K$ s_3 is constant while f_3 slowly decreases as the temperature is further reduced. This latter effect is small in comparison to the change in frequency between 0.6K and T_λ as can be seen from the expanded scale on the left hand side of figure 3.1. The same qualitative behaviour in f_3 and s_3 was observed at 34.09 and 47.70 MHz.

For measurements of s_3 within a few millikelvin ($\sim$ 7 mK) of T_λ an XY chart recorder was used. This enabled s_3 and R11 to be recorded continuously and resulted in a series of s_3 vs R11 traces similar to the one shown in figure 2.9. The processed data expressed as the acoustic impedance normalised to its lambda-point value is shown in figure 4.21.

3.2 Transmission Circuit

The starting point in the analysis of the raw data is the transmission circuit shown in figure 3.3. Since the crystal is driven very near f_s its equivalent circuit reduces (Berlincourt et al (1964), Firth (1965)) to a

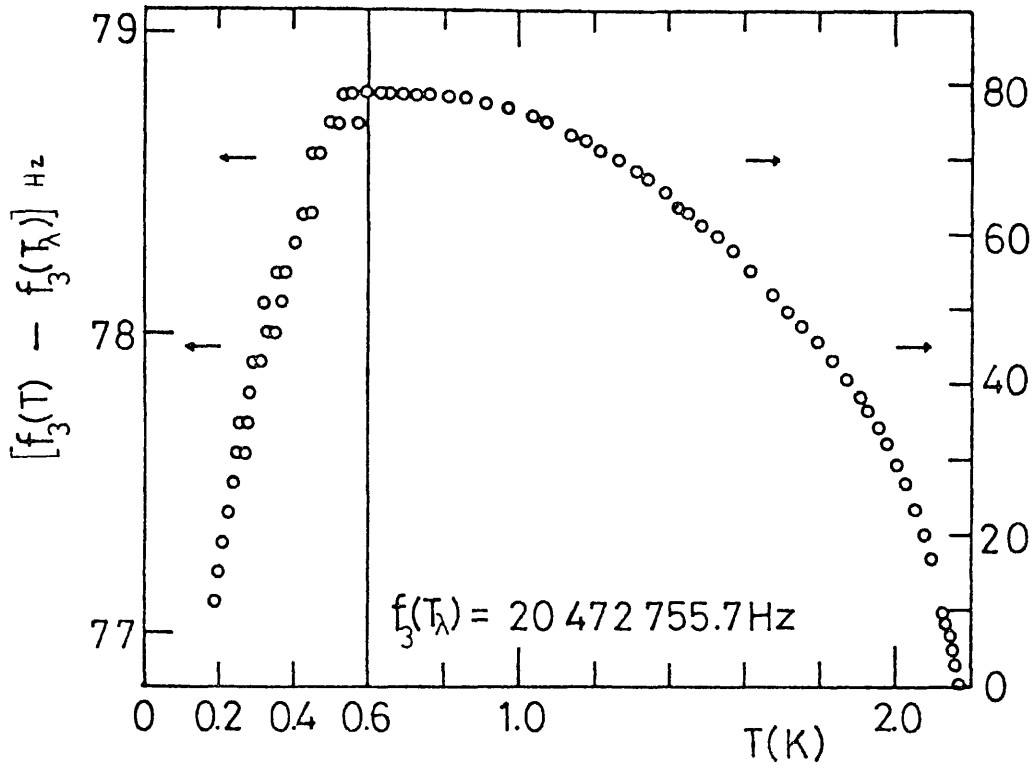

FIG.3.1 f_3 AS A FUNCTION OF TEMPERATURE BELOW T_λ

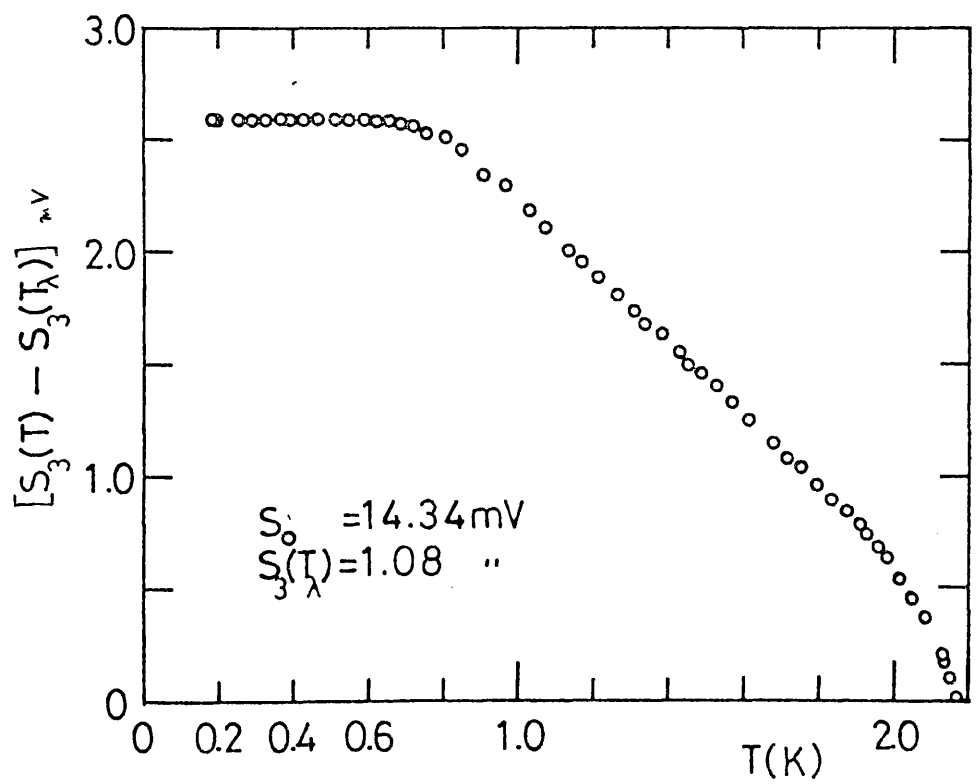

FIG.3.2 s_3 AS A FUNCTION OF TEMPERATURE BELOW T_λ

simple series LCr branch shunted by C_o, the crystals' static capacitance. The 50 Ω loads on either side of the crystal represents the coaxial attenuators which in effect decouples the crystal from the rest of the circuit. The electrical impedance Z_e of the crystal at frequency f is

$$\frac{1}{Z_e} = i2\pi fC_o + \frac{1}{r + i\left(2\pi fL - \frac{1}{2\pi fC}\right)} \qquad (3.2.1)$$

In terms of the circuit parameters, the mechanical resonant frequency f_s and the parallel resonant frequency f_p are defined (Anon (1957)) as:

$$f_s = \frac{1}{2\pi\sqrt{LC}} \qquad (3.2.2)$$

and

$$f_p = \frac{1}{2\pi}\sqrt{\frac{1}{LC}\left(1 + \frac{C}{C_o}\right)} . \qquad (3.2.3)$$

Introducing new variables Δf and Δf_p where

$$\Delta f = f - f_s$$

$$\Delta f_p = f_p - f_s \simeq \frac{f_s}{2}\frac{C}{C_o} , \qquad (3.2.5)$$

then

$$\frac{Z_e}{r} = \frac{1 + iM\left(\frac{\Delta f}{\Delta f_p} - \frac{1}{M^2} - \frac{\Delta f^2}{\Delta f_p^2}\right)}{\frac{1}{M^2} + \left(1 - \frac{\Delta f}{\Delta f_p}\right)^2} . \qquad (3.2.6)$$

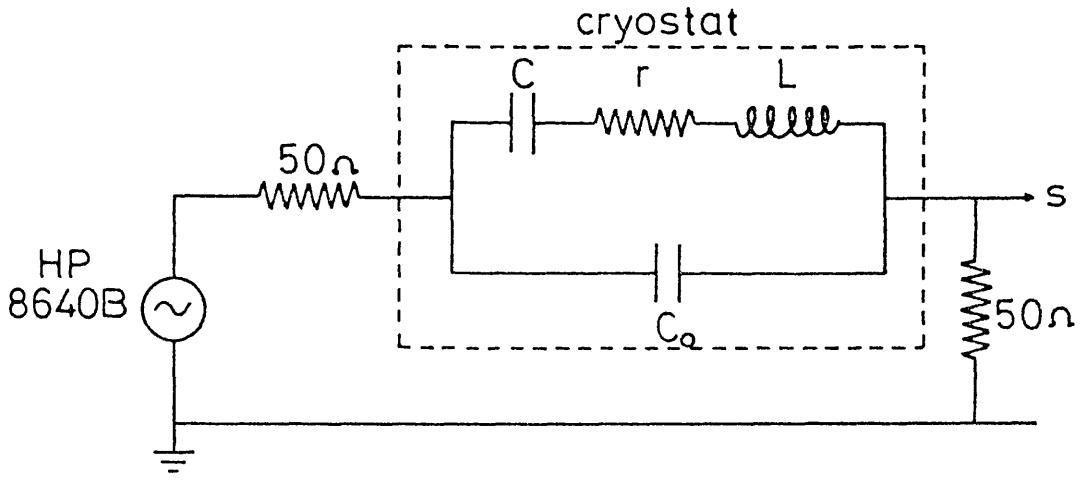

FIG.3.3 ELECTRICAL REPRESENTATION OF THE TRANSMISSION CIRCUIT

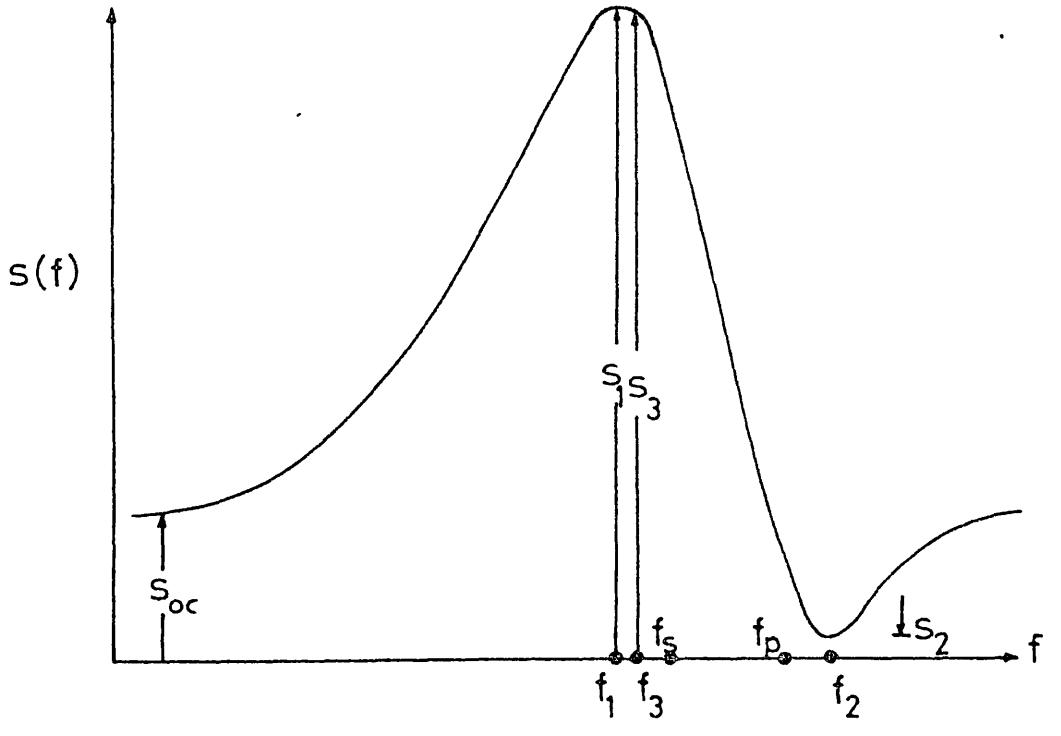

FIG.3.4 FREQUENCY RESPONSE OF THE TRANSMITTED SIGNAL

$M = 1/2\pi f_s C_o r$ and is known as the figure of merit.

The power P developed across the 50Ω load to the right of the crystal is

$$\frac{P}{P_o} = \left| \frac{100}{100 + Z_e} \right|^2 \qquad (3.2.7)$$

where $P \equiv P_o$ when the crystal leads are shorted (that is $Z_e = 0$) out of the circuit. Now P and P_o will give rise to d.c. signals s and s_o from the diode detector and since this is operated in its square-law region where $P \alpha s$ then

$$\frac{s}{s_o} = \left| \frac{100}{100 + Z_e} \right|^2 . \qquad (3.2.8)$$

(N.B. If there is a deviation from the theoretical square-law response then $P \alpha s^n$ must be used in the following analysis. The exponent n can easily be determined from the diode calibration curves as mentioned in section 2.4). The frequencies f_1 and f_2 corresponding to the maximum and minimum value of s can be found by differentiating equation (3.2.7) with respect to f. Ignoring terms of $1/M^4$ and smaller

$$f_1 - f_s = \Delta f_1 \simeq \frac{-\Delta f_p}{M^2}\left(\frac{r + 200}{r}\right) \qquad (3.2.9)$$

and

$$f_2 - f_s = \Delta f_2 \simeq \Delta f_p\left(1 + \frac{r}{200 + M^2 r}\right) . \qquad (3.2.10)$$

If at f_1, $s = s_1$ then to a very good approximation

$$\frac{s_1}{s_o} = \left(\frac{100}{100 + r}\right)^2 \quad . \qquad (3.2.11)$$

Also by substracting equation (3.2.9) from equation (3.2.10),

$$f_2 - f_1 = \Delta f_p \left(1 + \frac{2}{M^2}\left(1 + \frac{100}{r}\right)\right) . \qquad (3.2.12)$$

The shunt capacitance can be estimated from measurements of the off-resonance signal s_{oc} since

$$\frac{s_{oc}}{s_o} \simeq \frac{100^2}{100^2 + \frac{1}{(2\pi f C_o)^2}} \quad . \qquad (3.2.13)$$

Hence from equations (3.2.9) to (3.2.13) the crystals equivalent circuit parameters can be determined from the frequency response of the transmitted signal. For the purposes of defining the various symbols used above, figure 3.4 shows schematically the frequency response $s(f)$ of the transmitted signal about a crystal resonance.

As a means of verifying the validity of the transmission circuit the crystal parameters were determined from the above analysis and the theoretical response calculated and compared to an experimental trace of $s(f)$ produced by an XY chart recorder. Figure 3.5 shows such a comparison at 20.47 MHz. As can be seen the agreement between the theoretical response (open circles), computed from equations (3.2.6) and (3.2.8), and the XY trace (continuous line) is extremely good.

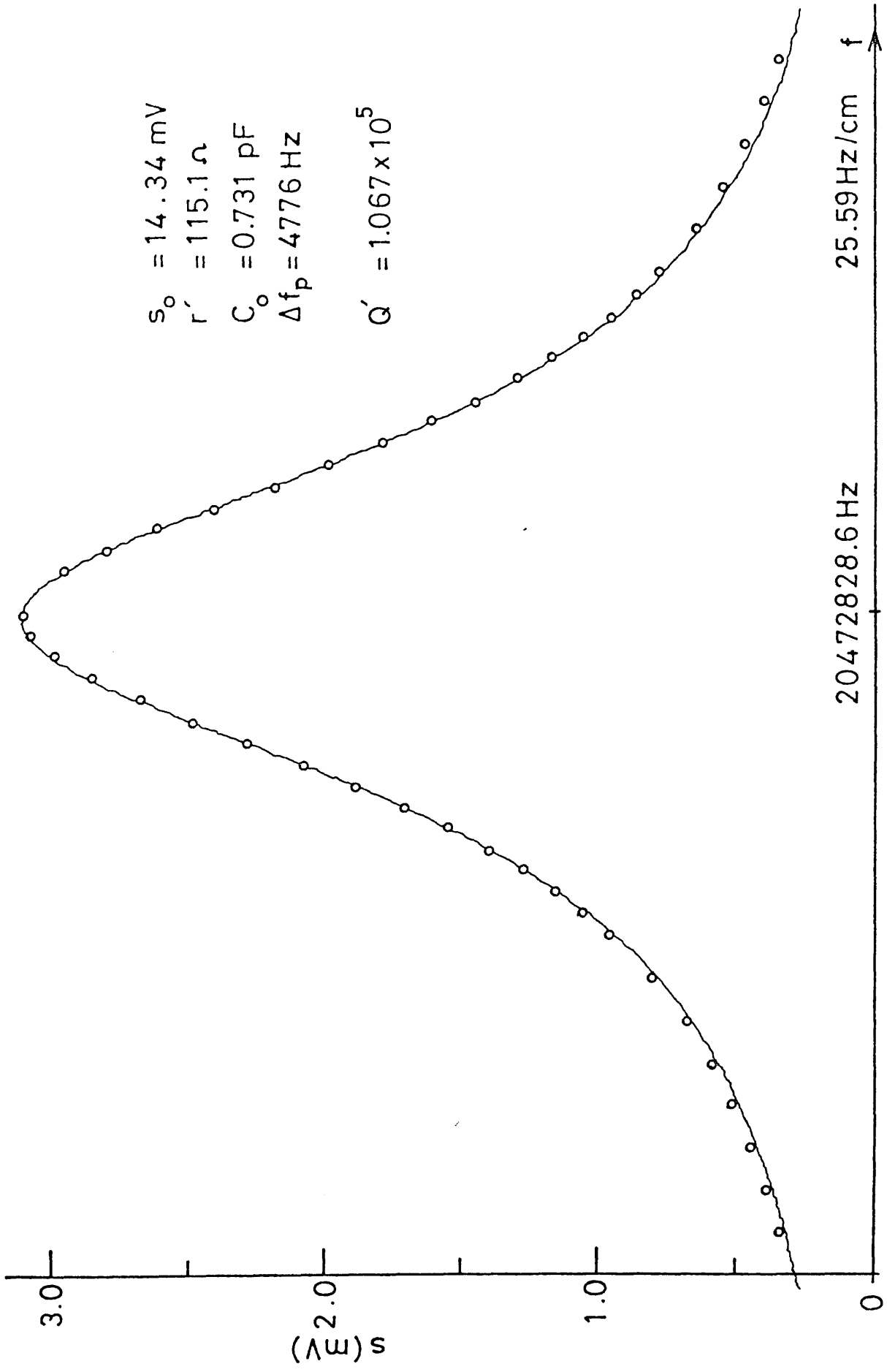

FIG. 3.5 A COMPARISON OF THE THEORETICAL AND EXPERIMENTAL FREQUENCY RESPONSE OF s(f)

The final parameter we require is the Q factor, Q, of the crystal alone which can be found as follows. Using figure 3.5 we can graphically estimate the Q factor, Q_c, of the circuit. Since this is inversely proportional to the circuit resistance at resonance we may write

$$Q_c(100 + r) \equiv K \quad , \tag{3.2.14}$$

where K is a constant, and hence

$$\frac{1}{Q} = \frac{r}{K} \ . \tag{3.2.15}$$

The constant K was determined from the low temperature ($T < 0.6K$) values of r and Q_c. If these are denoted by the primed symbols r' and Q_c' then

$$K = Q_c'(100 + r') \tag{3.2.16}$$

where

$$r' = 100\left(\sqrt{\frac{s_o}{s_1'}} - 1\right) \tag{3.2.17}$$

Typical values of r', Q_c' and Δf_p for an AT-cut quartz crystal are tabulated in figure 3.6. K can also be estimated from Δf_p and C_o since

$$\frac{1}{Q} = 2\pi f_s C\ r \tag{3.2.17}$$

and therefore

$$K = 1/4\pi\Delta f_p C_o \ . \tag{3.2.19}$$

f_s (MHz)	n	Δf_p (Hz)	Q'_c	r' (Ω)	$K = (100 + r')Q'_c$ (Ω)	$K = 1/4\pi\Delta f_p C_o$ (Ω)
20.496	3	4829	1.575×10^5	44	2.27×10^7	2.26×10^7
34.142	5	3065	2.584×10^5	38	3.57×10^7	3.56×10^7
47.784	7	2136	3.289×10^5	47	4.84×10^7	5.10×10^7
61.429	9	1618	3.378×10^5	50	5.07×10^7	6.74×10^7
$C_o = (0.730 \pm 0.006)$pF						

FIG.3.6 TYPICAL VALUES FOR AN AT-CUT QUARTZ CRYSTAL AT 4.2K

As can be seen from figure 3.6, the agreement between K calculated from equations (3.2.16) and (3.2.19) is better than 1% for the 3rd and 5th harmonics and about 5% at the 7th harmonic.

The lumped circuit parameters C and L can also be expressed in terms of the appropriate piezoelectric, h, and dielectric, ε_d, constants (Gooberman (1968)) of the quartz. If

$$C_o = a\ \varepsilon_d/d \qquad (3.2.20)$$

then

$$C = 4h^2C_o^2/n\pi^2 f_s\ R_q\ a \qquad (3.2.21)$$

and

$$L = R_q\ a/n16h^2C_o^2\ f_s\ . \qquad (3.2.22)$$

We can deduce a value of h from K since from equation (3.2.15),(3.2.18) and (3.2.21)

$$h = \frac{1}{2C_o}\sqrt{n\pi\ R_q\ a/2K}\ . \qquad (3.2.23)$$

Taking the electrode area $a = 2 \times 10^{-6}$ m^2, $K = 2.27 \times 10^7 \Omega$ and $R_q = 8.862 \times 10^6$ kg m^{-2} s^{-1} then

$$h = 1.318 \times 10^9\ NC^{-1}$$

at 4.2K. At room temperature h has a value of about $2.336 \times 10^9\ NC^{-1}$.

3.3 The Lock-on Parameters f_3 and s_3

From the operation of the mixer in the feedback circuit we can define the lock-on frequency, f_3, as

$$\mathrm{Im}\left(\frac{100}{100 + Z_e(\Delta f_3)}\, e^{i\phi}\right) \equiv 0 \qquad (3.3.1)$$

where Δf_3 is the 'distance' of f_3 from f_s i.e. $\Delta f_3 = f_3 - f_s$ and ϕ is a phase factor. This was set by adjusting the length of the reference branch such that at some crystal resistance r' (since this adjustment usually took several minutes it was always done below 0.6K where the crystal resistance was constant) the lock-on position coincided with the maximum transmitted signal. For this special case, $\Delta f_3 = \Delta f_1$ and hence ϕ could be found from:

$$\mathrm{Im}\left(\frac{100}{100 + Z_e(\Delta f_1)}\, e^{i\phi}\right) = 0 \qquad (3.3.2)$$

Once adjusted, the reference branch and therefore ϕ remained unaltered throughout the run. At a difference resistance r, f_s was then estimated from f_3 and equation (3.3.1). This was initially solved on the computer by straight forward numerical methods. However, a simple approximate expression was derived which matched the program values to within 1% and was therefore used in all subsequent analysis. By considering the phase of the transmitted signal near f_1, Δf_3 is given by

$$\Delta f_3 = \frac{\Delta f_p}{M^2}\left(1 - \frac{2r'(100 + r)}{r^2}\right) . \qquad (3.3.3)$$

At the initial setting-up point $r = r'$ and $\Delta f_3 = \Delta f_1$ as required. Since $M = 1/2\pi f_s C_o r$ then

$$f_s = f_3 - 4\pi^2 f_3^2 C_o^2 \Delta f_p (r^2 - 2r'(100 + r)) . \qquad (3.3.4)$$

The value of the locked-on transmitted signal s_3 is, from equation (3.2.8),

$$\frac{s_3}{s_o} = \left| \frac{100}{100 + Z_e(\Delta f_3)} \right|^2 . \qquad (3.3.5)$$

Since $\Delta f_3/\Delta f_p \ll 1$ we can write

$$\frac{s_3}{s_o} = \frac{100^2}{(100 + r)^2 + r^2 \tan^2 \Phi(\Delta f_3)} \qquad (3.3.6)$$

where

$$\tan \Phi(\Delta f) = M\left(\frac{\Delta f}{\Delta f_p} - \frac{1}{M^2} - \frac{\Delta f^2}{\Delta f_p^2}\right) . \qquad (3.3.7)$$

For our crystals $M^2 \gg 1$ or

$$\tan \Phi(\Delta f_3) \sim \frac{1}{M} \qquad (3.3.8)$$

and hence to a very good approximation

$$r = 100\left(\sqrt{\frac{s_o}{s_3}} - 1\right) . \qquad (3.3.9)$$

This last equation shows that the lock-on position sits on the maximum transmitted signal i.e. $s_3 = s_1$.

3.4 Quartz: P and T Coefficients

All the measurements reported here are saturated vapour pressure measurements and hence equation (3.2.15) and (3.3.4) will give $f_s(T,SVP)$ and $Q(T,SVP)$ for the crystal immersed in a liquid helium environment. Both parameters will contain non-helium contributions arising from the pressure and temperature dependence of the intrinsic properties of the quartz. In this section these contributions are estimated and shown to be very small in comparison to the change in f_s and Q due to the helium alone. Using the IEEE convention (Anon (1949)) the shear wave velocity v depends on the elastic moduli C_{ij} of the quartz and the crystal orientation θ thus:

$$\rho_q v^2 = (C_{66} + 0.76311 \times 10^9 [Nm^{-2}])\cos^2\theta + C_{44}\sin^2\theta + 2C_{14}\sin\theta\cos\theta. \qquad (3.4.1)$$

The numerical factor in brackets is an empirical factor introduced by Stockbridge (1966a) to account for the 'piezoelectric stiffening'. These constants have been measured at room and at liquid nitrogen temperatures by McSkimin, Andreatch and Thurston (1965). We shall assume that the latter data can be used at liquid helium temperatures without serious error since the changes in elastic moduli between 77.4K and 4.2K is small for most solids. Using their values at 77.4K of

$$C_{66} = + 38.71521 \times 10^9 \ Nm^{-2}$$

$$C_{44} = + 59.64524 \times 10^9 \ Nm^{-2}$$

$$C_{14} = - 17.72384 \times 10^9 \ Nm^{-2}$$

and taking the density of quartz, ρ_q, at this temperature to be $\rho_q = 2.664 \times 10^3$ kg m^{-3} then we find for the AT-cut ($\theta = 30^o\ 10'$), $v = 3.326 \times 10^3 ms^{-1}$ and hence $R_q = 8.8618 \times 10^6 kg\ s^{-1}\ m^{-2}$. The effect of a change in pressure on f_s is found by differentiating equation (1.2.1) with respect to the pressure P. If the operator d/dP is denoted by $\dot{}$ then

$$\frac{\dot{f}_s}{f_s} = \frac{\dot{v}}{v} - \frac{\dot{d}}{d} \quad . \tag{3.4.2}$$

But from equation (3.4.1)

$$\frac{\dot{v}}{v} = \frac{1}{2}\left(\frac{\dot{\rho}_q v^2}{\rho_q v^2} - \frac{\dot{\rho}_q}{\rho_q}\right) \tag{3.4.3}$$

where

$$\dot{\rho_q v^2} = (\dot{C}_{66} - 4.0 \times 10^{-7}[m^2kg^{-1}]\rho_q)\ cos^2\theta + \dot{C}_{44}sin^2\theta + 2\dot{C}_{14}sin\theta cos\theta \quad . \tag{3.4.4}$$

The numerical constant is a further empirical factor introduced by Stockbridge (1966a) for the pressure differential of equation (3.4.1). The pressure derivatives of the elastic moduli have also been measured by Mc Skimin et al. At liquid

nitrogen temperatures they found:

$$\dot{C}_{66} = - 2.00$$

$$\dot{C}_{44} = + 1.77$$

$$\dot{C}_{14} = + 2.00$$

The pressure derivative of the density can be estimated from the bulk modulus κ. By definition

$$\kappa = - V \frac{dP}{dV} \qquad (3.4.5)$$

$$= - V \frac{dp}{d\rho_q} \frac{d\rho_q}{dV} \qquad (3.4.6)$$

and therefore

$$\frac{\dot{\rho}_q}{\rho_q} = \frac{1}{\kappa} = 2.5687 \times 10^{-11}\ N^{-1}m^2 \quad . \qquad (3.4.7)$$

To complete the calculation of $\dot{f}_s$ we also require the effect of pressure on the crystal thickness. For small pressure changes McSkimin et al found

$$\frac{\dot{d}}{d} = - a(\theta) \qquad (3.4.8)$$

where

$$a(\theta) = a_{\parallel} \cos^2\theta + a_{\perp} \sin^2\theta \qquad (3.4.9)$$

with

$$a_{\parallel} = 6.9307 \times 10^{-12} N^{-1}m^2$$

$$a_{\perp} = 9.3779 \times 10^{-12} N^{-1}m^2 \quad .$$

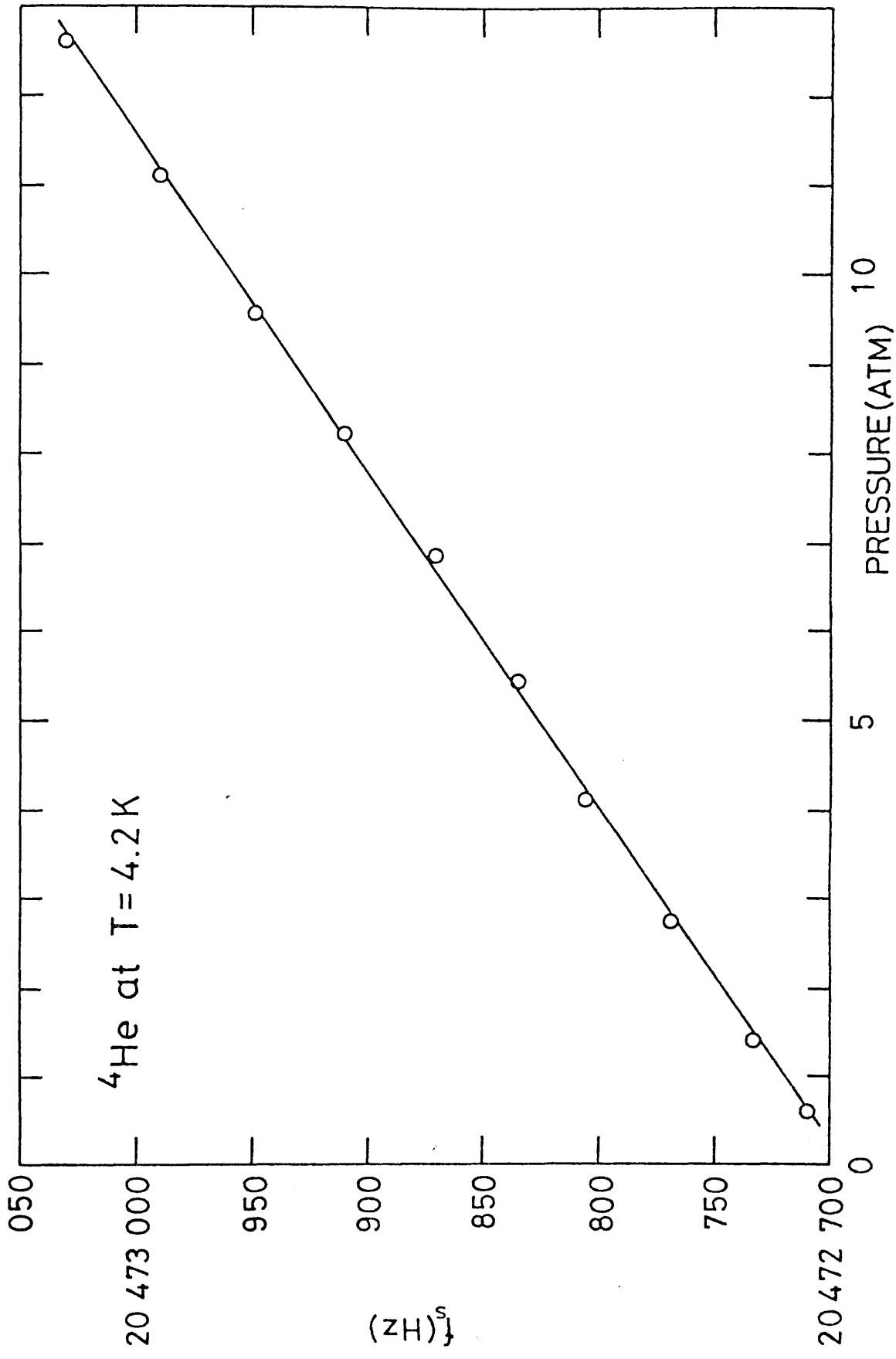

FIG.3.7 THE PRESSURE DEPENDENCE OF f_S AT 4.2K

This gives a $\dot{d}/d = -7.740 \times 10^{-12} N^{-1} m^2$ and hence, combining all the intermediate results above,

$$\frac{\dot{f}_s}{f_s} = 1.42 \times 10^{-6} \text{ atm}^{-1} \quad . \qquad (3.4.10)$$

For a pressure change of 40τ i.e. the change in the SVP of helium between 0.6K and T_λ, this would contribute a change in f_s of + 1.5 Hz for a base frequency of 20 MHz.

Figure 3.7 shows the variation in f_s between 0.63 and 12.6 atm at 4.2K. The gradient calculated by at least squares analysis is 26.5 ± 0.1 Hz atm^{-1} but this also includes a (- ve) contribution from the helium due to the variation of the acoustic impedance with pressure i.e. $\dot{X}$. Taking values of $\eta(P)$ from Tjerskra (1952) and $\rho_n(P)$ from Welber (1960) then

$$\frac{\dot{X}}{X} = \frac{1}{\sqrt{\eta\rho_n}} \frac{d}{dP} \sqrt{\eta\rho_n} \qquad (3.4.11)$$

$$\sim 0.04 \text{ atm}^{-1} \quad .$$

Translated into terms of a frequency shift at 20.47 MHz this accounts for a shift of approximately $-(3.1 \pm 0.4)$Hz atm^{-1} Therefore for the quartz crystal alone $\dot{f}_s = (29.6 \pm 0.5)$Hz atm^{-1} which is in favourable agreement with the expected value of 29.1 Hz atm^{-1} from equation (3.4.10). In a similar experiment the Q factor was measured at 0.5K at various pressures. For 0.18 and 1.17 atm the Q factors were 1.442×10^5 and 1.468×10^5 respectively. Hence for a pressure change of 40τ this effect should be negligible.

The frequency stability of AT-cut quartz crystals with temperature has been studied by Mossuz (1975) and Mossuz and Gagnepain (1976) in their search for a high-stability cryogenic oscillator. From accurate measurements at 4.2K they estimate the temperature coefficient of the resonant frequency to be $df_s/dT \lesssim 4 \times 10^{-9} f_s$ Hz K^{-1}. Hence for the frequencies used in our experiments this contribution should be negligible. In fact our measurements in a quasi-vacuum showed no appreciable change in f_s and Q from T_λ to 1.0K.

CHAPTER FOUR

4.0 RESULTS

4.1 Low Temperature Region: T < 600 mK

In this region the Q factor, Q', was (within experimental error) temperature independent. Since the viscous loading term in equation (1.1.4) becomes negligible below 0.6K, Q' was therefore identified with the intrinsic losses in the quartz material and crystal mounting assembly. Similarly we would also expect the resonant frequency to be constant in this region. But f_s decreased below 0.6K and was temperature dependent down to the lowest accessible temperature. This is shown in figures 4.1 to 4.9 where $\Delta f_s(T)$ is the mechanical resonant frequency below 0.6K relative to its 30 mK value. We attributed this non-viscous mechanism to the formation of a layer of helium atoms on the crystal surface. Under these conditions equations (1.2.5) and (1.2.7) are incorrect since they only apply to a situation where all reflecting boundaries are much further away from the crystal surface than δ. The effect of a thin solid layer is to introduce a back scattered wave from the layer/liquid boundary which decreases the resonant frequency but leaves the Q factor unchanged. In this context the crystal operates as a microbalance (Stockbridge (1966b), Yang (1973)), the resonant frequency shift being related to the adsorbed areal density $\sigma(T)$ thus

$$\Delta f_s'(T) = f_s(T) - f_s' \qquad (4.1.1)$$

$$= \frac{4\sigma(T) f_s'^2}{n R_q} \quad , \qquad (4.1.2)$$

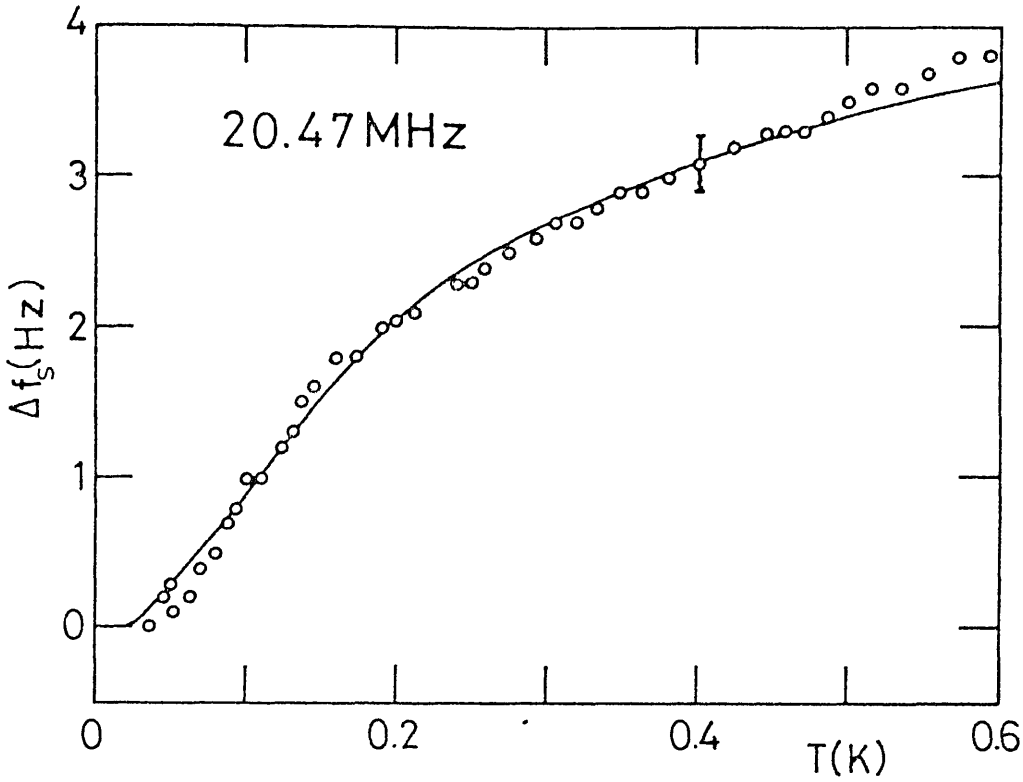

FIG.4.1 FREQUENCY SHIFT BELOW 600 mK (WARMING, 20 MHz)

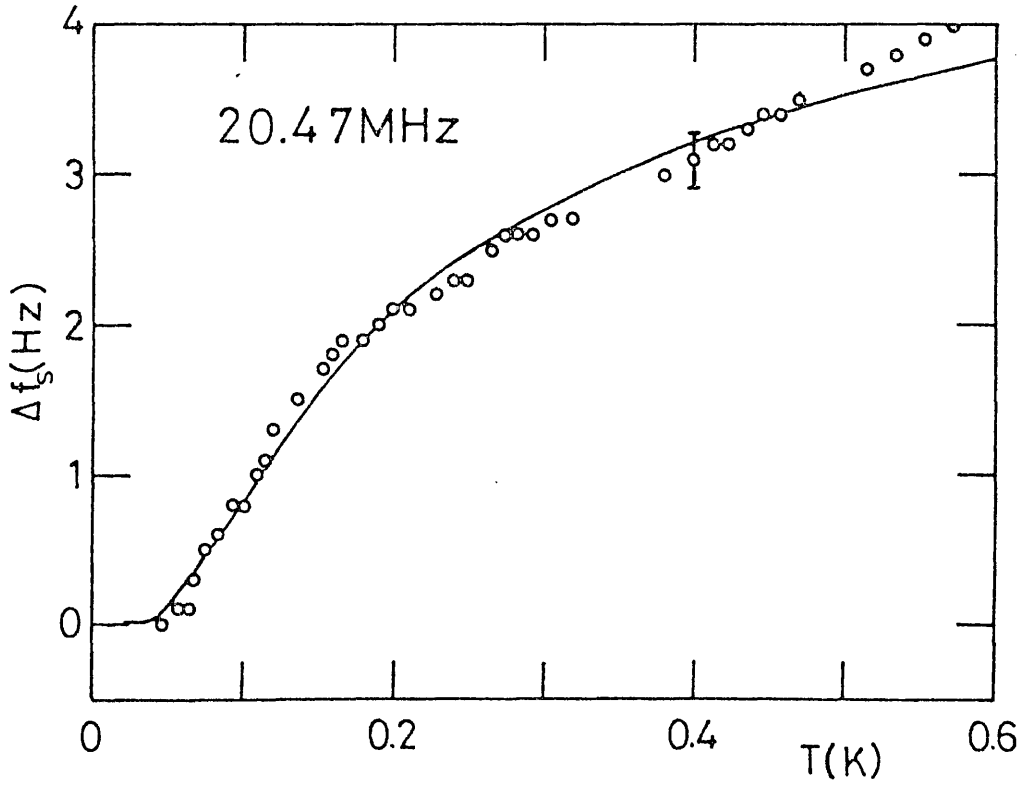

FIG.4.2 FREQUENCY SHIFT BELOW 600 mK (COOLING, 20 MHz)

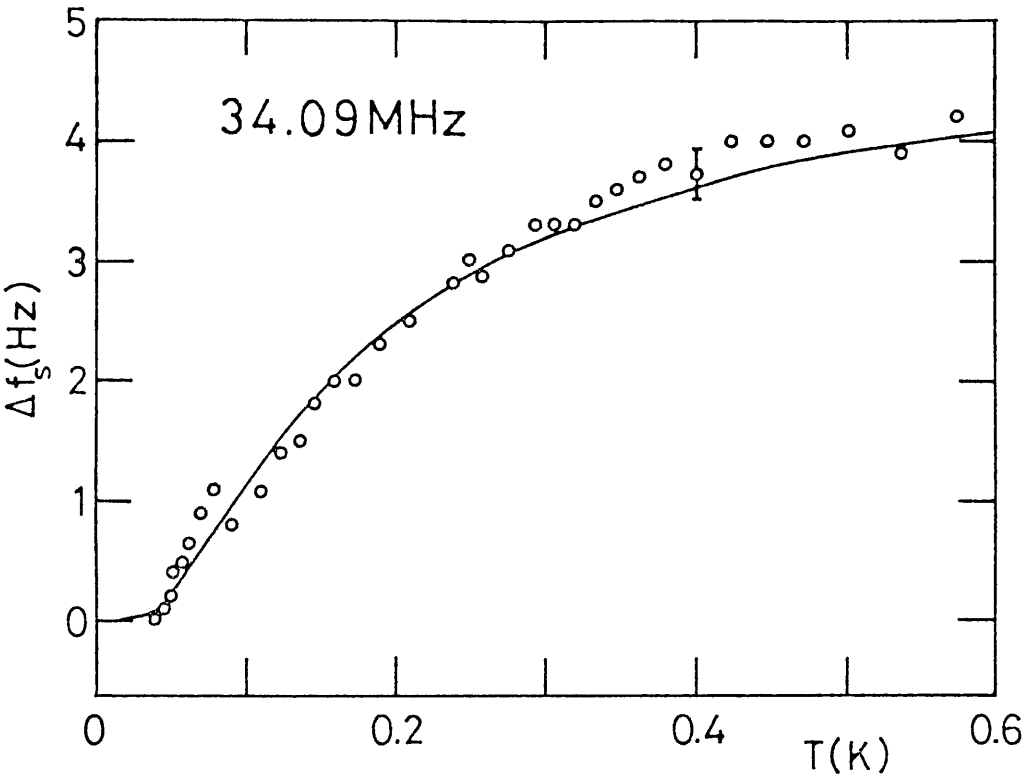

FIG.4.4 FREQUENCY SHIFT BELOW 600 mK (WARMING, 34 MHz)

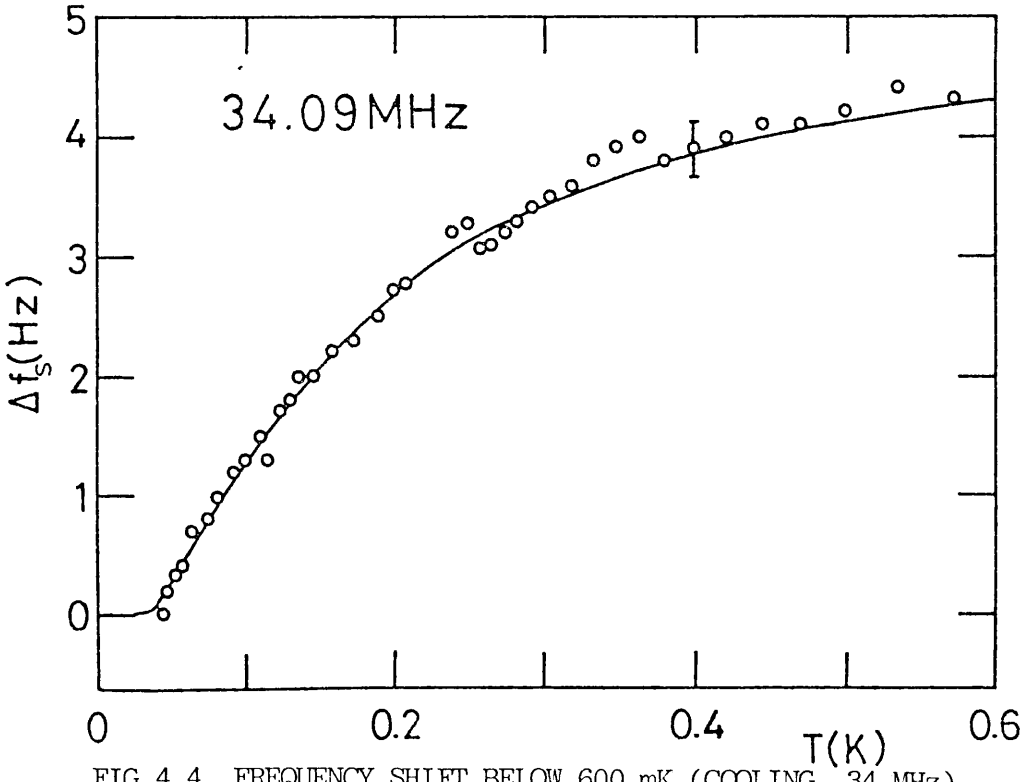

FIG.4.4 FREQUENCY SHIFT BELOW 600 mK (COOLING, 34 MHz)

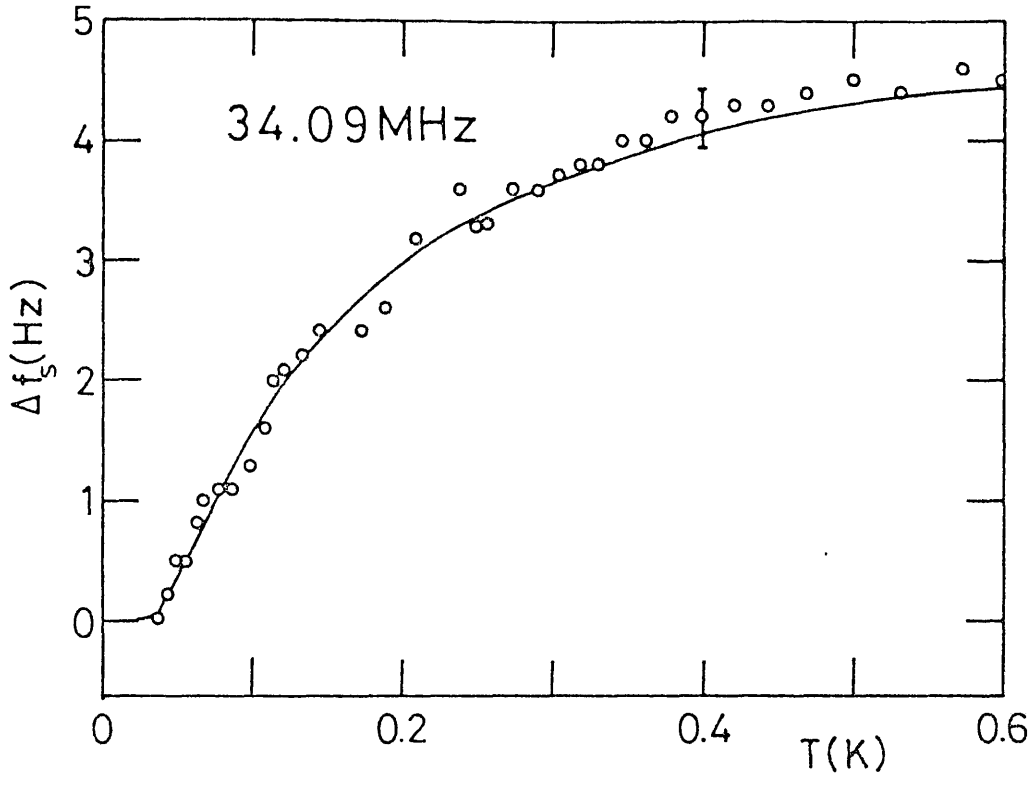

FIG.4.5 FREQUENCY SHIFT BELOW 600 mK (WARMING, 34 MHz)

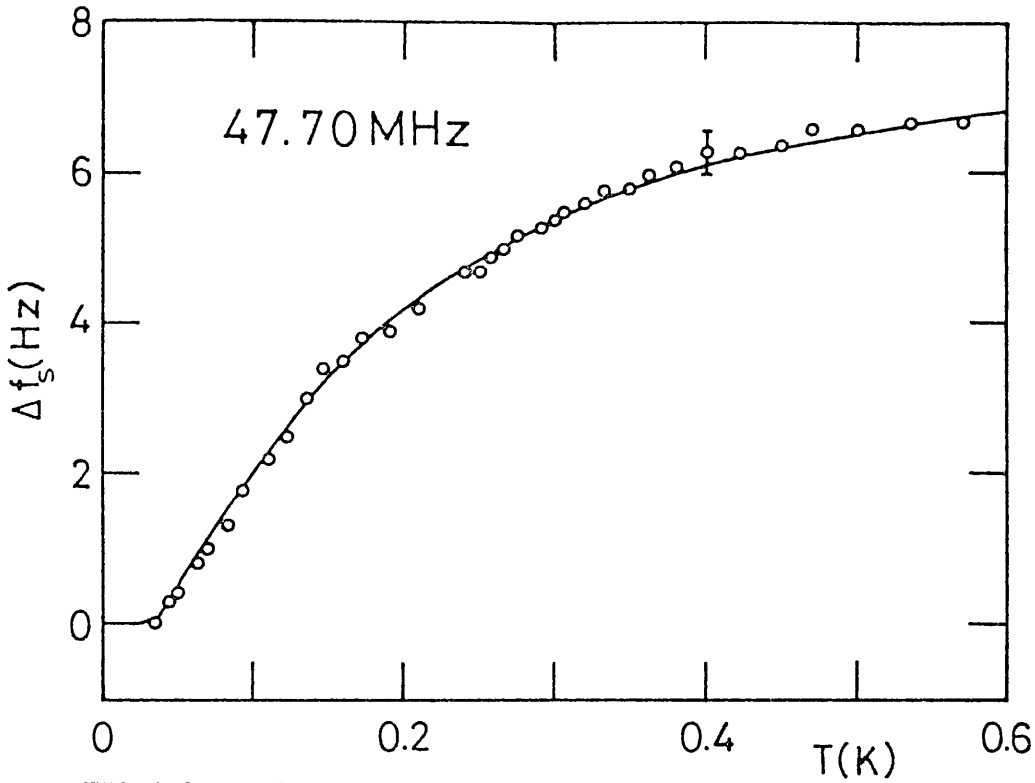

FIG.4.6 FREQUENCY SHIFT BELOW 600 mK (WARMING, 48 MHz)

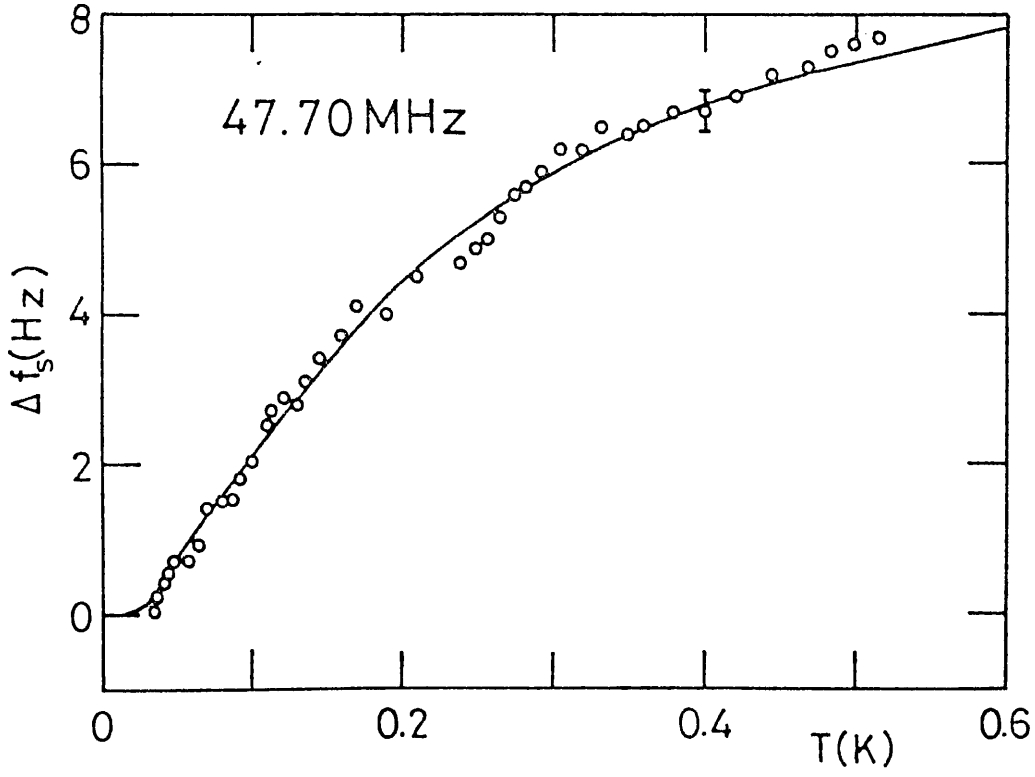

FIG.4.7 FREQUENCY SHIFT BELOW 600 mK (COOLING, 48 MHz)

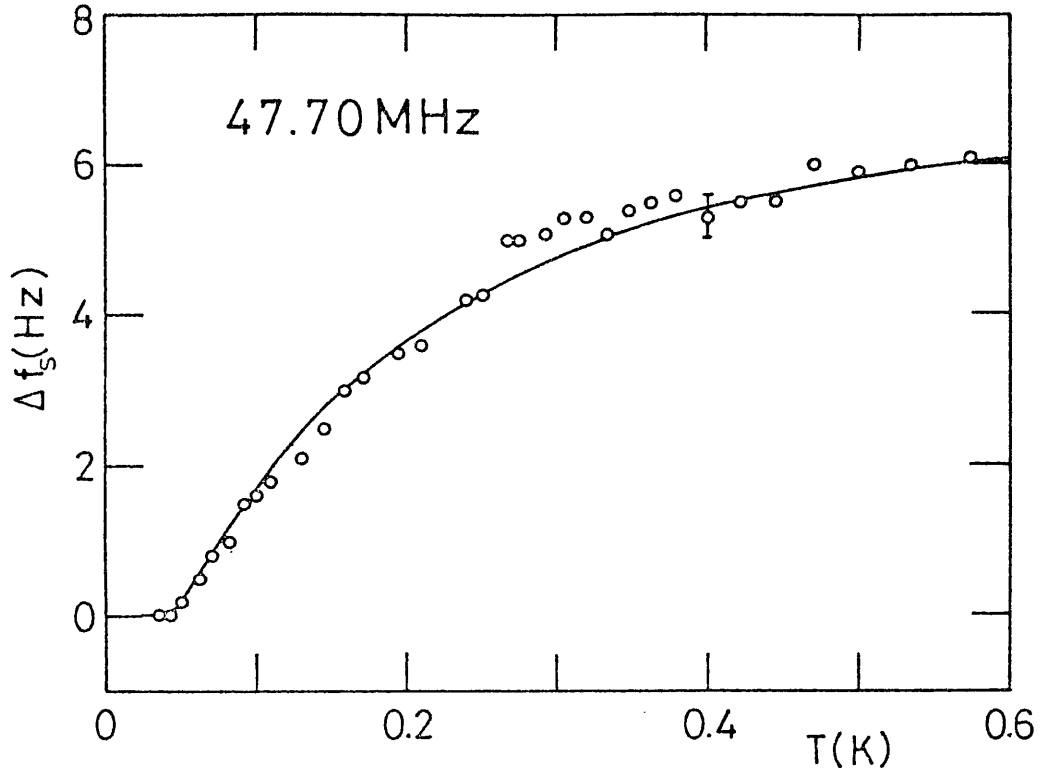

FIG.4.8 FREQUENCY SHIFT BELOW 600 mK (WARMING, 48 MHz)

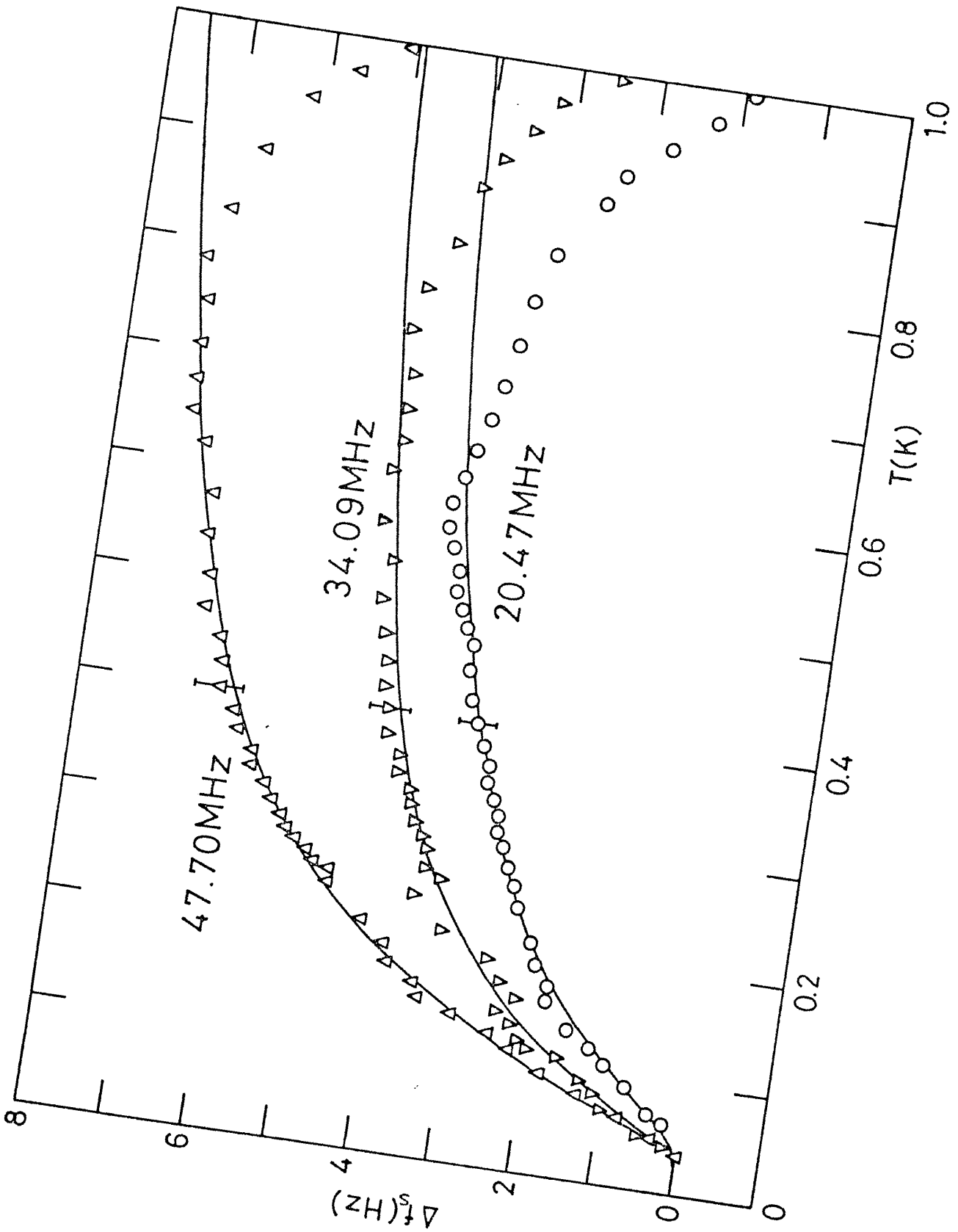

FIG.4.9 RELATIVE MAGNITUDE OF Δf_S AT 20,34 AND 48 MHz

where f_s' is the mechanical resonant frequency of the crystal in vacuo. Unfortunately in the cell used it was not possible to cool the crystal down below 1K in high vacuum (measurements with small amounts of helium-3 or helium-4 exchange gas showed a complicated behaviour) and hence measure f_s' directly. However, f_s' was estimated as follows. Using a least squares curve fitting routine $\Delta f_s(T)$ was fitted to an exponential curve of the form:

$$\Delta f_s(T) = A_1 + A_2 \exp(- A_3/K_B T) \quad . \qquad (4.1.3)$$

The solid line in the graphs shows the fitted curve and the values of A_2 and A_3/K_B are tabulated in figure 4.10 for each graph. Assuming that in this temperature region the viscous losses are completely negligible then

$$f_s' = f_s(o) + A_2 \qquad (4.1.4)$$

where

$$f_s(o) = f_s(30\ mK) + A_1 \quad . \qquad (4.1.5)$$

Hence from equation (4.1.2) ,

$$A_2(1 - \exp(- A_3/K_B T)) = \frac{4\sigma(T) f_s'^2}{n R_q} \qquad (4.1.6)$$

and if

$$\sigma(T) = \sigma(o)(1 - \exp(- A_3/K_B T)) \qquad (4.1.7)$$

then

Figure No	Crystal Frequency (MHz)	A_2 (Hz)	A_3/K_B (K)	$\sigma(o)$ (kg m^{-2})
4.1	20.47	5.03 (6)*	0.173(5)*	7.98×10^{-8}
4.2	20.47	4.87 (4)	0.177(4)	7.73×10^{-8}
4.3	34.09	5.37 (7)	0.149(6)	5.12×10^{-8}
4.4	34.09	5.67 (4)	0.132(4)	5.41×10^{-8}
4.5	34.09	5.76 (5)	0.128(40)	5.49×10^{-8}
4.6	47.70	8.94 (4)	0.145(2)	6.09×10^{-8}
4.7	47.70	10.10(10)	0.174(5)	6.88×10^{-8}
4.8	47.70	8.26 (6)	0.144(3)	5.63×10^{-8}

*Number in brackets indicates error in last figure(s) from curve fitting program.

Figure 4.10 TABLE OF CURVE FITTING PARAMETERS A_2 AND A_3

$$\sigma(o) = \frac{A_2\ nR_q}{4f_s'^2} \quad . \qquad (4.1.8)$$

The value of $\sigma(o)$ gives an estimate of the total density of the helium layer formed in this process. The results of $\sigma(o)$ from cooling and warming runs are tabulated in figure 4.10.

4.2 Middle Temperature Region: 0.6 < T < 2.17K

Clearly, the effects of the helium-4 adsorption process must be removed before $f_s(T)$ can be used to estimate $X(T)$ from equation (1.2.7). In the absence of such a layer the mechanical resonant frequency, $f_s''(T)$, would be

$$f_s''(T) = f_s(T) + A_2(1 - \exp(-A_3/k_BT)) \quad . \qquad (4.2.1)$$

Therefore

$$X(T) = \frac{n\pi R_q}{2}\left[\frac{f_s''(T) - f_s''(o)}{f_s''(o)}\right] \qquad (4.2.2)$$

or

$$X(T) = \frac{n\pi R_q}{2}\left[\frac{f_s(T) + A_2(1 - \exp(-A_3/K_BT)) - f_s'}{f_s'}\right] \quad . \qquad (4.2.3)$$

The change in Q factor, $\Delta\left(\frac{1}{Q(T)}\right)$, due to the temperature dependent viscous losses is

$$\Delta\left(\frac{1}{Q(T)}\right) = \frac{1}{Q(T)} - \frac{1}{Q'} \qquad (4.2.4)$$

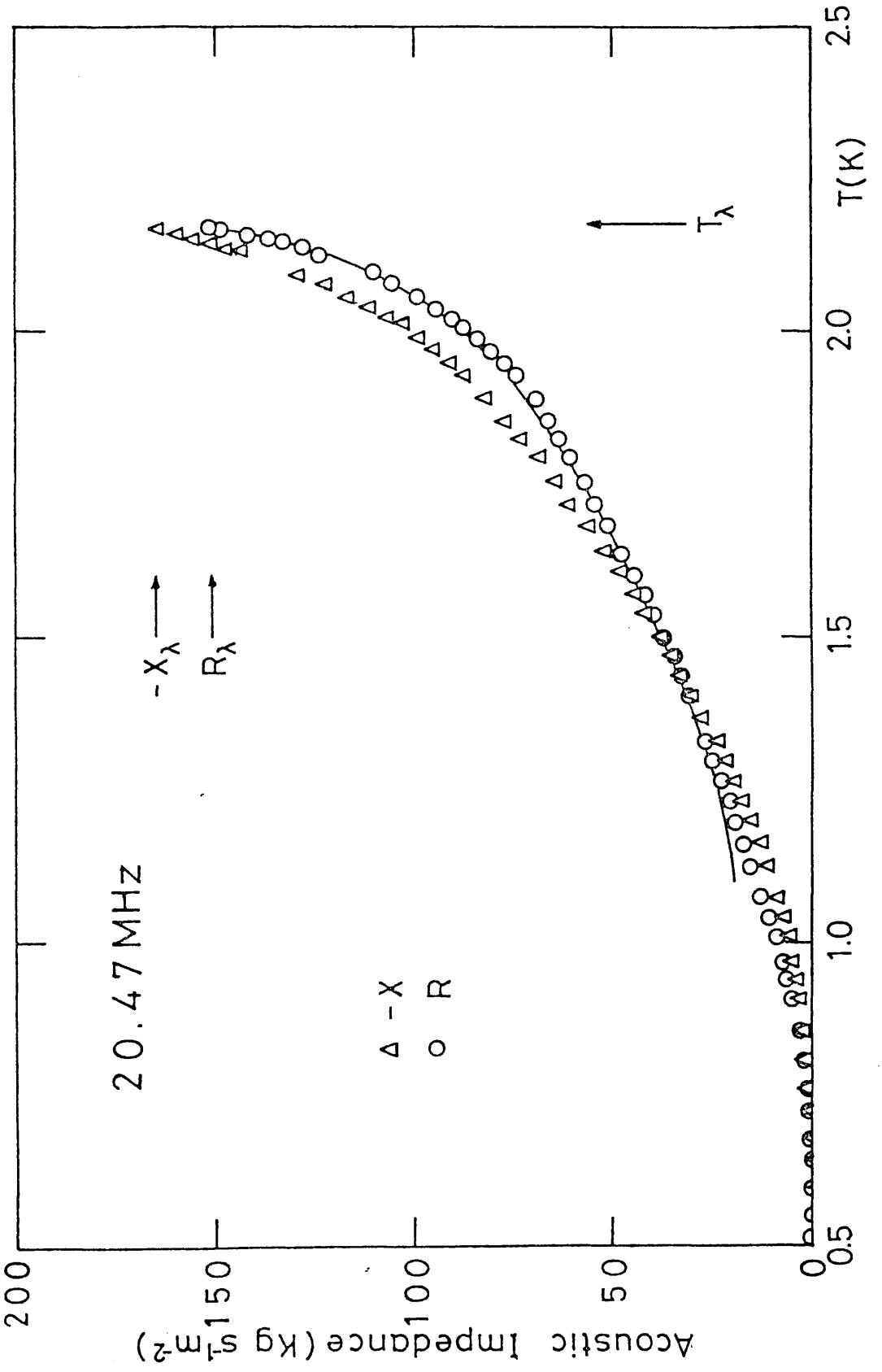

FIG.4.11 TEMPERATURE DEPENDENCE OF X AND R AT 20 MHz

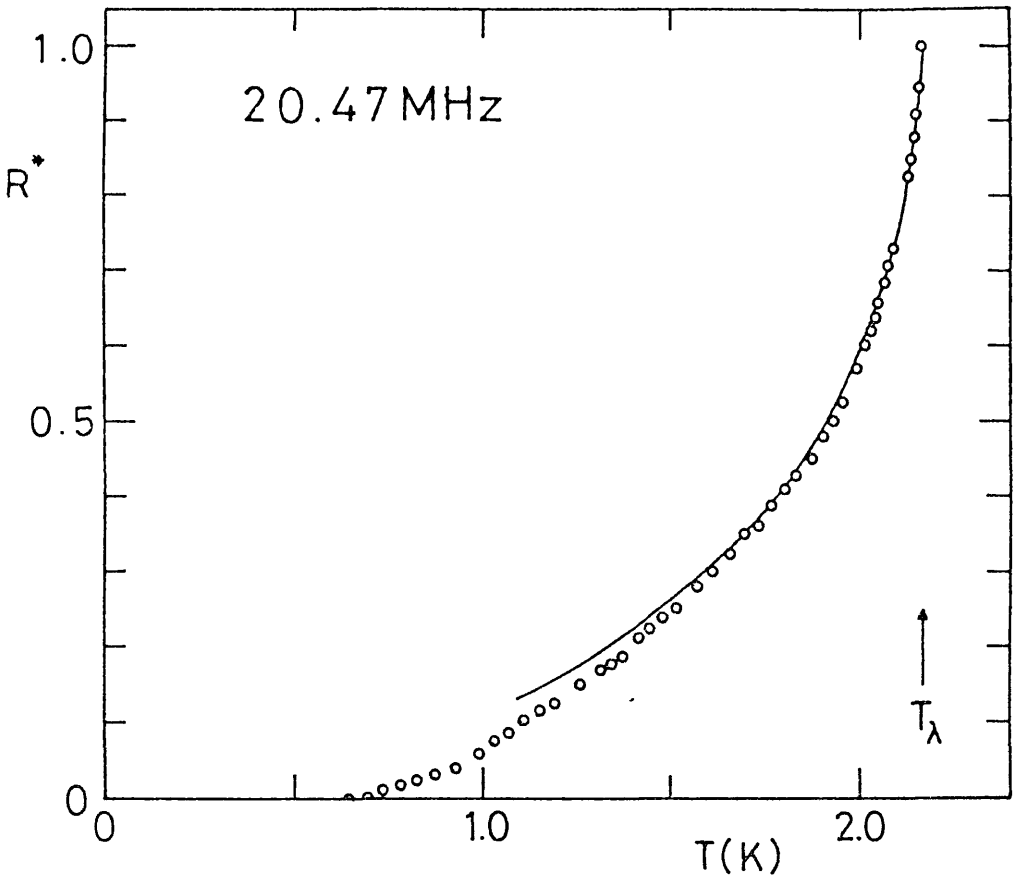

FIG.4.12 TEMPERATURE DEPENDENCE OF R/R_λ AT 20 MHz

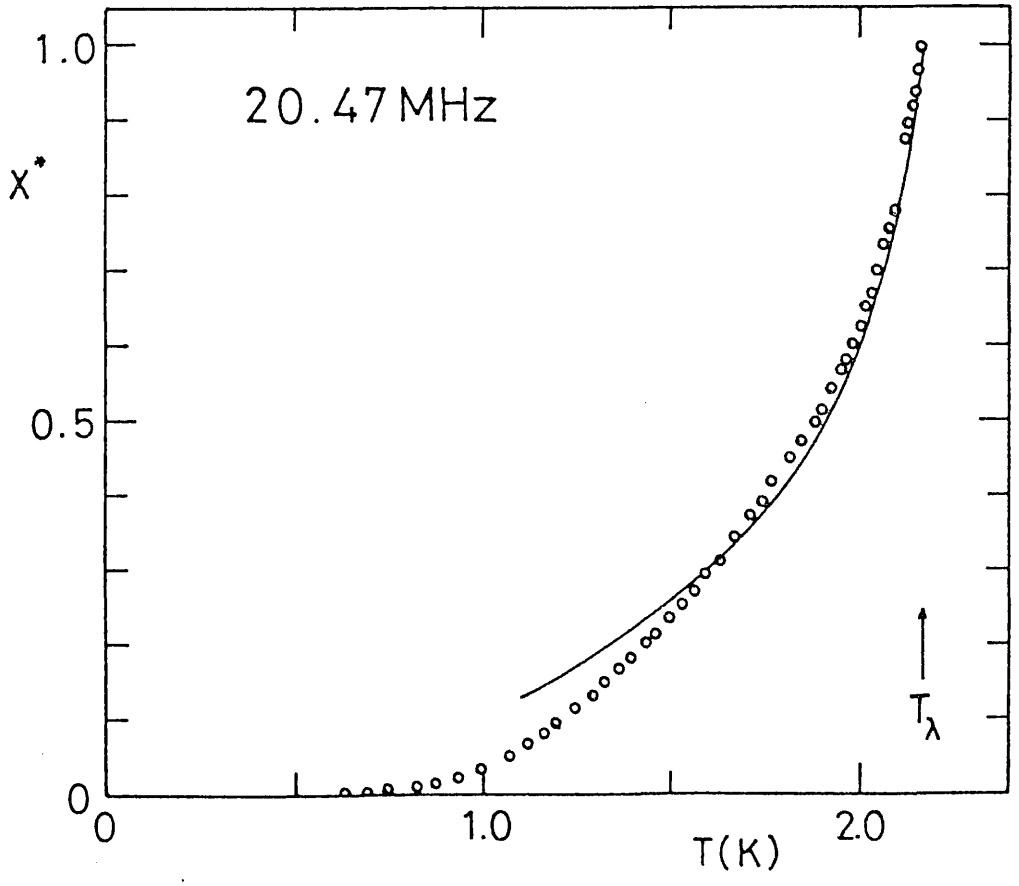

FIG.4.13 TEMPERATURE DEPENDENCE OF X/X_λ AT 20 MHz

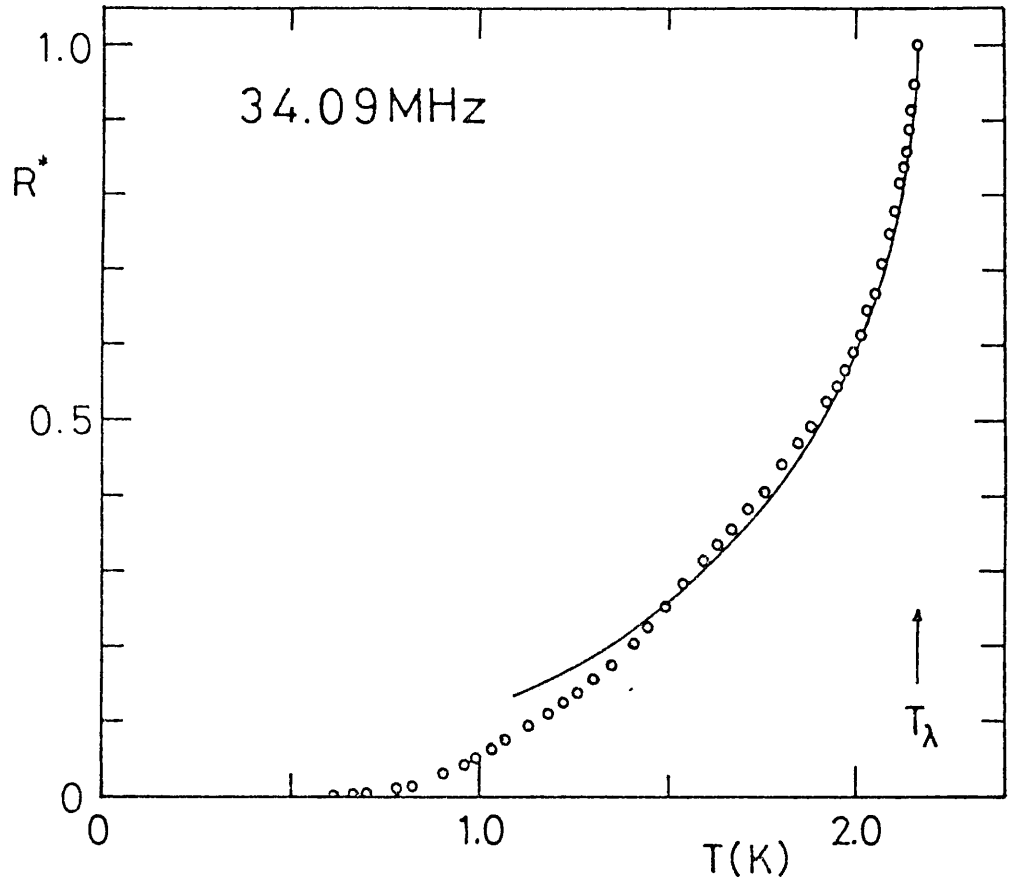

FIG.4.14 TEMPERATURE DEPENDENCE OF R/R_λ AT 34 MHz

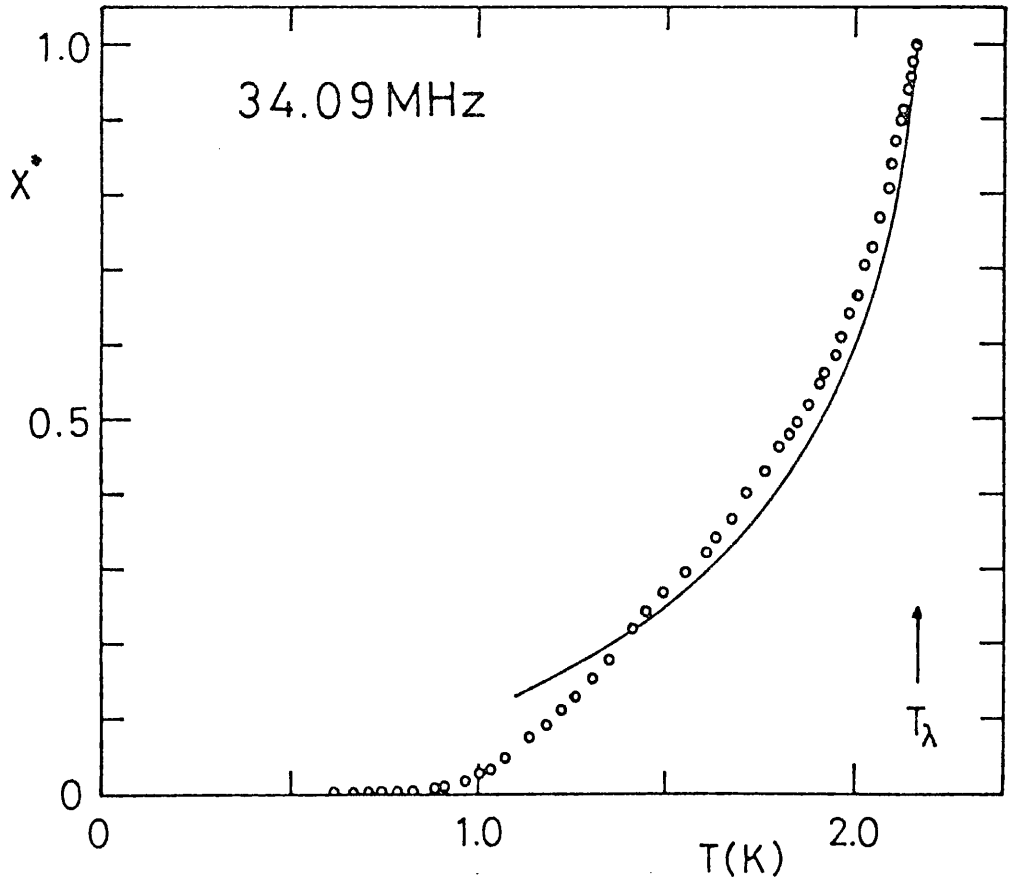

FIG.4.15 TEMPERATURE DEPENDECE OF X/X_λ AT 34 MHz

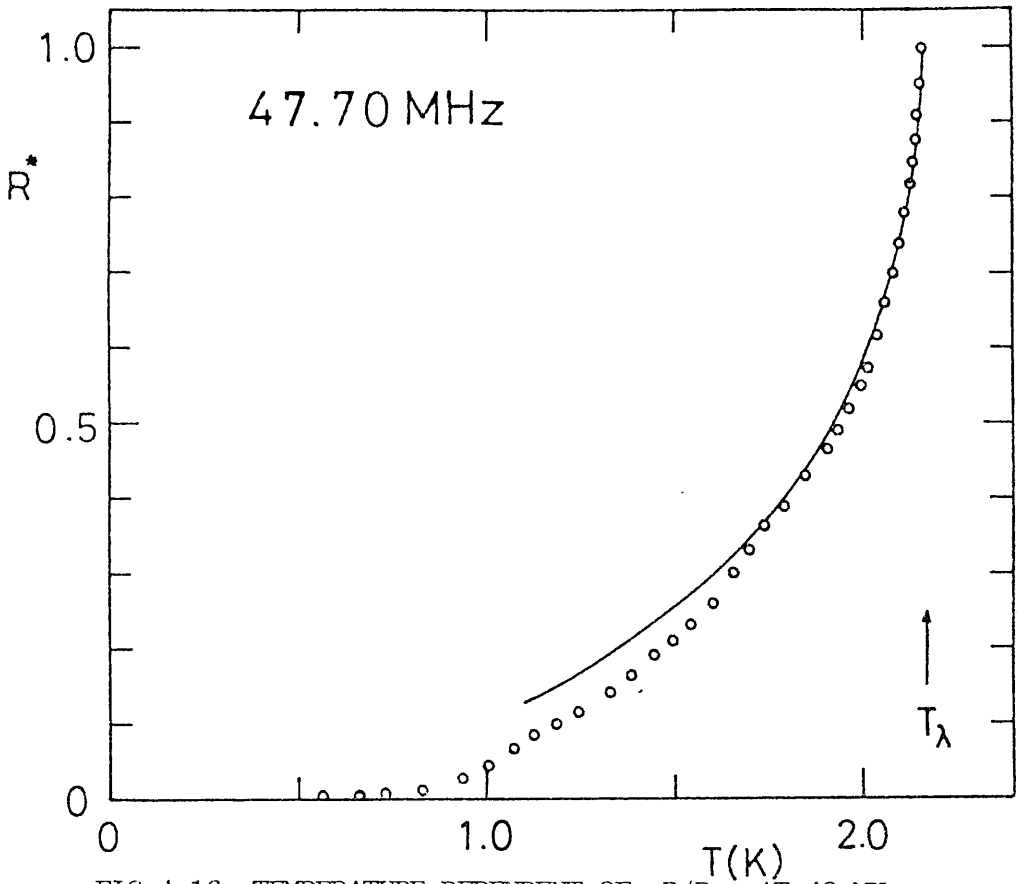

FIG.4.16 TEMPERATURE DEPENDENT OF R/R_λ AT 48 MHz

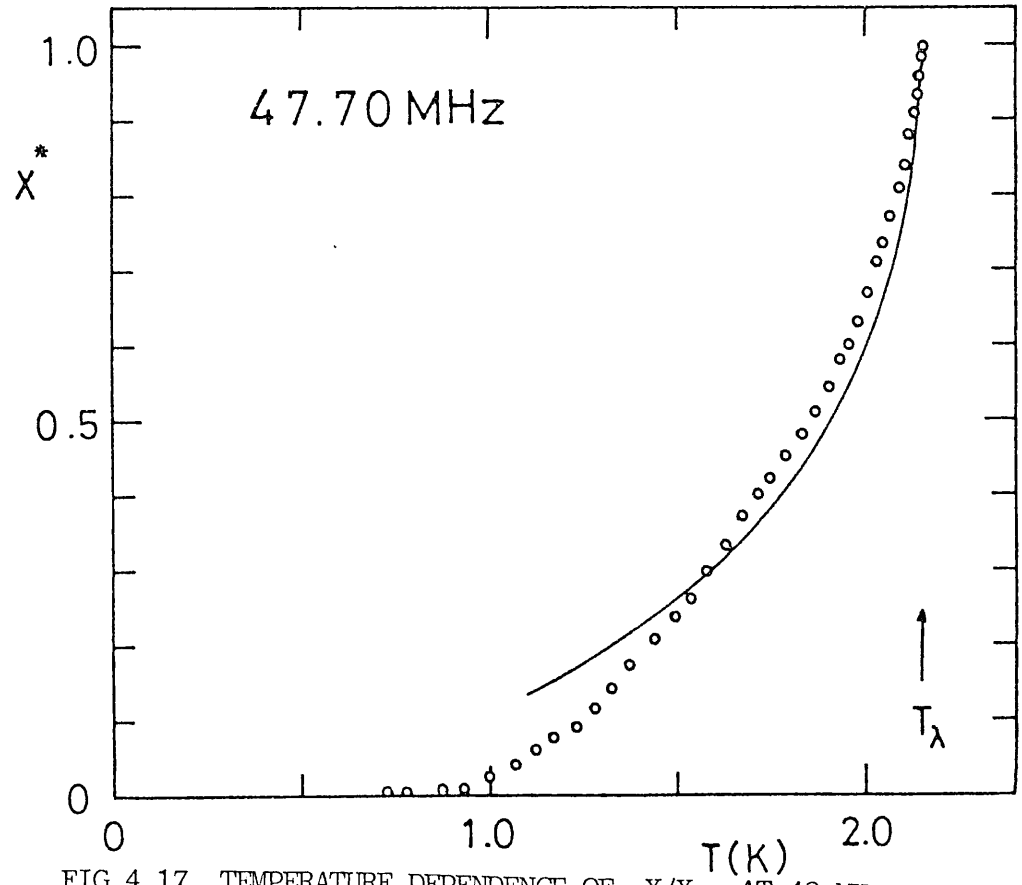

FIG.4.17 TEMPERATURE DEPENDENCE OF X/X_λ AT 48 MHz

or

$$= 4\pi\Delta f_p C_o (r(T) - r') \qquad (4.2.5)$$

using equations (3.2.15) and (3.2.19). r' and r(T) are given by

$$r' = 100\left(\sqrt{\frac{S_o}{S'_3}} - 1\right) \qquad (4.2.6)$$

where $S'_3 = S'_1$

and

$$r(T) = 100\left(\sqrt{\frac{S_o}{S_3(T)}} - 1\right) . \qquad (4.2.7)$$

Substituting these expressions into equation (1.2.5) we obtain

$$R(T) = 100n\pi^2 R_q \Delta f_p C_o \sqrt{S_o}\left(\frac{1}{\sqrt{S_3(T)}} - \frac{1}{\sqrt{S'_3}}\right) \qquad (4.2.8)$$

The absolute values of X and R at 20.47 MHz are shown in figure 4.11. The solid line was obtained from equation (1.1.4) using the ρ_n and η values from the data of Tough et al (1963). Normalised values X* and R* where

$$R^* = R/R_\lambda \qquad (4.2.9)$$

and

$$X^* = X/X_\lambda \qquad (4.2.10)$$

are shown in figures 4.12 to 4.17 for all (20.47, 34.09 and 47.70 MHz) run frequencies.

The agreement between X and R shows that, to a first approximation, HeII behaves like a classical viscous liquid. However, on closer inspection X falls less sharply than R below T_λ. At lower temperatures ($T < 1.5K$) this trend is reversed with R remaining larger and decreasing less rapidly than X. These differences are more pronounced if analysed in terms of the effective viscosities η' and η'' where, using equation (1.1.4),

$$\eta' = R^2/\pi f'_s \rho_n \qquad (4.2.11)$$

and

$$\eta'' = X^2/\pi f'_s \rho_n \qquad (4.2.12)$$

(N.B. η' and η'' are not the real and imaginary components of the viscosity.) Normalised values of η'/η'_λ and η''/η''_λ are shown in figures 4.18 to 4.20. For temperatures below 1.0K, ρ_n was taken from Bendt et al (1959). At 20.47 MHz the lambda-point viscosities were estimated to be

$$\eta'_\lambda = 24.3 \pm 0.4 \ \mu P$$

and

$$\eta''_\lambda = 28.4 \pm 0.5 \ \mu P$$

which is in good agreement with the accepted value of 27.4 μP quoted by Ahlers (1976). In general both η' and η'' fall rapidly below T_λ as do the low frequency (475 Hz - 3.3 kHz) measurements of Tough et al, shown as the solid line. Below 1.9K η' levels off before decreasing rapidly at lower temperatures while η'' decreases steadily as the temperature

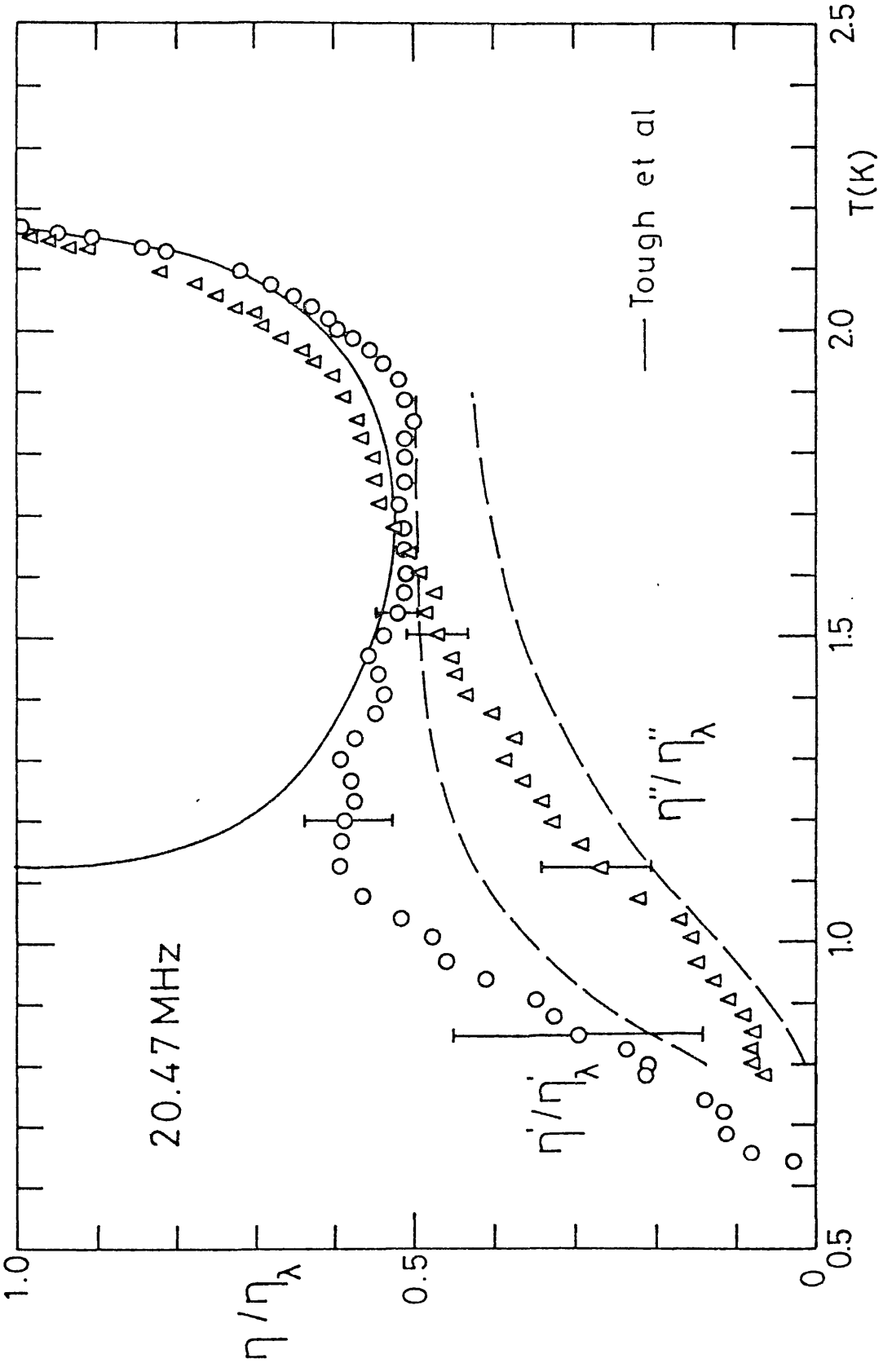

FIG.4.18 THE NORMALISED VISCOSITY VS TEMPERATURE AT 20 MHz

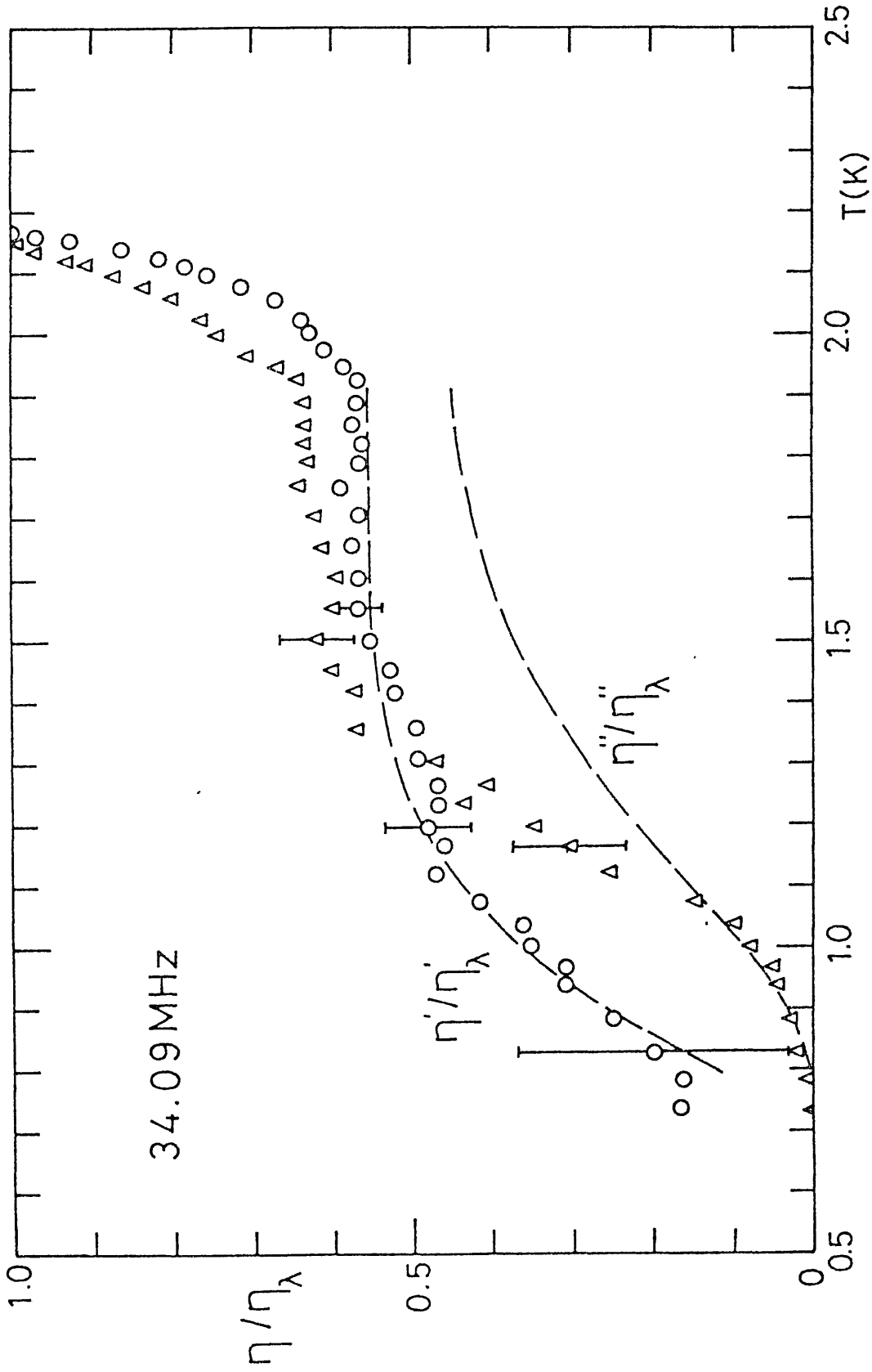

FIG.4.19 THE NORAMLISED VISCOSITY VS TEMPERATURE 34 MHz

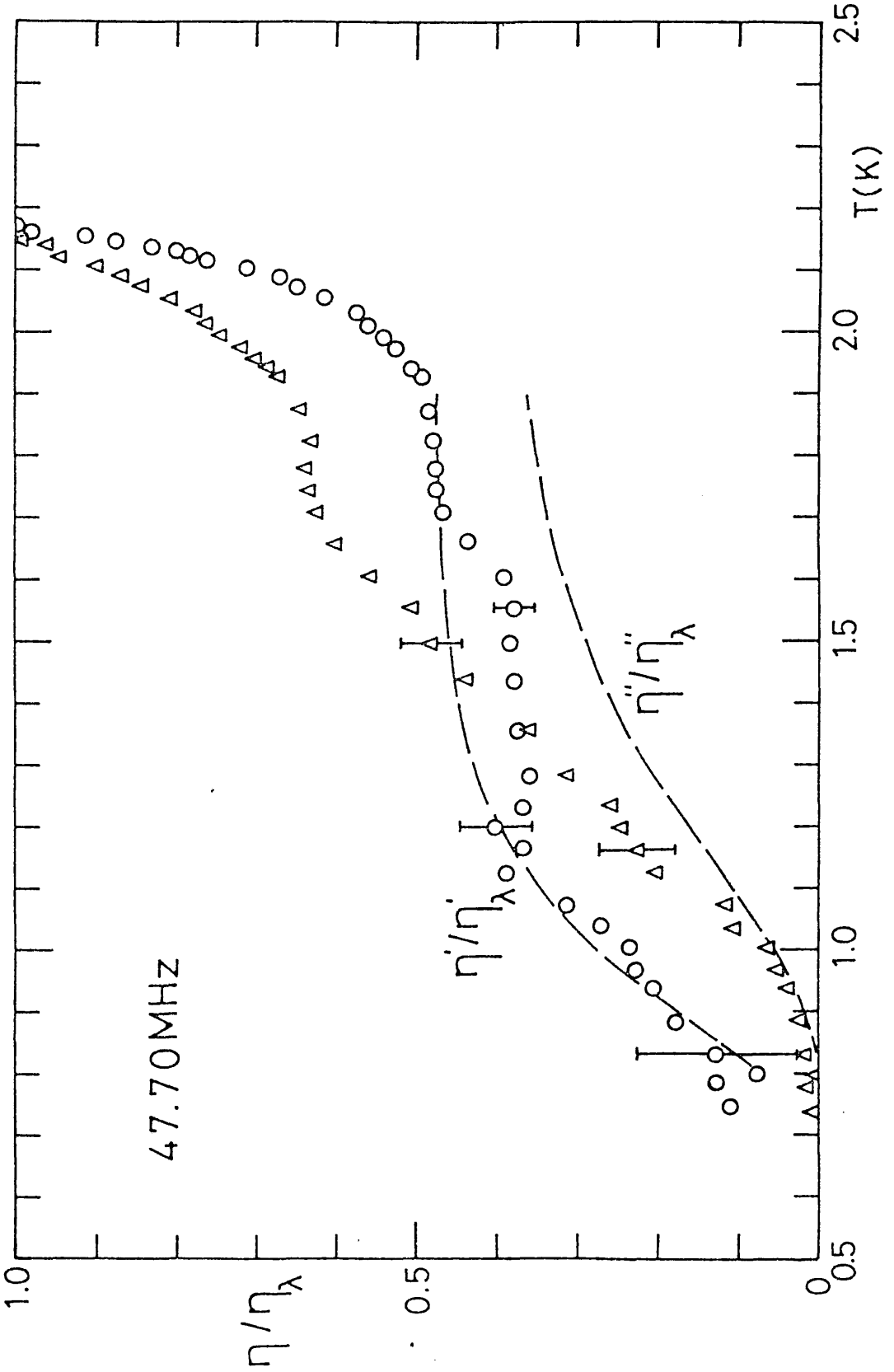

FIG.4.20 THE NORMALISED VISCOSITY VS TEMPERATURE AT 48 MHz

decreases. The most striking difference between the low and high frequency measurements occurs below 1.2K: Whereas the results of the latter show a dramatic increase in this region, no such increase is seen in the high frequency data. These effects are attributed to the large values of ℓ_p/δ in our experiments. This reduces the phonon viscous damping and hence the phonon contribution to η. In fact our results suggest that at MHz frequencies the viscosity is due to η_r only below 1.9K. The dashed curve (see section 5.2) show how η' and η'' should vary as a function of ℓ_r/δ assuming that the phonon contribution is negligible.

4.3 High Temperature Region: $T \sim T_\lambda$

For measurements of the viscous losses very close to T_λ an XY chart recorder was used which enabled s_3 and R11 to be recorded in a continuous fashion. This resulted in a series of XY traces, similar to the one shown in figure 2.9, for each frequency. Figure 4.21 shows the results of the processed data plotted as R* where from equations (4.2.8) and (4.2.9)

$$R^* = \frac{\frac{1}{\sqrt{s_3(T)}} - \frac{1}{\sqrt{s_3'}}}{\frac{1}{\sqrt{s_3(T_\lambda)}} - \frac{1}{\sqrt{s_3'}}} \qquad (4.3.1)$$

Also shown by the solid line marked 1.732 kHz is

$$R^* = \sqrt{\frac{\eta\rho_n}{\eta_\lambda\rho_\lambda}} \qquad (4.3.2)$$

obtained from equation (1.1.4). The values of η were taken from the precise measurements of Bruschi et al (1975) and ρ_n

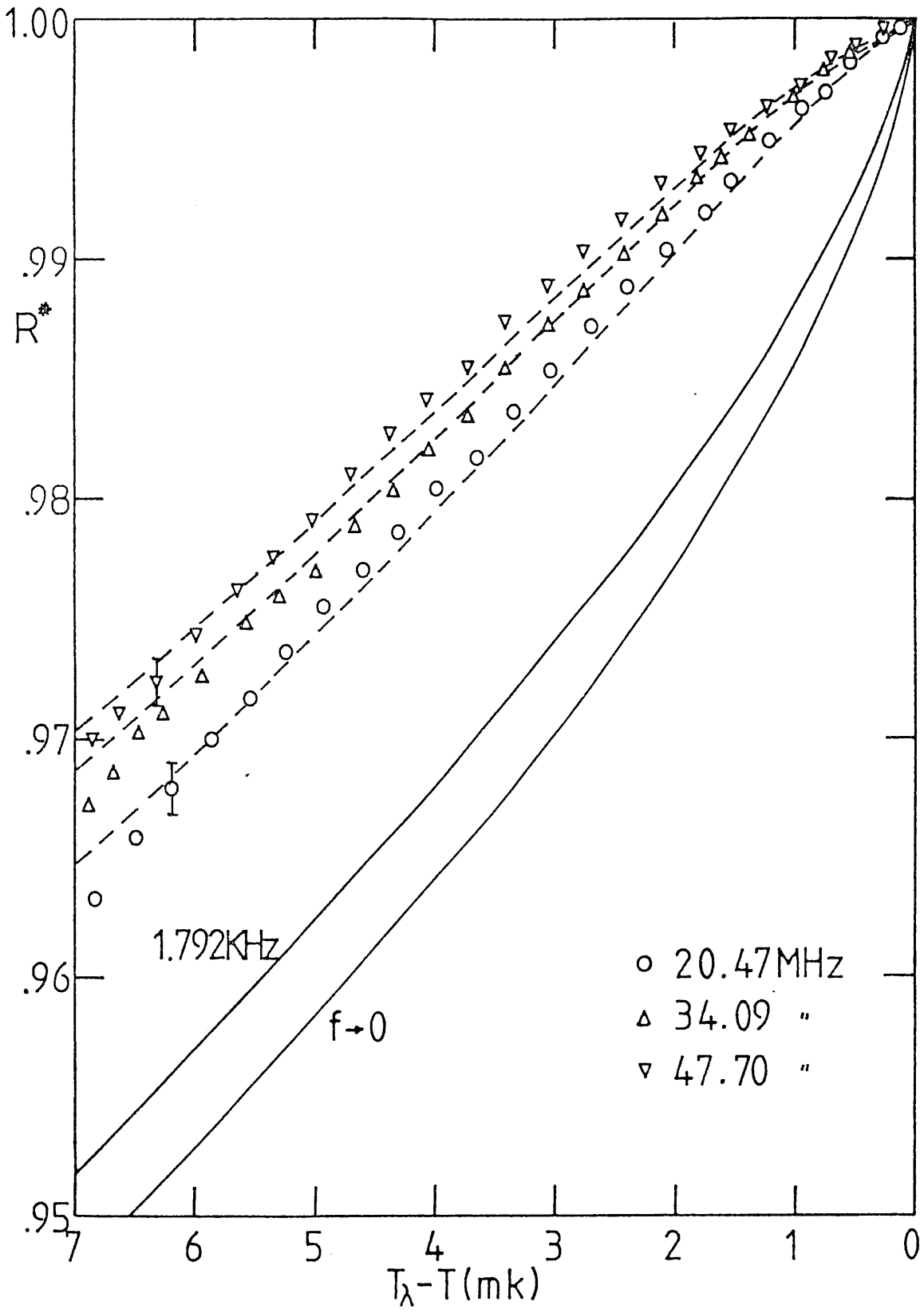

FIG.4.21 THE NORMALISED ACOUSTIC IMPEDANCE NEAR T_λ

from equation (1.4.7) of Tyson and Douglass (1966). If equation (1.1.4) were valid then R^* would be independent of frequency but this is clearly not the case. The higher the frequency the less sharp is the change in R^* near the lambda-point. This is attributed to the fact that the viscous penetration depth δ near T_λ becomes smaller than the superfluid healing length ξ_h and hence the viscous wave samples an enhanced normal fluid density adjacent to the crystal surface. This is discussed in greater detail in section 5.3.

CHAPTER FIVE

5.0 DISCUSSION OF RESULTS

5.1 Formation of a Helium Monolayer Below 600 mK

Many absorption isotherm experiments of unsaturated helium films (Brewer et al (1964), Chester et al(1972,1973), Yang (1973)) have shown that the liquid close to a solid surface is highly compressed by virtue of the van der Waals potential between substrate and helium atoms. This results in the formation of helium monolayers of varying thickness and density to be built-up on the substrate surface. The first monolayer is essentially a tightly bound solid under high pressure. Such a layer is presumably present in the experiments reported here but it would produce a temperature independent frequency shift, compared to the frequency in vacuo, and would therefore not be detected. Chester et al (1972, 1973) and Yang (1973) have estimated the density and binding energy of this layer on a quartz surface using a microbalance method. They found the density to be $(0.25 - 0.29) \times 10^3$ kg m^{-3} and obtained a value of 39 ± 6K for the binding energy. Taking the thickness of a statistical layer (Brewer (1978)) as 0.36 nm, the areal density of the first monolayer would be $(9.0 - 10.4) \times 10^{-8}$ kg m^{-2}. Assuming the second and subsequent layers to have normal fluid density then their areal densities would be 5.3×10^{-8} kg m^{-2}. As can be seen from figure 4.10 the value of $\sigma(o)$ lie in between these two cases which suggest that the effect is

probably caused by the formation of a monolayer. However, the binding energy of 0.15K is very much smaller than any other previously recorded and suggests that this process is associated with a more distant layer, possibly the second or even higher layer.

(Results from recent experiments have cast some doubt on this interpretation. See Postscript for further details.)

5.2 The Roton Viscosity and the Breakdown of Hydrodynamics

The results of η' at 20.47, 34.09 and 47.70 MHz are in reasonably good agreement with those of Tough et al (1963) from the lambda-point to 1.8K. But η'' is always larger than η' in this region and this trend becomes more noticeable the higher the run frequency. The reason for this remains unknown but the frequency shift and hence η'' tends to be more surface sensitive than the viscous energy losses which determine η'. Using the data at 20.47 MHz and identifying the approximately temperature independent region between 1.9-1.5K in η' with the roton viscosity, $\eta_r = 12.5 \pm 0.4$ μP. This is in excellent agreement with the value of 12.3 μP deduced from the capillary heat conduction measurements of Brewer and Edwards (1963). Hence we obtain from equations (1.3.3), (1.3.4) and (1.3.5) a value of

$$\frac{1}{\tau_r} = (1.08 \pm 0.03) \times 10^{13}\, T^{\frac{1}{2}} e^{-8.65/T} \qquad (5.2.1)$$

for the roton-roton scattering time, in good agreement with the measurements of Lea and Fozooni (1982).

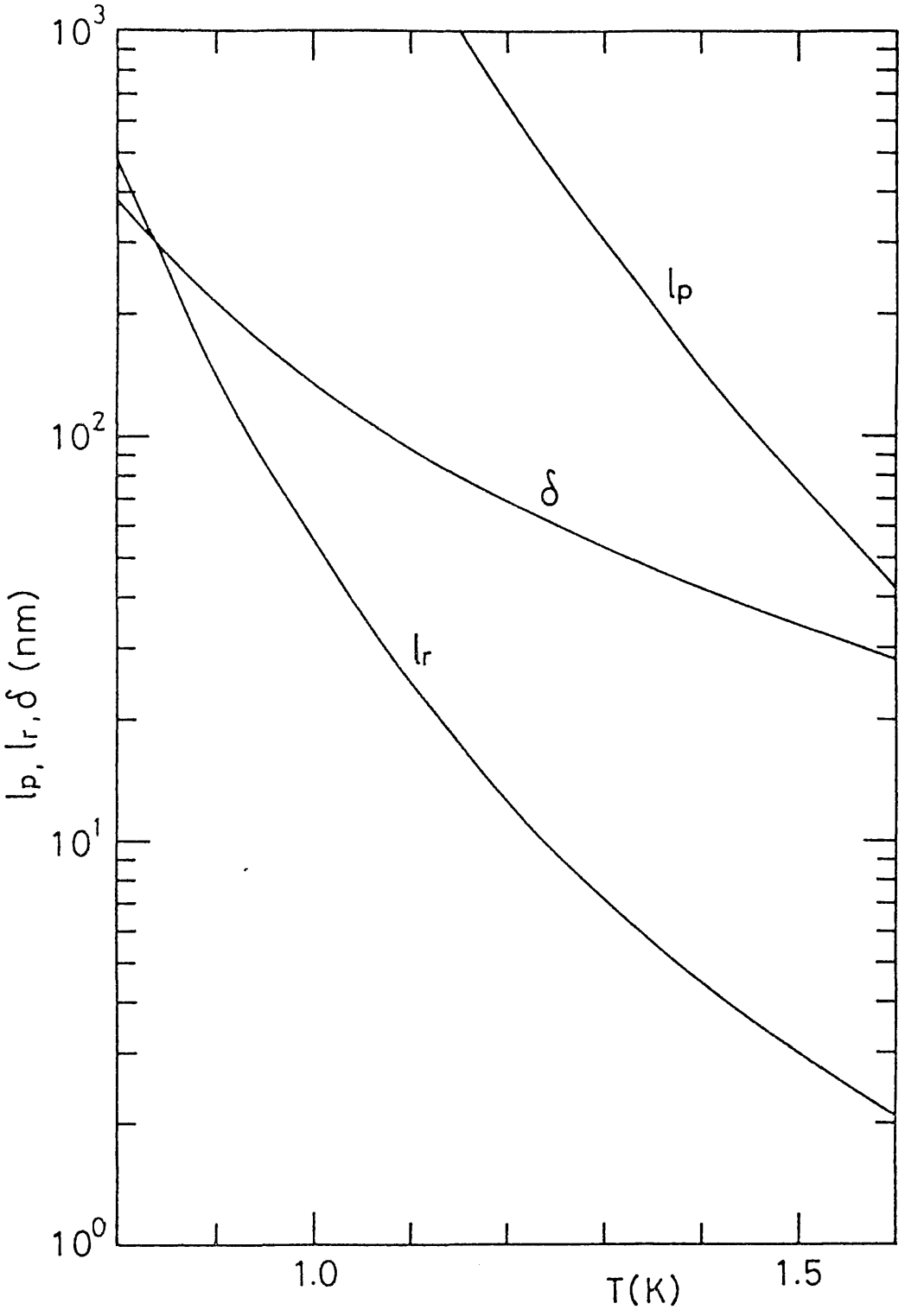

FIG.5.1 PHONON, ROTON MEAN FREE PATHS AND THE VISCOUS PENETRATION DEPTH AT 20 MHz

The most remarkable difference between the low and high frequency viscosity data occurs below 1.5K. The measurements of Tough et al show the expected viscosity increase due to the phonon component η_p but no such increase is seen in either η' or η''. This can be explained by recalling that to observe the true hydrodynamic viscosity the phonon and roton mean free paths must be less than δ, the viscous penetration depth. This is a necessary condition for (i) the configuration of the viscous wave to be well defined and (ii) to reduce the effect of slip - discussed below - at the crystal/liquid interface. From equation (1.3.10) it can be shown that at 20-50 MHz this condition is never satisfied by the phonons and therefore (Nadirashvili and Tsakadze (1978, 1979)) their contribution to the total viscosity is substantially reduced. Indeed below 1.8-1.7K $\ell_p/\delta > 1$ and our results suggest that the phonons are, hydrodynamically speaking, no longer seen. A similar hydrodynamic violation occurs for the rotons but at a lower temperatures (see figure 5.1) at which point both η' and η'' rapidly tend towards zero.

The derivation of equation (1.1.4) is based on the implicit assumption that the velocity profile is continuous across the crystal/liquid interface. Using classical kinetic theory Borovikov and Peshkov (1976) have given a simple expression for z for finite ℓ/δ, which includes the effect of slip, as follows: Consider a plane solid surface, normal to z, oscillating with a frequency f and a velocity along x of $u = u_o \exp(-i2\pi ft)$ in a rarefied gas of viscosity η and density ρ. The shear stress Π_{xz} at

the surface is given by (Kennard (1938)),

$$- \Pi_{xz} = \frac{1}{2} \eta \left. \frac{\partial U_x}{\partial z} \right|_o + \frac{\rho \bar{v}}{6}(U_x(o) - u) \quad (5.2.2)$$

where $\bar{v}$ is the mean atomic speed and $U_x(o)$ is the average tangential velocity of the atoms at the surface itself. Now the tangential velocity of an atom a distance L from the surface is $U_x(o) + L\partial U_x/\partial z$ and on being diffusely reflected it acquires a velocity u. Therefore

$$U_x(o) = \frac{1}{2}\left(U_x(o) + L \left. \frac{\partial U_x}{\partial z} \right|_o + u \right) \quad (5.2.3)$$

or

$$U_x(o) - u = L \left. \frac{\partial U_x}{\partial z} \right|_o \quad . \quad (5.2.4)$$

Classically, the slip length L is taken as the mean free path ℓ of the momentum carriers and then equation (5.2.2) becomes, since $\eta = \rho \bar{v} \ell / 3$,

$$- \Pi_{xz} = \eta \frac{\partial U_x}{\partial z} \quad (5.2.5)$$

which is the expected result. The shear impedance is defined thus:

$$Z = \frac{\Pi_{xz}}{u} \quad (5.2.6)$$

giving that

$$Z = \frac{- \eta \left. \frac{\partial U_x}{\partial z} \right|_o}{U_x(o) - \ell \left. \frac{\partial U_x}{\partial z} \right|_o} \quad . \quad (5.2.7)$$

From a solution of the one-dimensional equation for a viscous compressible liquid, equation (5.3.5), the velocity profile is

$$U_x(z) = U_x(o)\exp - (1 - i)z/\delta \; . \; \exp(- i2\pi ft) \qquad (5.2.8)$$

and hence

$$\frac{\partial U_x}{\partial z} = - \frac{(1 - i)}{\delta} U_x \quad . \qquad (5.2.9)$$

Substituting this into equation (5.2.7) gives

$$Z = \sqrt{\eta \rho \pi f} \left[\frac{(1 - i)}{1 + (1 - i)\ell/\delta} \right] \qquad (5.2.10)$$

where the term in square brackets is essentially a correction factor for finite ℓ/δ, tending to 1 as $\ell/\delta \to 0$. Applying this expression to HeII and assuming that at temperatures for which $\ell_p/\delta > 1$ the impedance is due to the roton component alone then

$$Z = \sqrt{\eta_r \rho_n \pi f} \left[\frac{(1 - i)}{1 + (1 - i)\ell_r/\delta_r} \right] \qquad (5.2.11)$$

where $\delta = \sqrt{\eta_r/\rho_n \pi f}$ since $\rho_n = \rho_r \gg \rho_n$ for $T > 0.9K$. Recalling the earlier definition of η' and η'' from equations (4.2.11) and (4.2.12) i.e.

$$Z = \sqrt{\eta' \rho_n \pi f} - i\sqrt{\eta'' \rho_n \pi f} \qquad (5.2.12)$$

then

$$\frac{\eta'}{\eta'_\lambda} = \frac{\eta_r}{\eta'_\lambda}\left[\frac{1 + 2\ell_r/\delta_r}{1 + 2\ell_r/\delta_r + 2\ell_r^2/\delta_r^2}\right]^2 \qquad (5.2.13)$$

and

$$\frac{\eta''}{\eta''_\lambda} = \frac{\eta_r}{\eta''_\lambda}\left[\frac{1}{1 + 2\ell_r/\delta_r + 2\ell_r^2/\delta_r^2}\right]^2 \quad . \qquad (5.2.14)$$

An expression similar to equation (5.2.13) has previously been used by Bertinat et al (1974) to correct helium-3 viscosity measurements for slip. The effective viscosity calculated from the above equations and fitted to the data are shown as dashed curves in figures 4.18 to 4.20. The agreement with the data for η' is very good but the measured value of η'' are generally greater than predicted from this simple theory. A slight improvement is found by assuming that only a fraction α of the rotons are diffusely reflected at the surface of the crystal. This enhances the slip factor such that ℓ/δ is replaced by $\left(\frac{2 - \alpha}{\alpha}\right)\ell/\delta$ in the above equations.

5.3 Determination of the Superfluid Healing Length

From the frequency dependence in R* shown in figure 4.21 it is evident that equation (1.1.4) becomes inappropriate for temperatures close to the lambda-point. The data indicates that as the frequency increases, and the penetration depth decreases, the viscous wave samples an enhanced normal fluid density near the crystal surface. Such a depletion

in ρ_s (or enhancement of ρ_n) is predicted on the basis of the GPM theory and should occur when δ becomes comparable to the superfluid healing length $\xi_h(T)$. Under these conditions equations (1.1.4) must be rederived so as to include the form of the superfluid density profile in the proximity of a solid surface. Adopting the convention used in the previous section, the power dissipated P_s per unit area of a plane oscillating with velocity $\mathrm{Re}(u_o \exp - i2\pi ft)$ in overcoming the viscous forces is

$$P_s(t) = \mathrm{Re}\ \Pi_{xz} \cdot \mathrm{Re}\ \dot{u}_o \exp(-i2\pi ft) \quad . \quad (5.3.1)$$

Using equation (5.2.8) and averaging over one complete oscillation then

$$\overline{P_s} = R\ u_o^2\ \overline{\cos^2 2\pi ft}$$

or

$$\overline{P_s} = \frac{1}{2} R\ u_o^2 \quad (5.3.2)$$

where $R \equiv \mathrm{Re}\ Z$. On the other hand the total kinetic energy E of an incompressible fluid is given by Landau and Liftshitz (1959) as

$$E = \int \frac{1}{2} \rho\ U^2\ dV \quad (5.3.3)$$

where ρ and U are the density and velocity respectively of an elemental volume of fluid dV. Applying this equation to a viscous wave generated by a plane oscillating in the

x direction gives

$$P_V(t) = \int_o^\infty \frac{\partial}{\partial t}\left(\frac{1}{2}\rho U_x^2\right) dz \qquad (5.3.4)$$

and since

$$\rho \frac{\partial U_x}{\partial t} = \eta \frac{\partial^2 U_x}{\partial z^2} \qquad (5.3.5)$$

$$P_V(t) = -\int_o^\infty \eta\left(\frac{\partial U_x}{\partial z}\right)^2 dz \qquad (5.3.6)$$

where $P_V(t)$ is the viscous energy loss in the fluid per unit time per unit area of the oscillating plane. Taking the real part of the velocity profile $U_x(z)$ from equation (5.2.8) and averaging over one oscillation:

$$\overline{P_V} = -\int_o^\infty \frac{2U_x^2(o)}{\delta} \exp(-2z/\delta)\, dz\ \overline{\cos^2(2\pi ft - z/\delta + \pi/4)}$$

or

$$\overline{P_V} = -\int_o^\infty U_x^2(o)\rho\pi f \exp(-2z/\delta)\, dz \qquad (5.3.7)$$

Now $\overline{P_s} \equiv -\overline{P_V}$ and provided there is no slipping i.e. $u_o = u_x(o)$,

$$R = 2\pi f \int_o^\infty \rho \exp(-2z/\delta) dz \qquad (5.3.8)$$

and the usual result $R = \sqrt{\eta\rho\pi f}$ is recovered when ρ (and hence δ) are position independent.

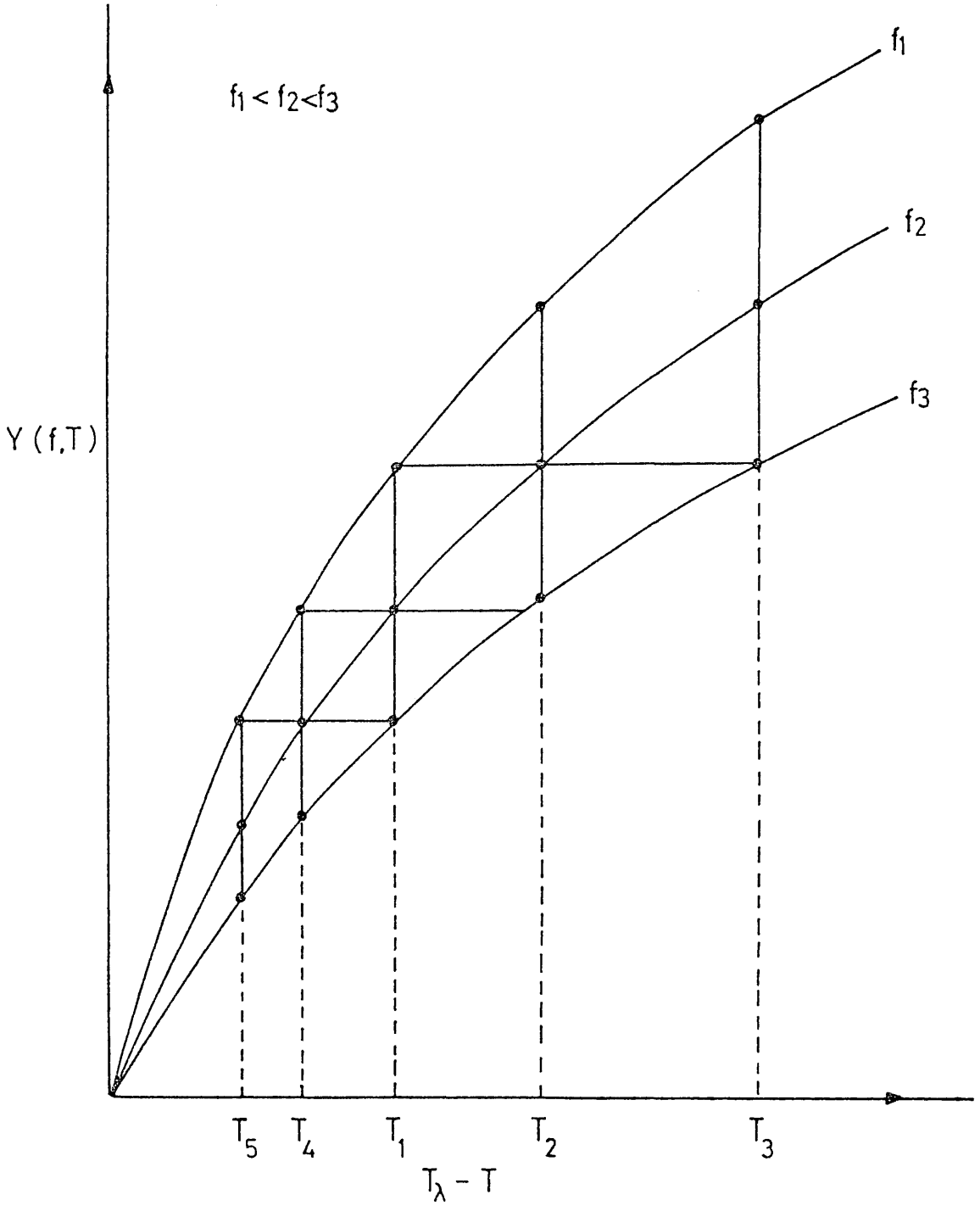

FIG.5.2 THE VARIABLE Y USED IN THE ANALYSIS OF THE T_λ DATA

To analyse the data in figure 4.21 it is important to note that δ is very much less temperature dependent than either ρ_n or η; using the values tabulated by Bruschi et al (1975), ρ_n decreases by 6.6% but δ by only 0.7% 10 mK below T_λ. Therefore in what follows it is assumed that δ is temperature and position independent and has lambda-point values of 17.07, 13.23 and 11.19 nm at 20.47, 34.09 and 47.70 MHz. In the case of the HeII equation (5.3.8) becomes

$$R(f,T) = 2\pi f \int_0^\infty \rho_n(z) \exp(-2z/\delta)dz \qquad (5.3.9)$$

since the superfluid component takes no part in the viscous dissipation process. The normalised acoustic resistance is then

$$R^* = 1 - \frac{2}{\rho\delta}\int_0^\infty \rho_s(z) \exp(-2z/\delta)dz \qquad (5.3.10)$$

where $\rho(=\rho_n + \rho_s)$ is the total helium density. But from GPM theory, equation (1.4.17) gives

$$\frac{\rho_s(z)}{\rho_s} = \tanh^2(z/\xi) \ ,$$

where $\xi = \sqrt{2}\,\xi_h$, and therefore

$$R^*(f,T) = 1 - \frac{\rho_s}{\rho}\left\{\frac{2}{\delta}\int_0^\infty \tanh^2(z/\xi) \exp(-2z/\delta)dz\right\} \ . \qquad (5.3.11)$$

From tables of Laplace transforms the factor in curly brackets, $p(\xi/\delta)$, has the form

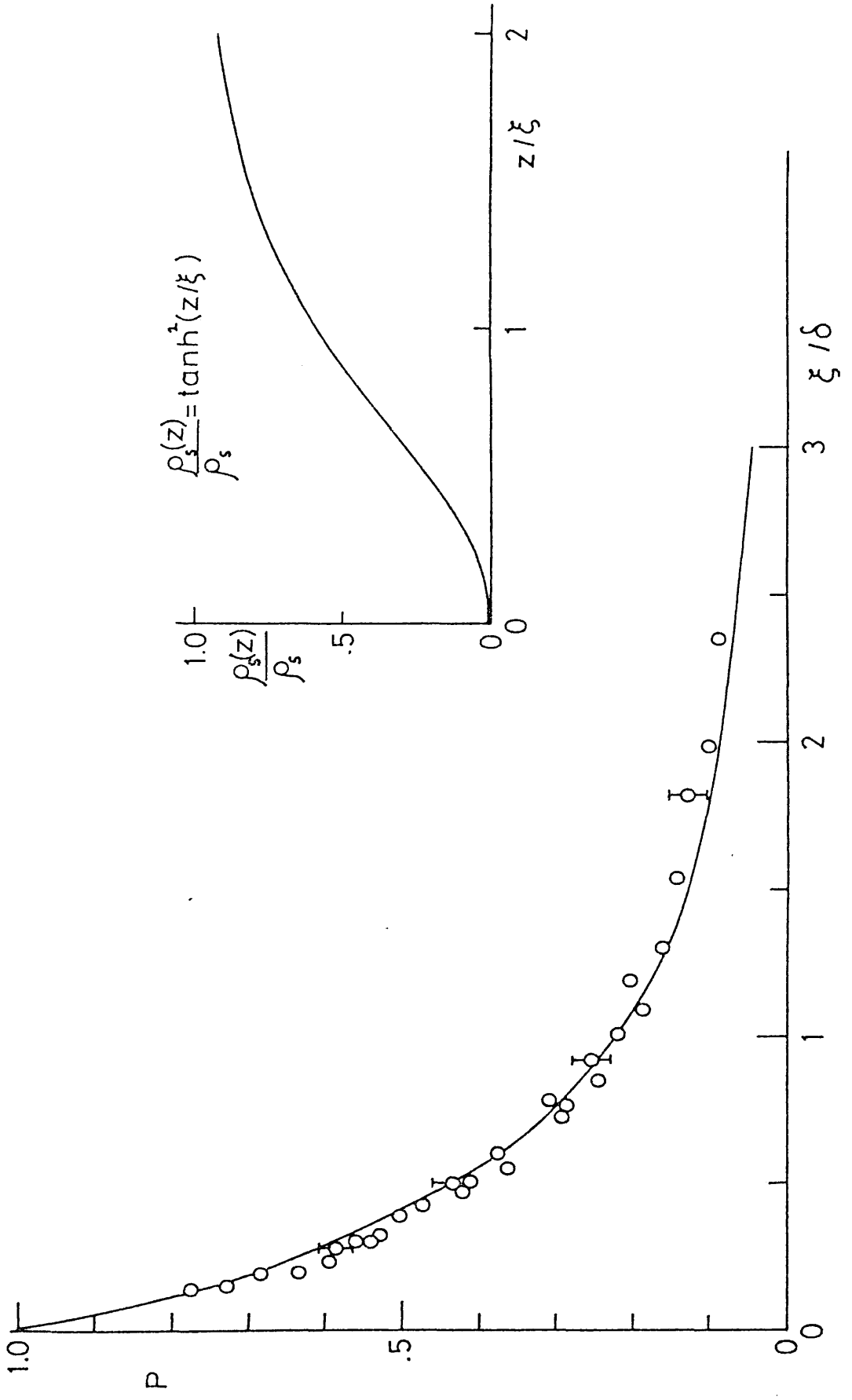

FIG.5.3 CORRECTION FACTOR p to R* FOR FINITE FREQUENCIES. INSERT: SUPERFLUID DENSITY PROFILE NEAR A SOLID SURFACE

$$p(\xi/\delta) = 1 + 2(\xi/\delta) - 2(\xi/\delta)^2\left[\psi(\xi/2\delta + \tfrac{1}{2}) - \psi(\xi/2\delta)\right] \quad (5.3.12)$$

where ψ is the digamma function (see for instance Abramowitz and Stegun (1965)). The function p is plotted in figure 5.3 for $0 < \xi/\delta < 3$. As can be seen for temperatures far from T_λ and low frequencies i.e. $\xi \ll \delta$, p tends to 1 giving

$$R^*(f,T) = 1 - \rho_s/\rho$$

which is the expected result if δ is constant.

It is possible to deduce the function $p(\xi/\delta)$, except for a constant multiplicative factor in ξ/δ, from the high frequency data as follows. By calculating a new variable $Y(f,T)$ where

$$Y(f,T) = (1 - R^*(f,T)) \cdot \frac{\rho}{\rho_s} \quad (5.3.13)$$

and taking the superfluid fraction values from equation (1.4.7) three curves, shown schematically in figure 5.2, are obtained. At a temperature T_1 and frequency f_1 the measured value of $Y(f_1,T_1)$ corresponds to an (unknown) value of $\xi/\delta = D$ say. Also at the same temperature there are two other values of Y, i.e. $Y(f_2,T_1)$ and $Y(f_3,T_1)$ corresponding to ξ/δ values of $\alpha_{21}D$ and $\alpha_{31}D$ respecitvely where $\alpha_{nm} = \sqrt{f_n/f_m}$. By choosing another temperature T_2 such that $Y(f_1,T_1) = Y(f_2,T_2)$, and therefore keeping $\xi/\delta = D$, two other values $Y(f_1,T_2)$ and $Y(f_3,T_2)$ are found which correspond to ξ/δ equal to $\alpha_{21}^{-1}D$ and $\alpha_{32}D$ respectively.

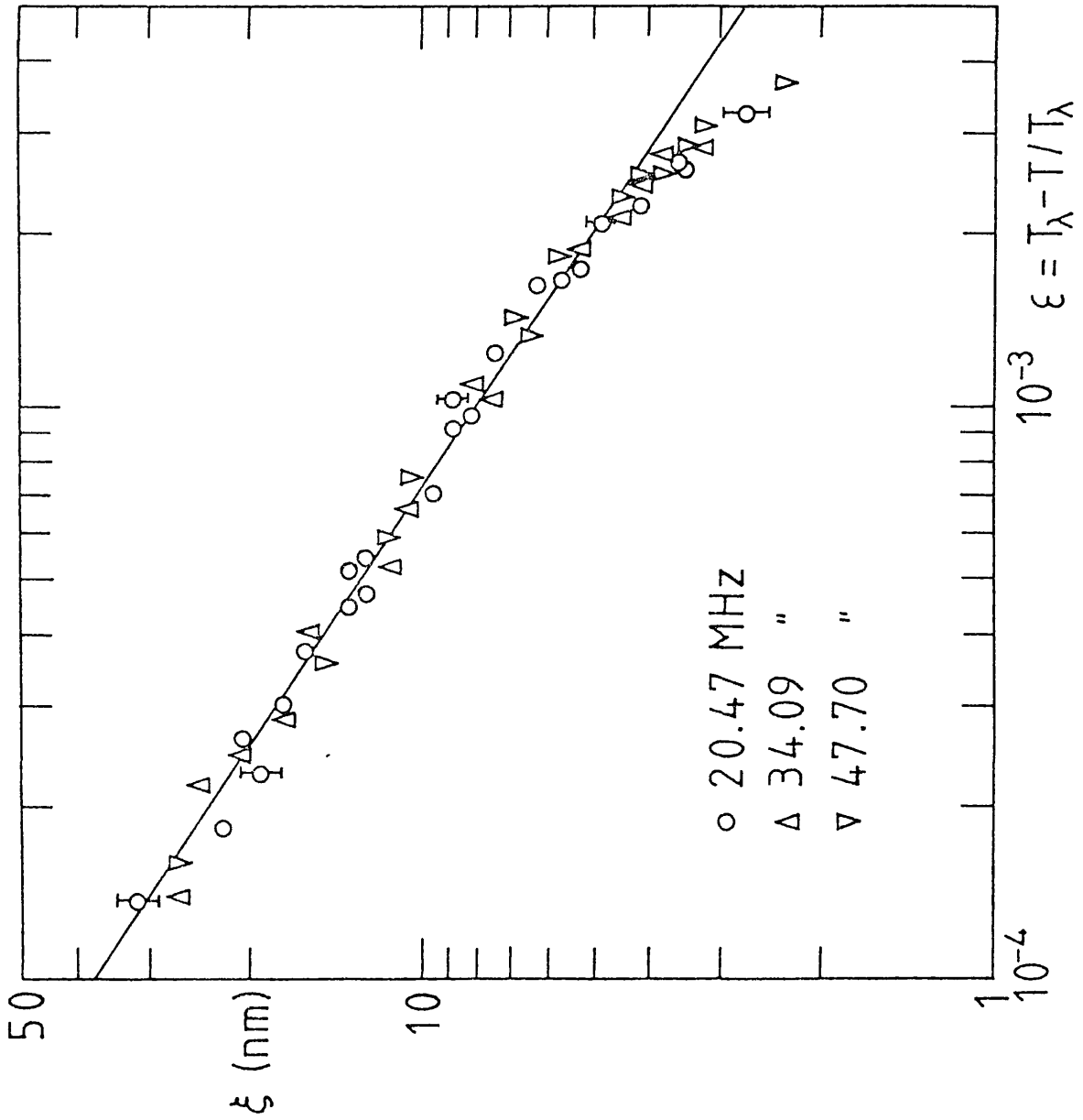

FIG.5.4 THE SUPERFLUID HEALING LENGTH AS A FUNCTION OF ε

Hence by repeating this process values of Y can be found corresponding to a series of ξ/δ values equal to $\alpha_{21}^{\ell}\alpha_{31}^{m}\alpha_{32}^{n} D$ where ℓ,m,n are integers. The constant D and hence the ξ/δ scale is found by fitting $Y(\alpha_{21}^{\ell}\alpha_{31}^{m}\alpha_{32}^{n})$ to $p(\xi/\delta)$. The results of this analysis are shown in figure 5.3. Once the value of D has been established it is then a simple matter to calculate $\xi(T)$ which is shown in figure 5.4. The solid line is

$$\xi(T) = 0.08\ \varepsilon^{-2/3}\ \text{nm} \qquad (5.3.14)$$

which has the expected temperature dependence and is seen to be a reasonably good fit to the data. The dashed curves in figure 4.21 shows the calculated acoustic impedance using this value of ξ and equations (5.3.11) and (5.3.12). The agreement between the data and theory shows that, within the assumptions of the model used to obtain equation (5.3.11), this analysis is self consistent. Although our value of ξ is almost three times smaller than the superfluid healing length it is identical to the characteristic length derived from the ultrasonic measurements of Williams and Rudnick (1970). In general, all measurements of characteristic lengths in helium-II give results with the same temperature dependence but with a wide range of amplitudes.

5.4 Concluding Comments

The aim of this work was to examine the potential of an AT-cut quartz crystal immersed in helium II firstly as a high-frequency viscometer and second as a sensitive method of probing the superfluid density profile next to a solid surface. The

following is essentially a brief summary of our findings and some additional comments.

The measurements show that below 1.5K the viscosity is drastically reduced below that of previous low frequency data. This reduction is explained in terms of the relative sizes of the phonon and roton mean free paths and the viscous wave penetration depth. There is reasonable qualitative agreement between these measurements and a simple slip model however this points up the need for a more detailed theory of the non-hydrodynamic regime from a solution of an appropriate kinetic equation. Such a theory would presumably show that for the frequencies used in our experiments the phonon contribution to the viscous damping is insignificant since $\ell_p > \delta$. Hence this technique provides a new method of studying the roton hydrodynamic and non-hydrodynamic regimes. The values of η_r and η_λ are in very good agreement with previous determinations of these parameters.

The acoustic impedance measurements near the lambda-point demonstrate yet another effect of a small viscous penetration depth on the hydrodynamic properties of the liquid. Deviations from the classical expression of equation (1.1.4) are interpreted in terms of a superfluid healing or coherence length ξ. A simple model is proposed based on energy conservation principles which enable ξ to be estimated assuming that the penetration depth is constant. This model is shown to be self consistent and yields a value of $\xi = 0.08\ \varepsilon^{-2/3}$ nm. This is in good agreement with the values of ξ tabulated in

figure 1.1. The superfluid density profile is also shown to be rather well described by the GPM theory. More detailed data near T_λ would enable the profile to be calculated directly by an inverse Laplace transform of the normalised acoustic impedance.

POSTSCRIPT

FURTHER EXPERIMENTS BELOW 600 mK

All the work presented here are the results of experiments conducted between September-December 1979. Most of these have since been repeated and extended to elevated pressures but the essential conclusions have not changed. However one aspect of the results which has caused some concern is our interpretation of the frequency shift Δf_s below 600 mK as being due to the formation of a helium monolayer on the crystal surface. Although the value for the absorbed areal density agrees with this picture, the activation or binding energy A_3/K_B is uncharateristically low. In order to resolve this problem Drs Lea and Fozooni conducted a series of experiments in a modified cell which allowed the crystal to be cooled to 30 mK in a nominally high vacuum. They observed that while both the Q factor and the resonant frequency were approximately temperature independent from 0.8 and 4.2K, frequency shifts occurred below 0.8K which were similar to the ones in this report. However the magnitude and sign of these shifts varied from run to run and were power dependent. When the cell was subsequently filled with liquid helium-4 the data in figures 4.1 to 4.9 were reproduced with no power dependence. Therefore our interpretation of this effect in terms of monolayer absorption is questionable. But whether the crystal is operating as a microbalance or some other mechanisms is responsible, $\sigma(T)$ can still be used as a parameter characterising this effect.

APPENDIX I

THE TRANSVERSE ACOUSTIC IMPEDANCE OF A WEAKLY INTERACTING FERMI-LIQUID

The purpose of the following section is to set down the details of a calculation of the transverse acoustic impedance of a weakly interacting Fermi-liquid carried out in the early stages of the project. Although this work is only relevant to some later experiments made by us (Lea and Retz (1981)) on dilute solutions of helium-3 in liquid helium-4, which have not been discussed here, it is an important contribution and therefore the author feels that it should be included in this report. A paper (Retz and Lea (1982)) presenting the results of this calculation for a Fermi-gas has already been published.

The basic formulation of the problem has been discussed by Flowers and Richardson (1978) in their calculation of the transverse acoustic impedance Z of an assembly of strongly interacting fermions: normal helium-3. For a weakly interacting system, where the (symmetric) Landau parameters $F_{\ell \geq 2} = 0$ and $-3 < F_1 \leq 6$, the initial part of the calculation proceeds in a similar fashion. The Landau kinetic equation is solved in a half-space with a plane solid surface oscillating transversely with angular frequency ω and velocity amplitude u_o. The collision term is approximated by a single relaxation time τ. The kinetic equation has an exact solution and Z is obtained from the value of the stress tensor at the surface from equation (5.2.6). For totally diffuse scattering of the helium-3 quasi-particles

from the surface

$$Z = \frac{3n}{4u_o}(b - 1)\bar{\phi}_1(o) \qquad (A.1)$$

where

$$b = \frac{1}{a}\left(\frac{3 + aF_1}{3 + F_1}\right)$$

$$a = (1 - i\omega\tau)$$

and n is the quasi-particle number density. The function $\overline{\phi_1}$ is related to the Laplace transform of the stress tensor and is given by

$$\overline{\phi_1}(s) = - \frac{4P_F}{3b} \frac{1}{s} \left[1 - \frac{\Delta_-(s)}{\Delta_-(o)}\right] , \qquad (A.2)$$

s being a complex variable, P_F the Fermi-momentum,

$$\ell n\Delta_-(s) = \frac{1}{2\pi i} \int_{-\beta - i\infty}^{-\beta + i\infty} \frac{\ell n\Delta(u)}{u - s}\, du \qquad (A.3)$$

for $0 < \beta < |Res_o|$ where $|Res_o| < 1$ and $0 < \beta < 1$ when $|Res_o| > 1$ and

$$\Delta(u) = 1 - \frac{3b}{2u^2}\left[\frac{u^2 - 1}{2u} \ell n\left(\frac{1 + u}{1 - u}\right) + 1\right] . \qquad (A.4)$$

s_o is defined by:

$$\Delta(s_o) \equiv 0 \qquad (A.5)$$

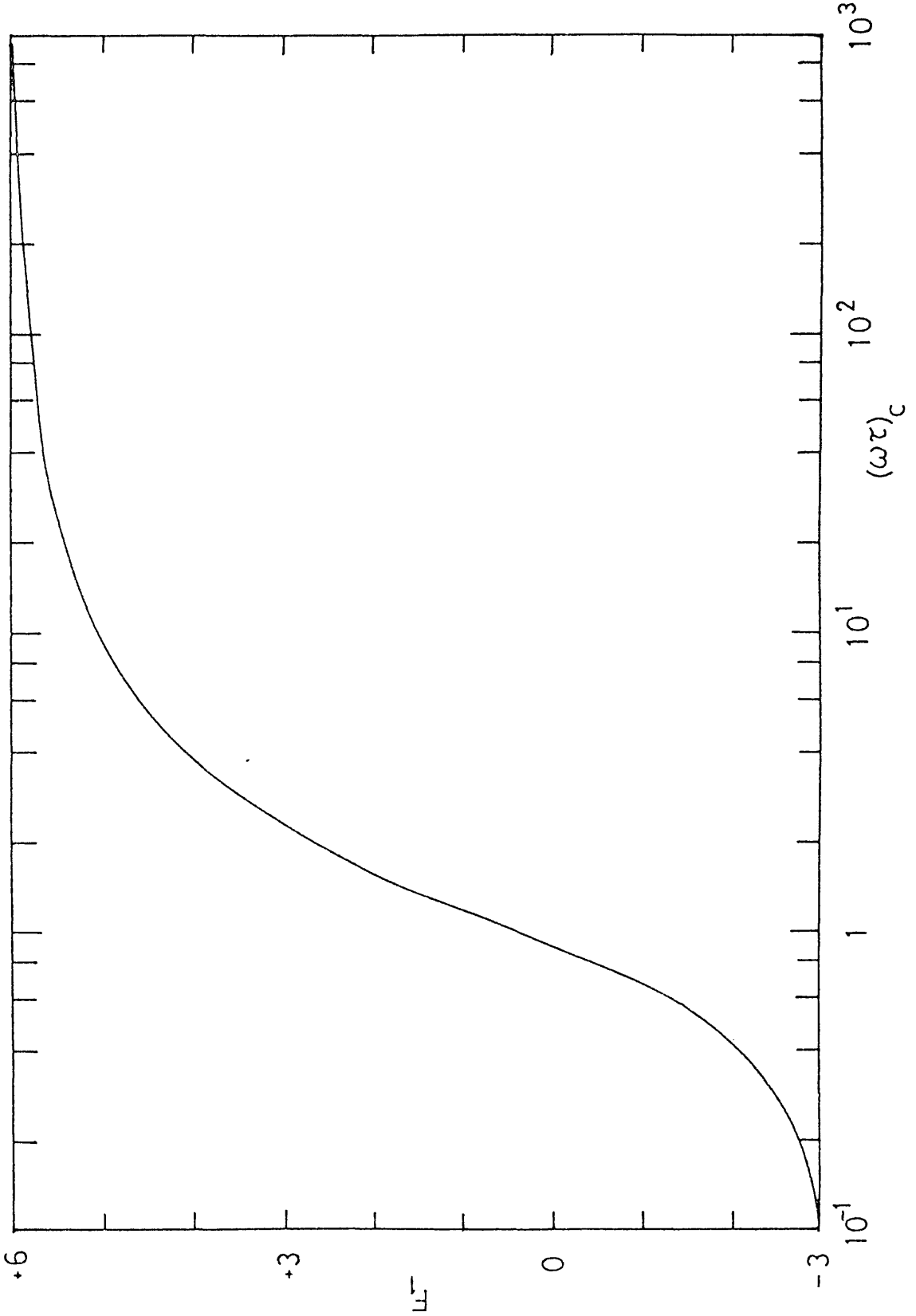

FIG.A.1 $(\omega\tau)_c$ LIMIT OF TRANSVERSE OSCILLATIONS IN A FERMI-LIQUID

and is proportional to the propagation constant of the transverse acoustic mode. (Flowers and Richardson obtain some different equations since they include F_2 and introduce another function G, expressed in terms of Δ, which is used to define a complex integral $\ell n g_-(s)$ analogues to $\ell n\ \Delta_-(s)$. However, taking these factors into account their expression for Z is equivalent to equations (A.1) to (A.5) above). Taking the limit $s \to 0$ of equation (A.2), to obtain $\overline{\phi_1}(o)$, then

$$Z = nP_F \left(\frac{b - 1}{b}\right)\frac{\Delta_-'(o)}{\Delta_-(o)} \qquad (A.6)$$

where $\Delta'(s) = d\Delta_-(s)/ds$. Hence Z can be determined from the evaluation of $\Delta_-(s)$ which is defined by equation (A.3). An inspection of the integrand shows that it has the following three singularities:

(i) a simple pole at $u = s$

(ii) branch points at $u = \pm 1$

and for $\omega\tau$ less than some critical value $(\omega\tau)_c$, which depends on F_1 as shown in figure A1,

(iii) branch points at $u = \pm s_o$.

When $\omega\tau > (\omega\tau)_c$, Lea et al (1973) have shown that equation (A.5) has no solution and therefore the singularity given in (iii) no longer exists. For $Re(s) > -\beta$ the integral can be evaluated by either one of the contours L or R shown in

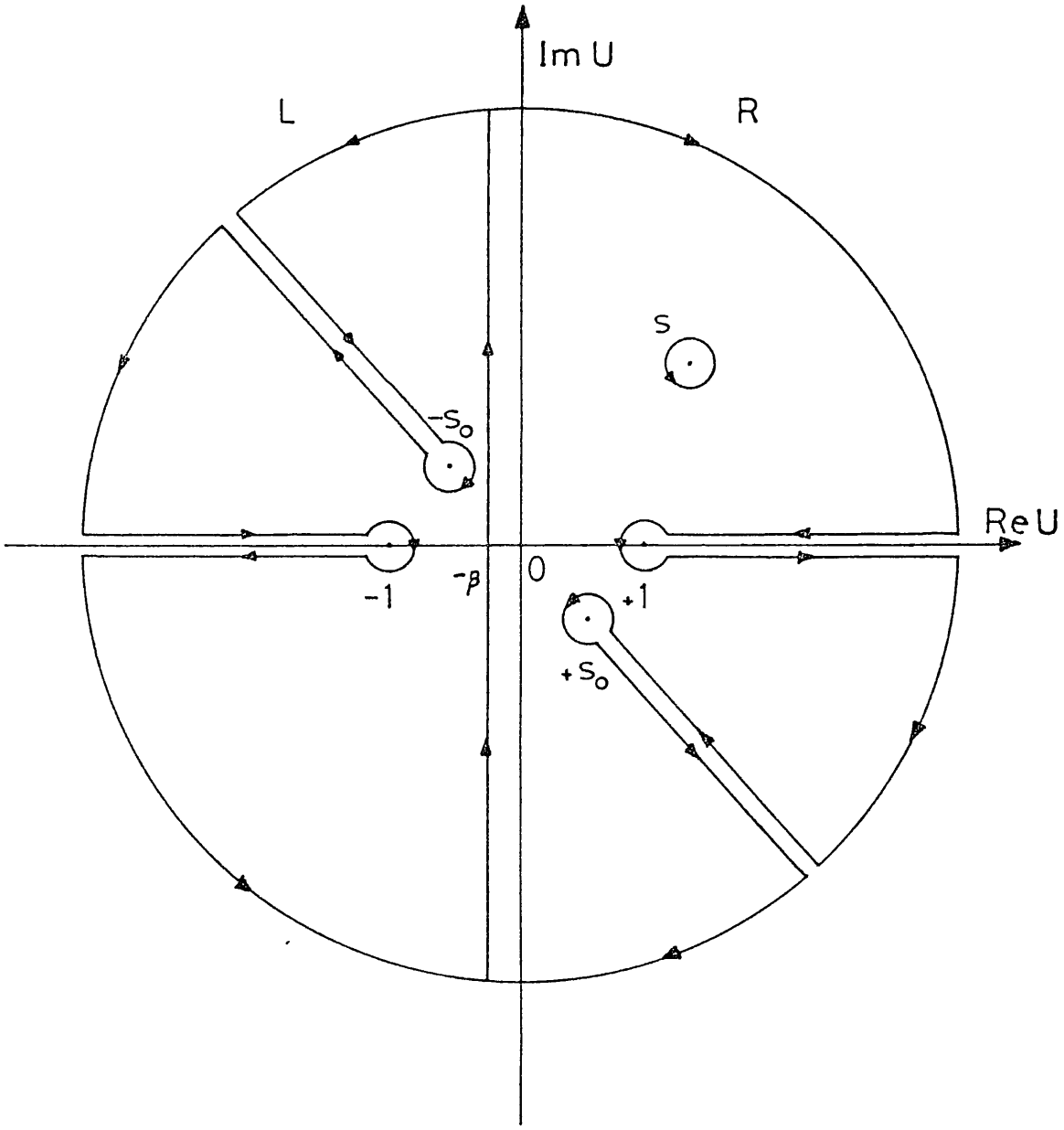

FIG.A.2 INTEGRATION CONTOURS FOR THE EVALUATION OF $\psi(s)$

figure A2. Following the procedure of Bekarevich and Khalatnikov (1960) the integral is evaluated over both contours, the expressions added and the result divided by 2. This gives

$$\ell n\ \Delta_{-}(s) = \frac{1}{2}\left[\ell n\ \Delta(s) + 2s\psi(s) + \ell n\left(\frac{s_o + s}{s_o - s}\right)\right] \quad (A.7)$$

where

$$\psi(s) = \frac{1}{2\pi i}\int_{\infty}^{1} \frac{\ell n\ \Delta^{+}(u) - \ell n\ \Delta^{-}(u)}{u^2 - s^2}\, du \quad (A.8)$$

and

$$\Delta^{\pm}(u) = 1 - \frac{3b}{2u^2}\left[\frac{u^2 - 1}{2u}\left(\ell n\left(\frac{1 + u}{1 - u}\right) \pm i\pi\right) + 1\right] . \quad (A.9)$$

The first term in equation (A.7) comes from the pole at $u = s$. The second is from the branch cuts along the real axis, $\Delta^{\pm}$ being the boundary value of Δ on the upper (Δ^{+}) and lower (Δ^{-}) edge of the cut around the L contour. The contribution from the other branch cuts in (iii) can be evaluated by introducing a real variable $X (X \geq 1)$ where $u = - Xs_o$ for L and $u = + Xs_o$ for R. The combined contribution is then

$$\frac{2s_o s}{2\pi i}\int_{\infty}^{1} \frac{2\pi i}{X^2 s_o^2 - s^2}\, dX \quad (A.10)$$

which can be integrated simply and gives rise to the third term in equation (A.7). Differentiating $\ell n\ \Delta_{-}(s)$ with respect to s we obtain

$$\frac{\Delta'_{-}(s)}{\Delta_{-}(s)} = -\frac{1}{2}\left[\frac{\Delta'(s)}{\Delta(s)} + 2s\psi(s) + 2s\frac{d\psi}{ds} + \frac{s_o}{s_o^2 - s^2}\right] \tag{A.11}$$

which is the required expression to calculate Z from equation (A.6). Since $\Delta(s)$ and $\psi(s)$ are even functions, for $s = 0$

$$\frac{\Delta'_{-}(o)}{\Delta_{-}(o)} = -\left(\psi(s) + \frac{1}{s_o}\right) \tag{A.12}$$

and hence

$$Z = -nP_F \frac{i\omega\tau}{1 + aF_1/3}\left(\frac{1}{s_o} + \psi(o)\right) , \tag{A.13}$$

for $\omega\tau < (\omega\tau)_c$. When $\omega\tau > (\omega\tau)_c$ the $1/s_o$ term vanishes and the impedance is given by:

$$Z = -nP_F \frac{i\omega\tau}{1 + aF_1/3}\psi(o) . \tag{A.14}$$

The integral $\psi(o)$ can be easily evaluated using standard numerical methods by changing the integration variable from u to $1/t$ say with the result that

$$\psi(o) = -\frac{1}{2\pi i}\int_o^1 \ell n\ \Delta^{+}(t) - \ell n\Delta^{-}(t)\ dt \tag{A.15}$$

where

$$\Delta^{\pm}(t) = 1 - \frac{3bt^2}{2}\left[\frac{1 - t^2}{2t}\left(\ell n\left(\frac{1 + t}{1 - t}\right) \pm i\pi\right) + 1\right]. \tag{A.16}$$

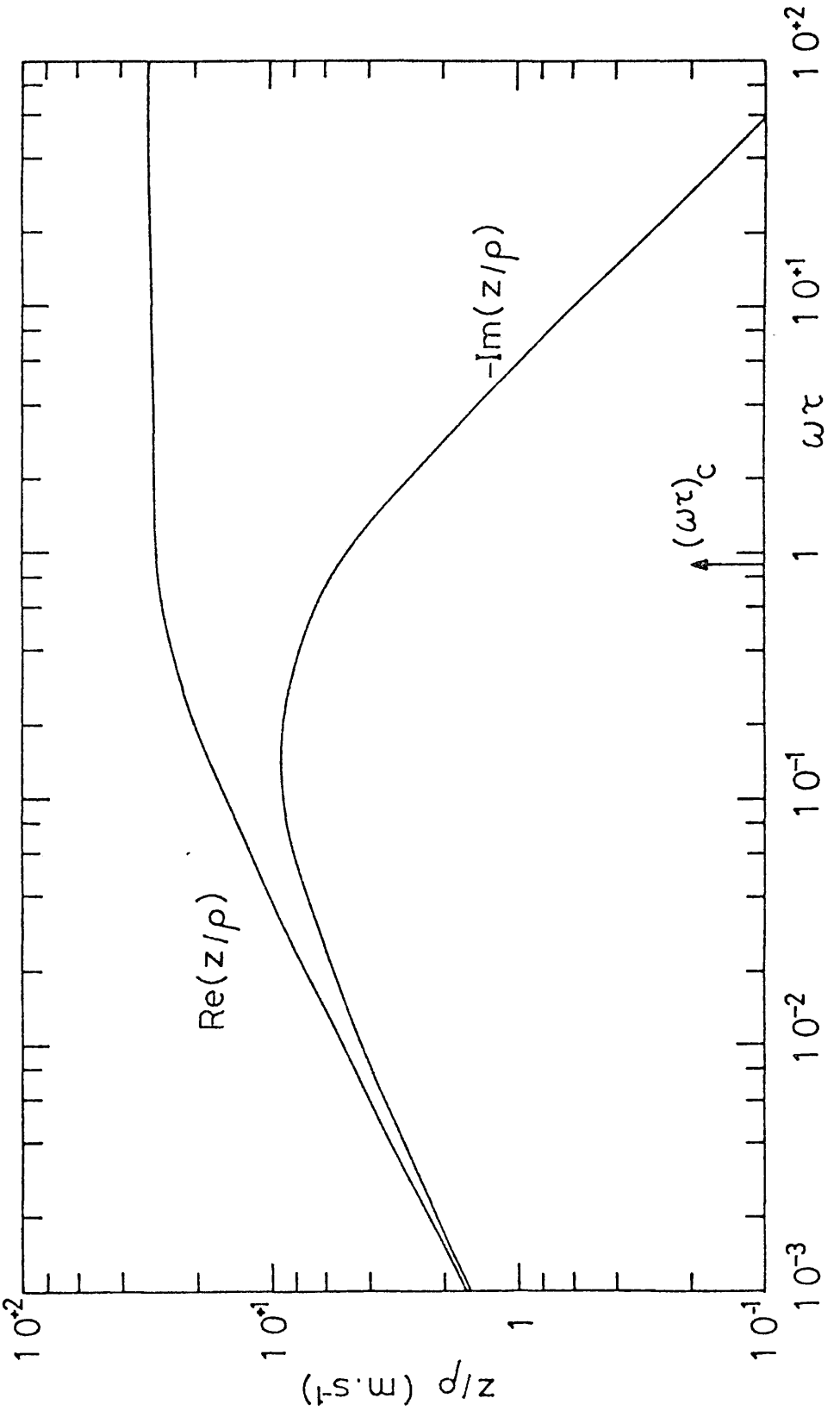

FIG.A.3 THE TRANSVERSE ACOUSTIC IMPEDANCE OF A FERMI-GAS

The phases of the logarithms are defined such that

$$\ell n\Delta^{+}(1) - \ell n\Delta^{-}(1) = 0$$

and

$$\ell n\Delta^{+}(o) - \ell n\Delta^{-}(o) = 2\pi i$$

(N.B. This differs from the definition used by Flowers and Richardson in which $\ell n\Delta^{+}(1) - \ell n\Delta^{-}(1) = -2\pi i$ and $\ell n\Delta^{+}(o) - \ell n\Delta^{-}(o) = 0$. However, this simply has the effect of replacing $\psi(o)$ in equations (A.13) and (A.14) by $\psi(o) - 1)$. Figure A3 shows Z/ρ for a non-interacting liquid, i.e. a Fermi-gas, obtained by putting $F_1 = 0$. ρ is the liquid density given by

$$\rho = \frac{nP_F}{V_F(1 + F_1/3)}$$

The Fermi-velocity, V_F, was taken to be 165.3 ms^{-1}.

It is instructive to consider the various limiting cases of Z from the above equations. In the hydrodynamic limit, $\omega\tau \ll 1$, the transverse acoustic mode is a viscous wave. The solution to equation (A.5) may be found by expanding $\ell n \frac{1 + u}{1 - u}$ in powers of u which gives that

$$s_o^2 \doteq \frac{- 5\ i\omega\tau}{1 + F_1/3} \quad .$$

Substituting this into equation (A.13) and taking the limit

$\omega\tau \to 0$ then

$$Z = (1 - i)\sqrt{\eta\rho\omega/2}$$

which is the classical result with η, the viscosity, given by Fermi-liquid theory as $\frac{\rho V_F^2 \tau}{5}(1 + F_1/3)$. In the non-hydrodynamic or collisionless limit, $\omega\tau \gg 1$, equation (A.5) has no solution and therefore a propagating transverse mode cannot exist. The momentum transport in this region is by single particle excitations only. (For a strongly interacting system e.g. $F_1 > 6$, as discussed by Flowers and Richardson, the behaviour is quite different: A propagating normal mode exists for all $\omega\tau$ which for $\omega\tau \gg 1$ is called transverse zero sound). The impedance is entirely real,

$$\frac{Z}{\rho V_F} = \frac{3 + F_1}{F_1}\,\psi(o) \qquad (A.17)$$

where

$$\psi(o) = \frac{1}{\pi}\int_o^1 \tan^{-1}\left[\frac{\pi}{2}\,\frac{t(1 - t^2)}{(1 - t^2)(1 - t\,\tanh^{-1}t) - (F_1 - 6)/3F_1}\right]dt \qquad (A.18)$$

which agrees with the expression derived by Fomin (1976). The integral can be evaluated exactly for a Fermi-gas by considering the integrand in the $F_1 \to 0$ limit. In this case

$$\psi(o) = \frac{1}{\pi}\int_o^1 \frac{F_1}{3 + F_1}\,\frac{3\pi}{4}\,t(1 - t^2)dt \qquad (A.19)$$

$$= \frac{3}{16}\,\frac{F_1}{3 + F_1} \quad . \qquad (A.20)$$

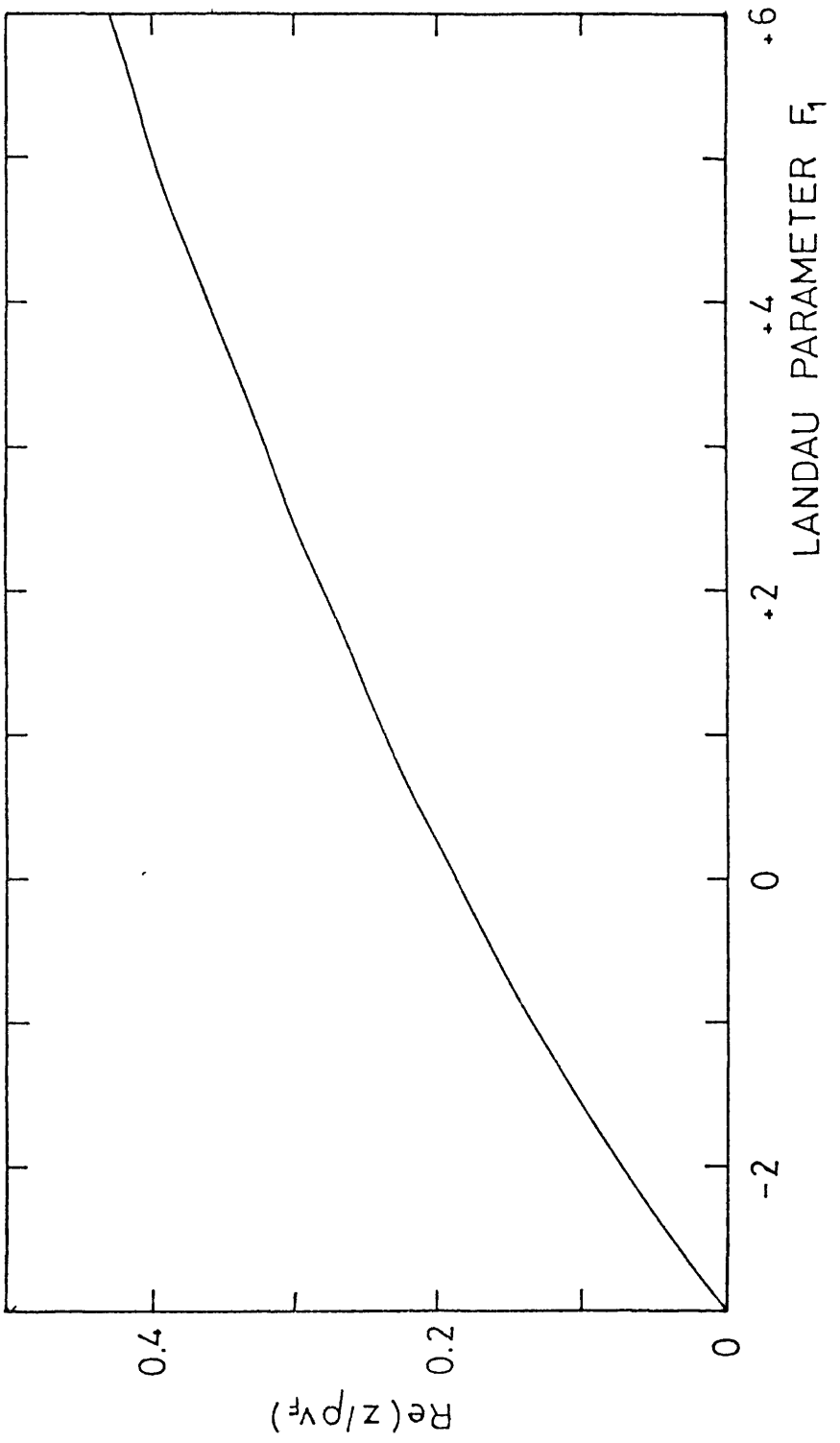

FIG.A.4 THE TRANSVERSE ACOUSTIC IMPEDANCE IN THE COLLISIONLESS LIMIT

Therefore

$$\frac{Z}{\rho V_F} = \frac{3}{16} ,$$

which has also been derived by Butcher (1978) from purely ballistic arguments by considering the change in momentum of gas particles diffusely reflected from a transversely oscillating boundary. For other values of F_1 equation (A.18) has to be evaluated numerically. Figure A4 shows $Z/\rho V_F$ in the collisionless limit for $-3 < F_1 \leqslant 6$.

APPENDIX II

Physica 107B (1981) 223-224
North-Holland Publishing Company

QUARTZ CRYSTAL RESONATOR STUDIES OF LIQUID HELIUM

M.J. Lea and P.W. Retz

Department of Physics
Bedford College, University of London
Regent's Park, London, NW1 4NS, United Kingdom

A shear-mode quartz crystal resonator was used both as a microbalance and a high frequency viscometer (20, 34 and 48 MHz) in liquid He II. The results show the thermal mobilisation of a ^{4}He monolayer on a surface and the breakdown of hydrodynamics in the high frequency viscosity.

We present here some measurements of the properties of liquid He II using a shear-wave thickness mode quartz crystal resonator immersed in the liquid. The resonant frequency f and the quality factor Q of the crystal are changed by the helium in two ways. First, the crystal acts as a microbalance [1], since any mass adsorbed on the surfaces decreases the resonant frequency of the n^{th} harmonic by

$$\Delta f_1 = - 4f^2\sigma/R_q n \qquad (1)$$

(σ is the adsorbed mass per unit area; R_q is the acoustic impedance of the quartz) but should not alter Q. Secondly, the crystal acts as a high frequency viscometer [2], as viscous loading decreases both f and Q by

$$\Delta f_2 = 2fX/n\pi R_q \; ; \quad \Delta(1/Q) = 4R/n\pi R_q \qquad (2)$$

where R and $X(<<R_q)$ are the real and imaginary parts of the transverse specific acoustic impedance Z of the helium. From two-fluid hydrodynamics

$$Z = R + iX = (1 - i)\sqrt{\eta\rho_n\pi f} \qquad (3)$$

where η and ρ_n are the viscosity and normal fluid density. The crystal then excites a viscous wave with a penetration depth $\delta = \sqrt{\eta/\pi\rho_n f}$.

Our crystals [3] had a fundamental frequency of 6.83 MHz and were used at the 3rd (20.47 MHz), 5th (34.09 MHz) and 7th (47.70 MHz) harmonics. $f(T)$ and $Q(T)$ were measured for a crystal in liquid helium from 30 mK to the λ-point, with a power dissipation between 2 and 200 nW (no power dependence was seen).

Below T_λ, $Q(T)$ and $f(T)$ increased rapidly as the viscous losses decreased but, below 0.6 K, Q was temperature independent with $Q(0) \simeq 10^5$, due to intrinsic losses in the resonator, while $f(T)$ decreased again as shown in Fig. 1. We interpret this as due to the formation of a solid layer on the crystal surfaces. The temperature dependence is then due to thermal excitation from this layer giving an adsorbed areal density $\sigma(T) = \sigma(0)(1 - exp(-\theta/kT))$, where θ is an activation or mobilisation energy. The change in f from its value at absolute zero is then

$$\Delta f(T) = 4f^2\sigma(0)\exp(-\theta/kT)/R_q n \qquad (4)$$

Measurements of $\Delta f(T)$ below 0.6 K at 20, 34 and 48 MHz were fitted to Eq.(4) as in Fig.1, giving $\sigma(0) = (6.3 \pm 0.4) \times 10^{-8}$ kg m^{-2} and $\theta/k = 0.15 \pm 0.01$ K. The areal density of a monolayer ^{4}He atoms at normal fluid density is 5.3×10^{-8} kg m^{-2}. This suggests we are observing the thermal mobilisation of a monolayer of ^{4}He atoms. The very low value of θ suggests that it is the second or subsequent monolayer on the substrate of gold plating.

Above 0.6 K, Z was found using Eq.(2) from $Q(T)$ and the frequency shift $f(T) - f(0)$ which was corrected to allow for the temperature dependent adsorption described above. Effective viscosities were derived from R and X using

$$\eta' = R^2/\rho_n\pi f \; ; \quad \eta'' = X^2/\rho_n\pi f \qquad (5)$$

and the known values of ρ_n [6] for He II. (N.B. η' and η'' are *not* the real and imaginary parts of η). At T_λ we find, using the data at 20.47 MHz that $\eta_\lambda = 24.3 \pm 0.4$ μP and $\eta'' = 28.4 \pm 0.5$ μP in agreement with the accepted value of 24.7 μP [4] and a recent measurement of 27.4 μP [5]. The temperature dependence of the normalised effective viscosities, η'/η_λ and η''/η_λ at 20.47 MHz are shown in Fig.2. Both η' and η'' fall rapidly below T_λ; η' remains approximately constant between 1.9 and 1.2 K before decreasing rapidly at lower temperature while η'' decreases steadily as the temperature decreases. Also shown in Fig.2 are measurements of the viscosity of He II from wire viscometers [6], vibrating at low frequencies. The temperature dependences of the low and high frequency viscosities are strikingly different. There is good agreement between 1.5 and 1.9 K when the temperature independent roton viscosity η_r is dominant [7]. But below 1.5 K the low frequency viscosity increases rapidly as phonon-roton scattering decreases exponentially and the phonon viscosity η_p increases. But no such increase is seen in η' or η'' at 20 MHz.

0378-4363/81/0000–0000/$02.50

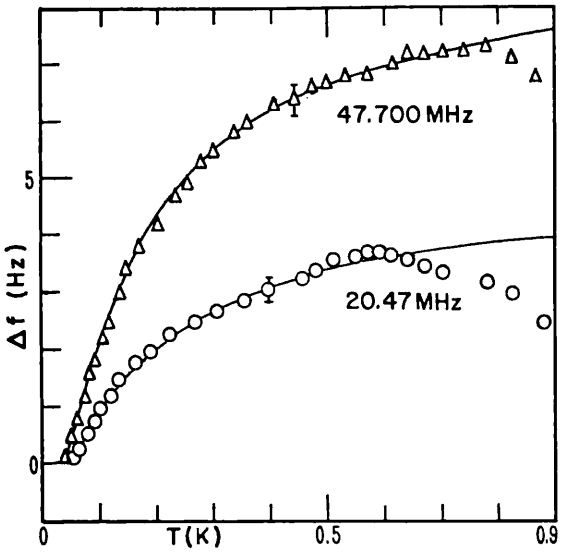

Fig.1. The change in resonant frequency of a quartz crystal immersed in liquid He II. The solid lines show fits of the data below 0.6 K to Eq.(4).

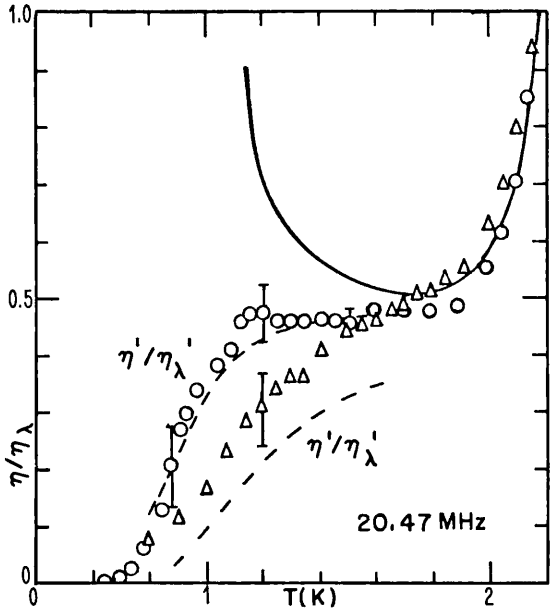

Fig.2. The effective normalised viscosities derived from the data using Eq.(5). The solid lines show the data of Tough et al [6]. The dashed lines are values calculated from Eq.(6).

Following Nadirashvili and Tsakadze [8] we believe this is due to the large values of the ratio ℓ_p/δ in our experiments, where ℓ_p is the phonon mean free path. At 20 MHz we estimate $\ell_p/\delta \simeq 1.5$ at 1.6 K, rising to 35 at 1 K. For $\ell/\delta > 1$ the concepts of viscosity and penetration depth become inappropriate. Z remains well defined but must be derived from the kinetic equation, though a simple expression for finite ℓ/δ has been given by Borovikov and Peshkov [9]. For diffuse scattering of excitations at the interface, Eq.(3) becomes

$$Z = \frac{1-i}{1+(1-i)\,\ell/\delta}\sqrt{\eta\rho_n\pi f} = \sqrt{\eta'\rho_n\pi f} - i\sqrt{\eta''\rho_n\pi f} \quad (6)$$

where η' and η'' are the effective viscosities. Despite the limitations of Eq.(6) it is very useful in understanding our results. First, at 20 MHz, the contributions to R and X due to the phonons is negligibly small at all temperatures. Below 1.9 K our experiments measure *only* the roton viscosity $\eta_r = 12.5 \pm 0.4\ \mu P$. Below 1.2 K, η' and η'' tend to zero, and we interpret this as due to finite values of ℓ_r/δ where ℓ_r is the roton mean free path. Taking the mean free time t_r between roton-roton collisions as $1.04 \times 10^{-13} T^{-\frac{1}{2}} \exp(8.65/T)$ [7] and a mean roton speed of $\sqrt{2kT/\pi\mu}$ where μ is the roton mass, we estimate $\ell_r/\delta \simeq 0.07$ at 1.6 K rising to 1 at 0.84 K. The temperature dependences of η' and η'', calculated from Eq.(6) and our estimates of ℓ_r/δ, are shown in Fig.2. The agreement with the data for η' is excellent, but the measured values of η'' are greater than calculated. Measurements at 34 and 48 MHz confirm these results with the breakdown of hydrodynamics when $\ell_r/\delta \simeq 1$ moving to higher temperatures as the frequency is increased.

We wish to thank A.K. Betts, F. Greenough, F.W. Grimes and A. King for technical assistance, Guernsey Education Council for a studentship (P.W.R.) and the Science Research Council (U.K.) for financial support.

REFERENCES

[1] Stockbridge, C.D., Vacuum Microbalance Techniques (Ed. Behrndt, K.H., Plenum, New York) Vol.5, p.147 (1966); Chester, M. and Yang, L.C., Phys.Rev.Lett. 29 (1972) 211.
[2] Yang, L.C., Ph.D. Thesis, University of California at Los Angeles (1973), and Borovikov, A.P., Priv.Tek.Eksp. 1 (1976) 184 [Instrum. & Exp.Tech. (U.S.A.) 19 (1976) 223] for previous measurements in the range 1.3 K to 2.2 K.
[3] AT-cut quartz crystal resonators were generously supplied by GEC Hirst Research Centre, Wembley, Middlesex, U.K.
[4] Ahlers, G., The Physics of Liquid and Solid Helium (Ed. Bennemann, K.H. and Ketterson, J.B., Wiley, New York) Vol.I, Chap.2 (1976).
[5] Bruschi, L., Mazzi, G., Santini, M. and Torzo, G., J.Low Temp.Phys. 18 (1975) 487.
[6] Tough, J.T., McCormick, W.P. and Dash, J.G., Phys.Rev. 132 (1963) 2373.
[7] Khalatnikov, I.M., Chap.1 of Reference [4].
[8] Nadirashvili, Z. Sh. and Tsakadze, Dzh. S., J.Low Temp.Phys. 37 (1979) 169.
[9] Borovikov, A.P. and Peshkov, V.P., Zh.Eksp. Teor.Fiz 70 (1976) 300. [Sov.Phys.-JETP 43 (1976) 156].

Physica 107B (1981) 225-226
North-Holland Publishing Company

THE TRANSVERSE ACOUSTIC IMPEDANCE OF DILUTE SOLUTIONS OF ^{3}He IN ^{4}He

M.J. Lea and P.W. Retz

Department of Physics
Bedford College, University of London
Regent's Park, London NW1 4NS, United Kingdom

Measurements of the transverse acoustic impedance of dilute solutions of ^{3}He in ^{4}He at 20.47 MHz show evidence for the slip of ^{3}He quasiparticles at a vibrating surface. The fraction of ^{3}He quasiparticles diffusely scattered at a surface of gold plated quartz was found to be 0.25 for a 5.3% solution, compared with 0.05 for a polished quartz surface.

We present here measurements of the transverse acoustic impedance $Z = R + iX$ of dilute solutions of ^{3}He in superfluid ^{4}He (molar concentrations c = 0.014, 0.031, 0.053, 0.060 and 0.092) at a frequency of 20.47 MHz from 0.03 to 1 K. As in ^{4}He [1], we measured the resonant frequency $f(c,T)$ and the quality factor $Q(c,T)$ of a shear wave quartz crystal resonator in the liquid. Similar measurements were reported by Borovikov and Peshkov (BP) [2] for a resonator, inside the mixing chamber of a dilution refrigerator, which was covered with a superfluid film of the saturated dilute solution (c was then temperature dependent, decreasing to 0.064 at low temperature). The real part of Z was obtained from

$$R = n\pi\Delta(Q^{-1})\, R_q/4; \quad \Delta(Q^{-1}) = Q^{-1}(c,T) - Q^{-1}(0,0) \qquad (1)$$

where n is the harmonic number of the crystal resonance (n=3 at 20.47 MHz), R_q is the acoustic impedance of the quartz and $Q(0,0)$ is the value in pure ^{4}He below 0.5 K where R = 0. Values of $R(c,T)$ are shown in Fig.1. As in pure ^{4}He [1], the temperature dependent frequency shifts are due to $X(c,T)$ and to a solid adsorption, areal density $\sigma(T)$ (which we have assumed to be the same as in pure ^{4}He)

$$\Delta f = 2fX/n\pi R_q - 4f^2\sigma/nR_q \qquad (2)$$

The frequency changes for each concentration were reproducible and values of $X(c,T) - X(c,0)$ are shown in Fig.2 where the data is assumed to extrapolate linearly to T = 0. The absolute values of $X(c,0)$ could not be determined accurately, but were small and may be zero.

In the hydrodynamic region Z depends on the viscosity η and the normal fluid density ρ_n:

$$Z = (1 - i)\sqrt{\rho_n \pi f} \qquad (3)$$

and we expect contributions from phonons, rotons and ^{3}He quasiparticles. As discussed in [1] the phonons make a negligible contribution to η at 20 MHz while the roton viscosity is much reduced in mixtures because of roton-^{3}He scattering [3] and should be small at 1 K and negligible below 0.8 K. We use Eq.(3) to derive effective viscosities:

$$\eta' = R^2/\pi\rho_3 f; \quad \eta'' = X^2/\pi\rho_3 f \qquad (4)$$

with ρ_3 from an inertial effective mass $m^* = 2.54\, m_3$ [4]. At 1 K, η' is in good agreement with the data of Bertinat et al [5] who used a quartz crystal torsional viscometer at 40 kHz and with the capillary flow measurements of Kuenhold et al [6]. At lower temperatures $\eta'' < \eta'$ as X/R decreases. At 30 mK, η' is less than the effective viscosity at 40 kHz [5], which in turn is less than the hydrodynamic viscosity [6]. The data for ~5% solutions is shown in Fig.3. Following BP, these effects are due to slip of the ^{3}He quasiparticles, of which only a fraction α are diffusely scattered at the vibrating surface. At the lowest temperatures in the collisionless regime ($\omega\tau > 1$, τ is the relaxation time) for a degenerate Fermi gas (Fermi velocity v_F) Z is real [7]:

$$Z = \alpha(3/16)\rho_3 v_F \qquad (5)$$

Using Eq.(5) we find α = 0.25 for our 5.3% solution (BP found α = 0.22 for a saturated solution), presumably due to the roughness of

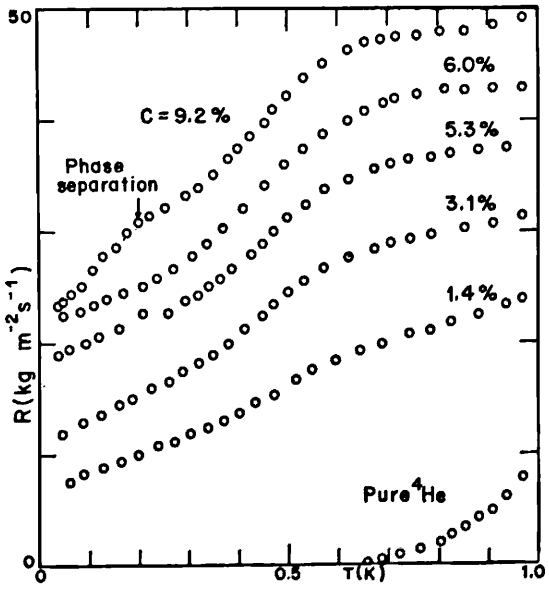

Fig.1. The real part of Z for dilute solutions of ^{3}He in ^{4}He.

0378-4363/81/0000–0000/$02.50

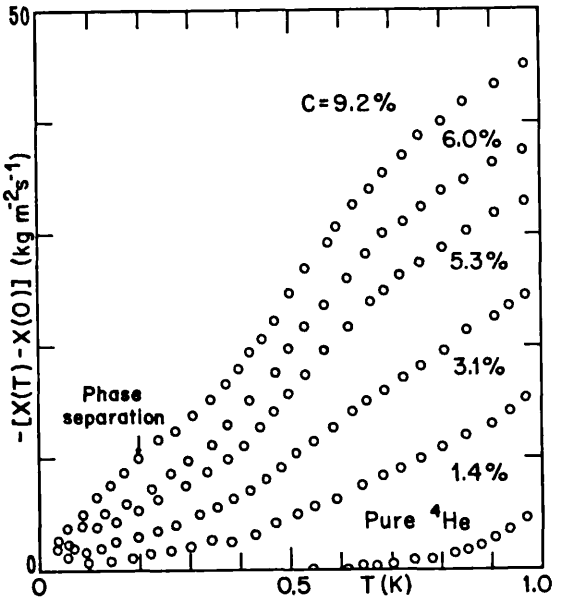

Fig.2. The imaginary part of Z for dilute solutions of ^{3}He in ^{4}He.

the gold plated quartz. At higher temperatures BP derived

$$Z = \frac{\eta}{\delta}\frac{(1-i)}{1+(1-i)\beta\ell/\delta} = \sqrt{\eta'\rho_3\pi f} - i\sqrt{\eta''\rho_3\pi f} \qquad (6)$$

where ℓ is the quasiparticle mean free path, δ is the viscous penetration depth ($= \sqrt{\eta/\rho_3\pi f}$ and $\ell/\delta = \sqrt{3\omega\tau/2}$. The enhancement factor $\beta = (2-\alpha)/\alpha$ in the quasi-hydrodynamic region ($\beta\ell/\delta>1$, $\omega\tau<1$) which corresponds to the 40 kHz data [5]. We can calculate the effective viscosity for a 5% solution from Eq.(6) and calculations of τ[8] and η[9] and the results at 40 kHz for β = 38, and hence α = 0.05 for a polished quartz surface [5], are shown in Fig.3. Eq.(6) is not strictly valid in the collisionless region ($\beta\ell/\delta>1$, $\omega\tau>1$), which corresponds to 20 MHz at low temperatures, but reduces to Eq.(5) if we put $\beta = 4/3\alpha$ and should then be a reasonable approximation. Calculations of η' at 20 MHz for β = 4.9, and hence α = 0.27, are shown for a 5% solution in Fig.3. The agreement with our data is reasonable below 0.5 K. The discrepancy above 0.5 K indicates that τ [8] is too long in the classical region, as suggested before [9, 4].

We thank A.K. Betts, F. Greenough, F.W. Grimes, and A. King for technical assistance, Guernsey Education Council for a studentship (P.W.R.) and the Science Research Council (U.K.) for a grant.

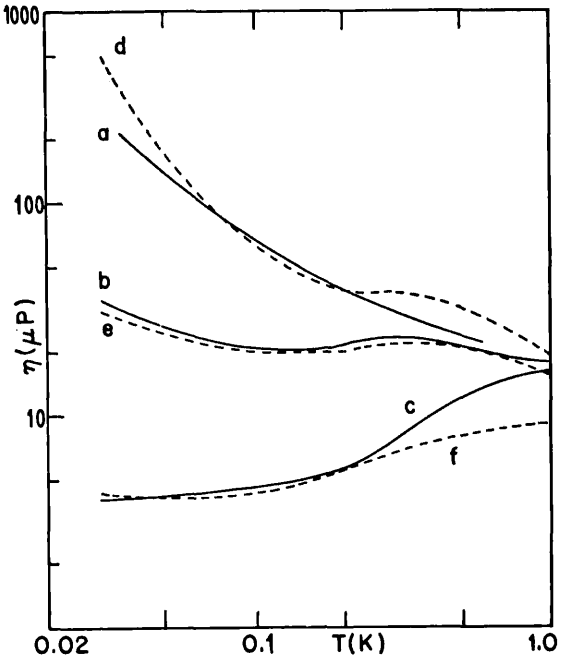

Fig.3. Measurements of the effective viscosity for 5% solutions: (a) by capillary flow [6], (b) at 40 kHz [5], (c) at 20 MHz (5.3% solution). Calculations for a 5% solution: (d) Baym and Saam [9], (e) with slip at 40 kHz, (f) with slip at 20 MHz.

REFERENCES

[1] Lea, M.J. and Retz, P.W., LT 16 Proceedings, Vol. p.

[2] Borovikov, A.P. and Peshkov, V.P., Zh.Eksp. Teor.Fiz. 70 (1976) 300 [Sov.Phys. - JETP 43 (1976) 156].

[3] Zharkov, V.N., Zh.Eksp.Teor.Fiz. 33 (1957) 929 [Sov.Phys. - JETP 6 (1958) 714].

[4] de Voogt, W.J.P. and Kramers, H.C., Physica 85B (1977) 73.

[5] Bertinat, M.P., Betts, D.S., Brewer, D.F. and Butterworth, G.J., Phys.Rev.Lett. 28 (1972) 472.

[6] Kuenhold, K.A., Crum, D.B. and Sarwinski, R.E., Phys.Lett. 41A (1972) 13.

[7] Jensen, H.H., Smith, H., Wölfle, P., and Nagai, K., J.Low Temp.Phys. 41 (1980) 473.

[8] Baym, G. and Ebner, C., Phys.Rev. 164 (1967) 235.

[9] Baym, G. and Saam, W.F., Phys.Rev. 171 (1968) 172.

J. Phys. C: Solid State Phys., **15** (1982) L207–L210. Printed in Great Britain

LETTER TO THE EDITOR

The transverse acoustic impedance of a Fermi gas

P W Retz† and M J Lea
Department of Physics, Bedford College, Regent's Park, London NW1 4NS, UK

Received 29 December 1981

Abstract. The effective transverse acoustic impedance of a Fermi gas is calculated for both diffuse and partially diffuse reflection of the gas particles at a transversely vibrating solid surface.

There have been several calculations of the transverse acoustic impedance Z of a Fermi liquid (Flowers and Richardson 1978, Richardson 1978, Jensen *et al* 1980 and others) which have been used to interpret experimental data on pure liquid ^{3}He. We present here explicit computations of Z for a Fermi gas, which should be appropriate for dilute solutions of ^{3}He in liquid ^{4}He at low temperatures, and for which data has recently been obtained (Lea and Retz 1981). We also give a simple expression for the effective impedance of the gas as seen by a transversely vibrating surface from which only a fraction α of the Fermi gas particles are diffusely reflected.

Consider a plane solid surface, normal to z, oscillating with an angular frequency ω and a velocity along x of $U_0 \exp(-i\omega t)$, immersed in a gas of n fermions per unit volume, each of mass m and with a Fermi momentum of p_F. The transverse acoustic impedance is

$$Z = \Pi_{xz}/U_0 \tag{1}$$

where Π_{xz} is a component of the momentum flux tensor at the surface. The Landau kinetic equation for Π_{xz} was solved using Wiener–Hopf techniques (e.g. Flowers and Richardson 1978) with the symmetric Landau parameters $F_{l\geqslant 2} = 0$ and for $-3 < F_1 \leqslant 6$ with a single relaxation time τ. The Fermi gas results are then obtained by putting $F_1 = 0$. For $\omega\tau$ less than some critical value $(\omega\tau)_c$, Z is given by

$$Z = R + iX = -i\omega\tau n p_F(\psi + 1/s_0) \tag{2}$$

where, for $F_1 = 0$,

$$\psi = \frac{-1}{2\pi i}\int_0^1 \{\ln \Delta(u, +1) - \ln \Delta(u, -1)\}\, du$$

$$\Delta(u, v) = 1 - \frac{3u^2}{2(1 - i\omega\tau)}\left[\frac{1 - u^2}{2u}\left(\ln\frac{1+u}{1-u} + i\pi v\right) + 1\right].$$

s_0 is defined by $\Delta(s_0^{-1}, 0) = 0$ and is proportional to the propagation constant of the

† Present address: Oxford Instruments, Osney Mead, Oxford, UK.

0022-3719/82/080207 + 04 $01.50

transverse acoustic mode which, for $\omega\tau \ll 1$, is a viscous wave. But for $\omega\tau > (\omega\tau)_c = 0.89$ for $F_1 = 0$ (Lea *et al* 1973) no root s_0 exists and Z is then given by

$$Z = -i\omega\tau n p_F \psi \tag{3}$$

and the momentum transport is by single-particle excitations. ψ† was evaluated numerically as a function of $\omega\tau$ and is discontinuous at $(\omega\tau)_c$, but Z, which is the experimentally accessible quantity, remains continuous. For a strongly interacting Fermi liquid (e.g. $F_1 > 6$) as discussed by Flowers and Richardson (1978) the root s_0 exists for all $\omega\tau$ and is related to transverse zero sound for $\omega\tau \gg 1$. The behaviour of Z for a Fermi gas is qualitatively similar to that found for a Fermi liquid. For $\omega\tau \ll 1$, Z is given by the hydrodynamic result

$$Z = (1 - i)(\eta\rho\omega/2)^{1/2} \tag{4}$$

where η is the viscosity and ρ the density of the gas. In the ballistic or collisionless limit, $\omega\tau \gg 1$, Z is real with

$$Z = R_\infty = \tfrac{3}{16} n p_F. \tag{5}$$

Values of the real and imaginary parts of the normalised impedance $Z^* = R^* + iX^* = (R + iX)/R_\infty$ are given in table 1 and plotted in figure 1.

Table 1. The normalised transverse acoustic impedance of a Fermi gas (equations (2) and (3)).

$\omega\tau$	R^*	$-X^*$
0.01	0.167	0.139
0.02	0.234	0.182
0.04	0.325	0.228
0.06	0.391	0.253
0.08	0.444	0.269
0.1	0.488	0.280
0.2	0.640	0.291
0.4	0.793	0.261
0.6	0.868	0.223
0.8	0.911	0.190
1	0.936	0.164
2	0.981	0.094
4	0.995	0.049
6	0.998	0.033
8	0.999	0.025
10	0.999	0.020

These exact results may be compared with an approximate solution of the transport equation given by Richardson (1978) for a strongly interacting Fermi liquid. On setting the Landau parameters to zero and using a single relaxation time, his expression becomes

$$Z^* = 2/[1 + (1 + iA/\omega\tau)^{1/2}] \tag{6}$$

where $A = \frac{3}{4}$. The maximum deviation in Z^* from the exact results is less than 0.01,

† We have defined the phases of the logarithm by $\ln \Delta(1, 1) - \ln \Delta(1, -1) = 0$. An alternative definition, used by other authors, $\ln \Delta(1, 1) - \ln \Delta(1, -1) = -2\pi i$ replaces ψ in equations (2) and (3) by $\psi - 1$.

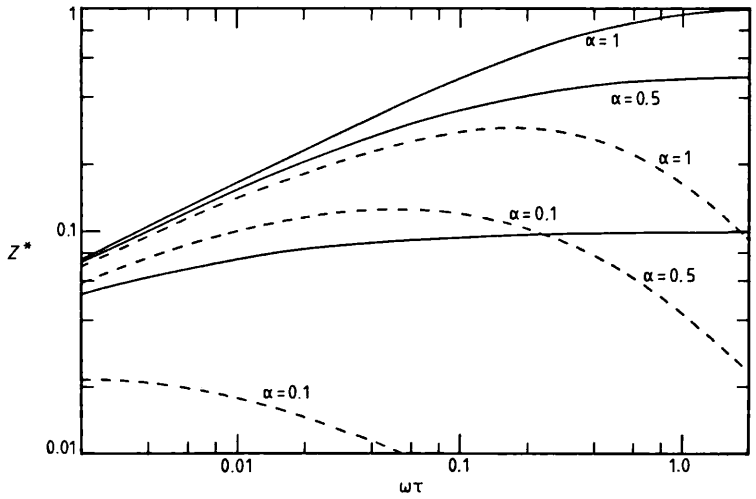

Figure 1. The normalised acoustic impedance of a Fermi gas, for $\alpha = 1, 0.5$ and 0.1. The full curves are the real part R^* and the dotted curves are the imaginary part $-X^*$.

although there is a small systematic deviation in the hydrodynamic limit, $\omega\tau \ll 1$. Jensen *et al* (1980) have suggested $A = \frac{45}{64}$; the maximum deviation is then 0.02 but the result is exact for $\omega\tau \ll 1$. Hence the expression given by Richardson for a strongly interacting Fermi liquid can also be used with minimal error for a Fermi gas. It is especially useful since the full expression allows for finite F_1 and F_2, two relaxation times, and is much more amenable to computation than equations (2) and (3).

The differences between these calculations are small and much more important, particularly for solutions of ^{3}He in ^{4}He, is the effect on the measured impedance Z if only a fraction α of the ^{3}He quasiparticles are diffusely reflected at the vibrating surface. For pure specular reflection, $\alpha = 0$, no transverse momentum is transferred to the gas and Z is zero. For $0 < \alpha < 1$ the calculation of $Z(\alpha)$ from the transport equation is difficult. However, the following simple kinetic theory should give a reasonable approximation if $Z(1)$ is known from the calculations above.

If the mean transverse velocities of the atoms approaching the surface just prior to reflection is $U_2 \exp(-i\omega t)$ and of those leaving the surface is $U_1 \exp(-i\omega t)$ then

$$\Pi_{xz} = \tfrac{1}{4} nmc(U_1 - U_2)$$

where c is the mean particle speed. For a Fermi gas

$$\Pi_{xz} = \tfrac{3}{16} np_F(U_1 - U_2). \tag{7}$$

Therefore, from equation (1), and using normalised quantities $Z^* = Z/\frac{3}{16}np_F$, $u_1 = U_1/U_0$ and $u_2 = U_2/U_0$, we have

$$Z^*(\alpha) = u_1 - u_2. \tag{8}$$

Also, for a fraction α of particles diffusely reflected

$$u_1 = \alpha + (1 - \alpha)u_2. \tag{9}$$

If we also assume that the ratio of the velocities u_2/u_1 in the gas is independent of α

then, since for $\alpha = 1$, $Z^*(1) = u_1 - u_2 = 1 - u_2$, we can write for all α

$$u_2/u_1 = 1 - Z^*(1). \tag{10}$$

Hence from equations (8)–(10) we obtain

$$Z^*(\alpha) = \frac{Z^*(1)}{1 + \beta Z^*(1)}. \tag{11}$$

where $\beta = (1 - \alpha)/\alpha$. $Z^*(\alpha)$ is plotted in figure 1 as a function of $\omega\tau$ for $\alpha = 0.5$ and 0.1. For $\omega\tau \gg 1$ equation (11) becomes

$$Z^*(\alpha) = \alpha$$

which was used by Lea and Retz (1981) to derive α for a gold-plated quartz crystal in a dilute solution of ^{3}He in ^{4}He. The effect of $\alpha < 1$ is to reduce the effective impedance and to enhance the slip between the gas and the vibrating surface. The most appropriate measure of slip in this situation is the ratio γ of the mean transverse velocity of the gas next to the surface to the velocity of the surface itself, i.e.

$$\gamma = \tfrac{1}{2}(u_1 + u_2) = \frac{1 - Z^*(1)/2}{1 + \beta Z^*(1)}. \tag{12}$$

Hence γ decreases from 1 in the hydrodynamic limit to $\alpha/2$ in the collisionless limit.

Equation (11) should also be a reasonable approximation for a Fermi liquid, when appropriate values of $Z^*(1)$ are used.

P W Retz would like to thank Guernsey Education Council for a Research Studentship.

References

Flowers E G and Richardson R W 1978 *Phys. Rev.* B **17** 1238–48
Jensen H H, Smith H, Wölfle P and Nagai K 1980 *J. Low Temp. Phys.* **41** 473–519
Lea M K, Birks A R, Lee P M and Dobbs E R 1973 *J. Phys. C: Solid State Phys.* **6** L226–30
Lea M J and Retz P W 1981 *Proc. 16th Int. Conf. on Low Temp. Phys: Physica* B + C **107** No 1 225–6
Richardson R W 1978 *Phys. Rev.* B **18** 6122–38

ACKNOWLEDGEMENTS

It is a pleasure to convey my thanks to the many people who have helped me in this work, particularly to my supervisor, Dr M J Lea for his constant advice and encouragement throughout this project. I am also indebted to Professor E R Dobbs for his help and guidance during my post-graduate years at Bedford College.

For advice on the technical aspects, I would like to extend my thanks to Mr W Baldock and the technical staff of the department for their assistance. Especially to Mr F Greenough for maintaining and operating the dilution refrigerator; Mr F Grimes and Mr A King for their help with the design and construction of the sonic cells; Mr A K Betts for discussions on the electronics used in the experiments.

I would also like to thank Mr and Mrs J Y Rose and their youngest daughter, Melanie, for their kindness and patience during the later stages of this work.

Finally, I gratefully acknowledge the financial support of the Guernsey Education Council in the form of a Research Studentship.

P W RETZ

April 1983

REFERENCES

Abramowitz M and Stegun I	'Handbook of Mathematical Functions' (Dover, New York, 1965)
Ahlers G	in 'The Physics of Liquid and Solid Helium' eds: Bennemann K H and Ketterson J B (Wiley, New York, 1976) Chap.2, Vol.I
Anon*	Proc. IRE 37, 1378 (1949)
Anon*	Proc. IRE 14, 353 (1957)
Anon*	Metrologica 15, 65 (1979)
Atkins K R and Rudnick I	in 'Progress in Low Temperature Physics' ed: Gorter C J (North-Holland, Amsterdam, 1970) p.37, Vol.XI
Bekarevich I L and Khalatnikov I M	Zh. Eksp. Teor. Fiz. 39, 1699 (1960) [Sov. Phys. - JETP 12, 1187 (1961)]
Bendt P J, Cowan R D and Yarnell J L	Phys. Rev. 113, 1386 (1959)
Berlincourt D A	in 'Ultrasonic Transducer Materials' ed: Mattiat O E (Plenum, New York, (1971))
Berlincourt D A, Curran D R and Jaffe H	in 'Physical Acoustics' eds: Mason W P and Thurston R N Academic Press, New York, 1964), p.169, Vol.1A
Bertinat M P, Betts, D S, Brewer D F and Butterworth G J	J. Low Temp. Phys. 16, 479, (1974)
Betts D S	'Refrigeration and Thermometry Below One Kelvin' (Sussex Univ. Press, UK, 1976)
Binder K and Hohenberg P C	Phys. Rev. B6, 3461 (1972)
Borovikov A P	Prib. Tek. Eksp. 1, 184 (1976) [Instrum. and Exp. Tech., USA, 19, 223 (1976)]
Borovikov A P and Peshkov V P	Zh. Eksp. Teor. Fiz 70, 300 (1976) [Sov. Phys. - JETP 43, 156 (1976)]
Brewer D F	in 'The Physics of liquid and Solid Helium' eds. Bennemann K H and Ketterson J B (Wiley, New York, 1978) Chap.6, Vol.II.

Brewer D F and Edwards D O	Proc. 8th Int. Conf. Low Temp. Phys. ed: Davies (Butterworth, 1963) p.96
Brewer D F, Symonds A J and Thomson A L	Phys. Lett. 13, 298 (1964)
Brooks J S and Donnelly R J	J Phys. Chem. Ref. Data 6, 51 (1977)
Bruschi L, Mazzi, G, Santini M and Torzo G	J. Low Temp. Phys. 18, 487 (1975)
Butcher K J	Ph.D. Thesis, Univ. of London (1978)
Chester M and Yang L C	Phys. Rev. Lett. 31, 1377 (1973)
Chester M, Yang L C and Stephens J B	Phys. Rev. Lett. 29, 211 (1972)
Cowley R A and Woods A D B	Can. J. Phys. 49, 177 (1971)
Dietrich O W, Graf E H, Huang C H and Passall L	Phys. Rev. A5, 1377 (1972)
Donnelly R J	Phys. Lett. 39A, 221, (1972)
Dwight H B	'Table of Integrals and Mathematical Data' (Macmillan, New York, 1961)
Firth D	'Quartz Crystal Oscillator Circuit Design Handbook' (Dept. of U S Army, Project No.3A99-15-004, 1965)
Fisher M E	Rev. Mod. Phys. 46, 597 (1974)
Flowers E G and Richardson R W	Phys. Rev. B17, 1238, (1978)
Fomin I A	Pis'ma Zh. Eksp. Teor. Fiz. 24, 90 (1976) [Sov. Phys. - JETP Lett. 24, 77 (1976)]
Ginzburg V L and Pitaevskii L P	Zh. Eksp. Teor. Fiz 34, 1240 (1958) [Sov. Phys. - JETP 34, 858 (1958)]
Gooberman G L	'Ultrasonics: Theory and Application' (English Univ. Press, UK, 1968)

Harrison J P	J. Low Temp. Phys. 37, 467 (1979)
Henkel R P, Smith E N and Reppy J D	Phys. Rev. Lett. 23, 1276 (1969)
Hohenberg P C, Aharony A, Halperin B I and Saggia E D	Phys. Rev. B13, 2986 (1976)
Ihas G C and Pobell F	Phys. Rev. A9, 1278 (1974)
Kennard E H	'Kinetic Theory of Gases' (McGraw-Hill, New York, 1938)
Khalatnikov I M	Usp. Fiz. Nauk. 59, 673 (1956)
Khalatnikov I M	'An Introduction to the Theory of Superfluidity' (Benjamin, New York, 1965)
Khalatnikov I M	in 'The Physics of Liquid and Solid Helium' eds: Bennemann K H and Ketterson J B (Wiley, New York, 1976), Chap.1, Vol.I
Landau L D	Zh. Eksp. Teor, Fiz. 11, 592 (1941) [J. Phys. Moscow 5, 71 (1941)]
Landau L D and Liftshitz E M	'Fluid Mechanics' (Pergamon Press, London, 1959)
Landau L D and Liftshitz E M	'Statistical Mechanics' (Pergamon Press, London, 1958)
Lea M J, Birks A R, Lee P M and Dobbs E R	J. Phys. C6, L226 (1973)
Lea M J and Fozooni P	Phys. Lett. 93A, 91 (1982)
Lea M J and Retz P W	Physica 107B, 223 (1981)
Lea M J and Retz P W	Physica 107B, 225 (1981)
Lounasmaa O V	'Experimental Principles and Methods Below 1K' (Academic Press, London, 1974)
Mamaladze Yu G	Zh. Eksp. Teor. Fiz 52, 729 (1967) [Sov. Phys. - JETP 25, 479 (1967)]

McSkimin H J, Andreatch P Thurston R N — J. App. Phys. 36, 1624 (1965)

Mossuz G — These de Docteur-Ingenieur, No.61, Faculte des Sciences de Basancon (1975)

Mossuz G and Gagrepain J J — Cryogenics 16, 652 (1976)

Nadirashvili Z Sh and Tsakadze Dzh S — Fiz. Nizk. Temp 4, 1509 (1978) [Sov. J. Low Temp. Phys. 4, 711 1978)]

Nadirashvili Z Sh and Tsakadze Dzh S — J. Low Temp. Phys. 37, 169 (1979)

Putterman S J — 'Superfluid Hydrodynamics' (North-Holland, Amsterdam, 1974)

Retz P W and Lea M J — J. Phys. C15, L207 (1982)

Roberts P H and Donnelly R J — J. Low Temp. Phys. 15, 1 (1974)

Scholtz J H, McLean E O and Rudnick I — Phys. Rev. Lett. 32, 147 (1974)

Smagin A G — Prib. Tek. Eksp. 6, 143 (1974) [Cryogenics 15, 483 (1975)]

Sobyanin A A — Zh. Eksp. Teor. Fiz. 63, 1780 (1972) [Sov. Phys. - JETP 36, 941 (1973)]

Stockbridge C D — in 'Vacuum Microbalance Techniques' ed: Behrndt K H (Plenum, New York, 1966a) p.179, Vol.5

Stockbridge C D — in 'Vacuum Microbalance Techniques' ed: Behrndt K H (Plenum, New York 1966b) p.193, Vol.5

Tjerskra H H — Physica 18, 853 (1952)

Tough J T, McCormick W D and Dash J G — Phys. Rev. 132, 2373 (1963)

Tyson J A and Douglass D H — Phys. Rev. Lett. 17, 472 (1966)

Welber B	Phys. Rev. 119, 1816 (1960)
Williams R D and Rudnick I	Phys. Rev. Lett. 25, 276 (1970)
Wilks J	'The Properties of Liquid and Solid Helium' (Clarendon Press, Oxford, 1967)
Yarnell J L, Arnold, G P Bendt P J and Kerr E C	Phys. Rev. 113, 1379 (1959)
Yang L C	Ph.D. Thesis, Univ. of Cal. at Los Ang. (1973)

---

*Proceedings papers or documents prepared by a Committee

Anon (1949):	"Standards on Piezoelectric Crystals, 1949", Chairman: Brainerd J G
Anon (1957):	"IRE Standards on Piezoelectric Crystals - The Piezoelectric Vibrator: Definition and Methods of Measurement, 1957", Chairman: Jaffe H
Anon (1979):	"The 1976 Provisional 0.5K to 30K Temperature Scale", Chairman: Durieux M